A Singular-Value-Decomposition-Based Method For Impact Assessment Of Power Electronic Interfaced Generation On The Harmonic Response In Electrical Power Systems

Armando Daniel Torres Acosta

Technische Universiteit Delft

TU Delft Delft University of Technology

Challenge the future

A Singular-Value-Decomposition-Based Method For Impact Assessment Of Power Electronic Interfaced Generation On The Harmonic Response In Electrical Power Systems

by

Armando Daniel Torres Acosta

in partial fulfillment of the requirements for the degree of

Master of Science
in Electrical Engineering

at the Delft University of Technology,
to be defended publicly on Thursday September 5, 2019 at 03:00 PM.

Supervisor:	Dr. ir. J.L. Rueda Torres	
Thesis committee:	Prof. ir. M.A.M.M. van der Meijden,	IEPG, TU Delft
	Dr. ir. J.L. Rueda Torres,	IEPG, TU Delft
	Dr. T. Batista Soeiro,	DCE&S, TU Delft

This thesis is confidential and cannot be made public until December 31, 2020.

An electronic version of this thesis is available at http://repository.tudelft.nl/.
Cover credtis to TenneT TSO B.V., available at https://www.tennet.eu/.

TU Delft Delft University of Technology

Abstract

The connection of offshore wind turbines to the European grid has been growing in the recent years. Many European countries are adopting this renewable energy and are increasing the number of wind power plant additions into their electrical transmission networks. Due to the phase out of conventional power plants (e.g. fossil fuel fired), new challenges are arising in terms of inertia, frequency stability, voltage stability and power quality, being the latter the main focus in the present work. It is important to study the harmonic frequencies that the wind parks are going to introduce in the electrical grid and how the grid is going to respond to this sustainable energy addition. The classical methods to identify the harmonics frequencies and to assess the stability in an electrical power system are performed by considering single-input single-output (SISO) systems. Nevertheless, when modelling a power system as a SISO system, information about the dynamics of the elements in the system is neglected. To overcome this disadvantage, a representation with more than one input and one output, a multiple-input multiple-output (MIMO) system, can be considered.

The present works concerns with the development of a method for studying the harmonic frequencies of any electrical power system. Since the main elements in the grid that contribute to the creation of harmonic frequencies are the inductances and the capacitances of the transmission lines and underground cables, the present work will focus on these passive elements and it will represent the transmission lines as PI sections and the underground cables as "fitted PI" sections. These representations are SISO systems, because the have only a voltage signal, measured in the sending end of a transmission branch, as input; and a voltage signal, measured in the receiving end of a transmission branch, as output. Therefore, it is necessary to find an approach to build a MIMO system. This is done via a concatenation of SISO linear-time-invariant (LTI) systems to create a MIMO system. Afterwards, the MIMO system is studied with a powerful mathematical tool called the singular value decomposition that not only will give information about the harmonic frequencies in the system, but it will show it is also possible to study which input of the system is affecting the system the most and which output will be the most affected. To finish the research, a sensitivity analysis is performed with respect to the variation of the capacitances and inductances in the transmission lines and the underground cables. This analysis will evaluate possible variations in the harmonic response of the MIMO system.

The proposed method to investigate the harmonic frequencies of an electrical power system can be applied to any power system. For sake of illustration of application, two different power system models are addressed. First, to understand each step in the method a small size test system is studied. This study shows how to apply the method and illustrates how to interpret the evaluation outcomes. Subsequently, a synthetic model of the Randstad regional transmission network is used to test the method in a relatively larger system model. This case study is of great importance due to the new wind parks that are going to be connected to this region in the coming years. Therefore, the harmonic frequencies observed in the synthetic model of the Randstad region will be obtained and an assessment of which transmission line or underground cable is the most affected by the harmonics in the system will be performed.

Acknowledgements

Quiero agradecer en primer lugar a mi familia, mis padres, Armando y Marisela y a mi hermana Sofi por todo su apoyo, comprensión y amor que me brindaron durante esta aventura. Este trabajo está dedicado a ustedes.

I want to thank my supervisor Dr. José Rueda for his support and advice during the realisation of this work. I would like to thank Prof. Mart van der Meijden for his pertinent feedback during the meetings where we discussed the details of the present project. I also want to thank to Dr. Thiago Batista for accepting to be part of my thesis committee.

I want to emphasise the help provided from Arcadio Perilla, his invaluable time dedicated to discuss matters of science and life is pretty much appreciated.

All my gratitude to my friends Arturo, Ale, Joel, Katherine, Jorge for all the laughs, amusement and support you have given to me. This thrilling experience would not have been the same without you guys.

I want to thank specially to my life companion, Celia. Thanks for encourage me through this adventure we walked together.

Finally, I want to thank the financial support provided by the National Council of Science and Technology (CONACYT).

Contents

List of Figures

List of Tables

1

Introduction

In the year 2018, Europe put in service 409 new offshore wind turbines to the grid [4]. Therefore, the new power connected to the grid was 2,649 MW. The main countries contributing to this offshore wind turbines connection are the United Kingdom (1,312 MW), Germany (969 MW), Belgium (309 MW), Denmark (61 MW), Spain (5 MW) and France (2 MW). The main location where this wind farms were connected was in the North Sea with 1,651 MW, representing the 62% of the installations. The Netherlands did not have any offshore wind turbine connections in this year. However, in the future years, large size wind power plants with nearly 3.5 GW of production are going to be connected to the Dutch electrical network [5]. Most of this power generation is going to be distributed through the Randstad electrical region. The Randstad is the territory consisting primarily of the four largest Dutch cities, such as Amsterdam, Rotterdam, The Hague and Utrecht [6].

All these offshore wind power plants are being built in the North Sea. Two 700 MW wind power plants are currently being commissioned and will be connected this year (2019) to the electrical grid in the Borssele substation. Another two wind farms have been planned for implementation in the coming years. The first one, the Hollandse Kust Zuid, will be conformed by two 700 MW wind farms and it is planned that in the years 2021 to 2022 will be connected to the Maasvlakte substation. The second one, the Hollandse Kust Noord, will be conformed by a 700 MW wind farm. In the year 2023, it is planned to be connected to the Beverwijk substation.

Due to the particular operating principles of the power electronic devices and variable nature of wind power, the harmonic interactions among wind generators within the same wind power plant, and between different wind power plants and the electrical transmission network, pose new challenges to the network stability and power quality [7]. Understanding the modified dynamic behaviour of the Randstad region is essential to define appropriate mitigation measures to ensure optimal operation of the wind power plants, as well as optimal compliance of the network requirements concerning stability and power quality harmonic distortion.

It is of high importance to know the resonance (harmonic) frequencies of the Randstad region in order to implement appropriate mitigation methods. The approach that was taken in the present work in order to discover the harmonic frequencies, was the passive one. This means that only capacitances, inductances and resistances are going to be taken into account in the modelling of the system. This approach is taken to show the basics of obtaining the harmonic frequencies. However, a much complex approach, e.g. a frequency dependent model,

can be explored.

In order to explain the methodology to find the harmonic frequencies of the Randstad region, a simpler *small size test system* is going to be studied and developed through each chapter of the present work. Once this system has been studied, a synthetic Randstad region model will be analysed and its harmonic frequencies will be found.

The present work will focus on the passive elements of the network. Therefore, the transmission lines are going to be modelled as state-space representations of PI sections and the underground cables will be modelled as state-space representations of "fitted PI" sections. The current methods available in the literature related to find the harmonic frequencies of an electrical system are performed to single-input single-output systems. However, by nature the electrical systems are multiple-input multiple-output systems. Therefore, the first objective is to find a methodology to represent the *small size test system* as a multiple-input multiple-output (MIMO) system. Then, the transfer function of the system is found. The latter is necessary to use a powerful mathematical tool to discover the harmonic frequencies. This tool is called Singular Value Decomposition (SVD). The latter, uses the dynamics of the system in the frequency domain and takes into account how the input(s) of the system affects the direction(s) and the gain(s) of the output(s) of the system [8]. The SVD can also be used to analyse the system at a certain harmonic frequency and show which input(s) of the system will have more influence in the system dynamics and which output(s) will be the most affected by that input(s).

Once the *small size test system* has been explained, the 380 kV transmission lines and underground cables that are part of the synthetic model of the Randstad region are going to be modelled as a MIMO system and the transfer function of the region will be found. Then, the latter is going to be analysed to discover the harmonic frequencies of the system and a study of their inputs and the outputs is going to be performed. Finally, a sensitivity analysis is going to be implemented to observe how the harmonics of the system change as a function of the length of the components in the system.

The output of the present work will provide a methodology to model any electrical network via its passive electrical elements, and to perform a harmonic analysis. The latter, will help the TSOs to take action in terms of which harmonics must not be injected to the system due to the voltage magnitude increment that they will produce in a transmission branch.

1.1. State of the art and scientific gap

In [9] an EMT model of the Randstad region was developed. The values for the transmission lines, generators, wind power plants, loads, DC cables, two-phase transformers, three-phase transformers, capacitor and inductor banks were taken from the PSS/E software. In this software a synthetic European electrical network is modelled. Afterwards, they were converted to their proper representations in the RTDS software. Then, the correct initialisation of the dynamic components and the implementation of a three-phase fault were performed. In order to build only the 380 kV transmission lines existing in the Randstad region, the previous work was used as a reference. Therefore, the name of the buses, the configuration of the 380 kV network and the connection of the wind power plants were known beforehand. Since the objective of the present work is to create a methodology to discover the harmonic frequencies of the network, only the transmission lines and underground cables were taken into account in the model.

There are also useful methods to analyse the stability of power systems that are based on power electronics such as the impedance and eigenvalue-based methods [10]. In the impedance-based method the system is analysed through the frequency domain Nyquist criterion and the system is separated into the impedance of the source and the load. The source subsystem is modelled by its Thevenin equivalent circuit and the load subsystem is modelled by its input impedance. Then, the stability of the system is performed based on the source-load impedance ratio [11]. Nevertheless, the vulnerability of this method is the limited observability of certain states due to its dependence on the description of the source and load subsystems. Therefore, it is necessary to investigate the stability of the system in all the source and load subsystems that the system has, due to the fact that this method only assess single-input single-output systems. One way to overcome this vulnerability is to implement the method in the critical locations of the system. Those locations can be selected where a passive component or a controller gain could affect the stability of the system. By stability meaning that the the system must produce a bounded output for a given bounded input [12].

The eigenvalue-based method is a global stability analysis method that determines the stability of the system regardless of the location of the source of instability. Such as in [13], where it is used to identify the harmonic-frequency oscillation modes of a distributed generation inverter. However, this method requires a detailed modelling of the system under study in a state-space point of view. Moreover, the eigenvalues are only suitable for the study of single-input single-output systems. In a multiple-input multiple-output system they are a poor measure for the stability of the system [14].

The harmonic resonance is certainly one of the most important consequences of harmonics in the power systems. The cause of harmonic resonance is well understood in electrical engineering. Nevertheless, the tools to analyse this phenomena are limited. One of the most used methods to identify the resonance frequencies of a power system is the frequency scan [15]. The harmonic resonance is caused by the energy exchange between the capacitive and the inductive elements in the power system [16]. Due to the fact that a power system has numerous elements of this type it is necessary to develop a method that takes into account both types of elements as well as the system inputs, either voltages or currents injections, and the system outputs, such as voltages.

One method to analyse multiple-input multiple-output systems is the singular value decomposition. It has been recently used in [17] in order to size the voltage-droop gain of a Multi-Terminal HVDC (MTDC) system considering the AC and the DC system dynamics. In the latter work, the converters were modelled as current injectors and the DC lines by standard PI sections. Furthermore, in [18] the authors improved the work in [17] by adding the dynamics of the DC grid converter control loops and computing again the voltage-droop gain.

In the study performed by [19], the authors used the SVD mathematical tool to minimise the impact of the disturbances in the AC side via the optimisation of the DC voltage droop settings in a multiterminal VSC-HVDC.

In [20] the SVD is used to size the voltage-droop parameter of the VSCs of an MTDC system and to asses the impact of four DC cable models on the response of the MTDC system.

The SVD has been used in many studies to asses the response of different transmission

power systems that are MIMO systems by nature. Nevertheless, a methodology to study the harmonics of a power system modelled as a MIMO system has not been developed. The classical methods addressed earlier in this section only take into account one current or voltage injection and only depict one output in the system. However, the physical power systems have many voltages and current injections and many voltage outputs, e.g. voltage outputs. Thus, a methodology that can address the system in a multiple-input multiple-output point of view is necessary.

1.2. Project scope and research questions

Based on the previous sections, the main goal of the present work has been defined and analysed in two research questions.

The objective of the present work is to develop an analytic method that can be used with a MIMO representation of the power system. It also has to asses the way the current injections by different power electronic interfaced generators impact the harmonic performances observed in different buses of an electrical power system.

Thus, two research questions have been formulated to address this objective,

1. How to derive a model of an electrical transmission power system to asses the harmonic response by considering a multiple-input multiple-output point of view?

2. How to analytically determine the influence of harmonic voltage injections on the harmonic performance observed in different buses of an electrical transmission power system?

1.3. Research methodology

To comply with the research questions of the present work, the next steps are proposed,

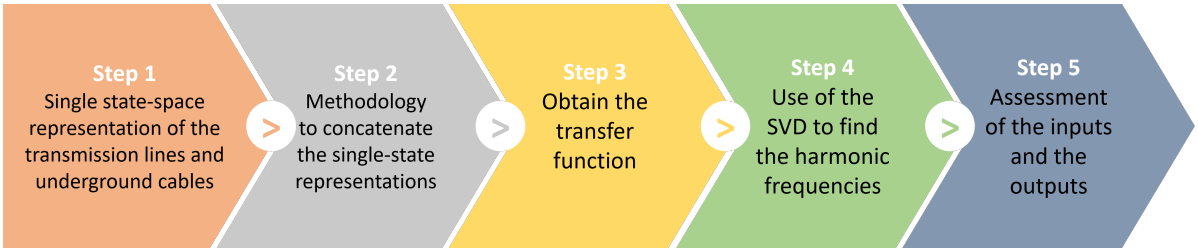

Figure 1.1: Steps followed in the present work

In order to explain in a simpler way the steps of Figure 1.1 are going to be performed to a *small size test system* in the next chapters. Afterwards, they will be applied to the synthetic Randstad transmission power system.

1.4. Project contributions

According to the scientific gap addressed earlier, the project contributions are summarised as follows,

- Two state-space representations for depicting the dynamics of the elements in the power system. The first one, to represent a transmission line and the second, to represent an underground cable.
- A methodology to concatenate each state-space representation of the elements in the power system. This methodology is necessary to represent a power system in a multiple-input multiple-output point of view.
- The necessary steps to obtain the transfer function matrix of the previous state-space representation of power system. This step is crucial to study the MIMO system with the singular value decomposition.
- A singular-value-decomposition-based method that asses the analytical relationship between harmonic voltage injections and the change of the frequency content in the global transfer function.

1.5. Thesis outline

The thesis is organised as follows, Chapter 2 presents the modelling in state-space representation of the transmission lines and underground cables that are going to be used throughout this work. This chapter also addresses the *small size test system* which is going to be useful when explaining the theory developed in each chapter.

Chapter 3 presents the steps of the methodology to concatenate linear time invariant systems represented by state-space models. At the end of this chapter can be seen how this methodology works using the *small size test system*.

In Chapter 4 the theory for the singular value decomposition is addressed, followed by a geometric explanation to have a better understating of how this mathematical tool works. Again, the *small size test system* is going to be used in order to explain their benefits.

In Chapter 5 the Randstad region is studied following the theory developed in the previous chapters. Finally, the conclusions of the present work and future research recommendations are addressed in Chapter 6.

2

Modelling approach

In this chapter is presented how the electrical passive elements of the transmission lines and underground cables were obtained. Then, it is explained in detail the derivation of the differential equations involving the dynamics of both elements and further, it is obtained the two state-space models. At the end of the chapter, the *small size test system* is introduced and it is showed numerically the single state-space representation of its elements.

2.1. Transmission power system in PSS/E

The existent Dutch electrical grid, can be consulted in detail in the map available in [21]. In this map can be observed the voltage levels of the transmission lines and substations as well as the power stations all over the Netherlands. It has also the advantage that it indicates the names of the cities where these components lie.

In the PSS/E software a synthetic European electrical grid has been developed. However, it is not visible at first sight and further steps need to be implemented to discover the required area of study. In order to achieve the latter, it is necessary to look for the *Network Data* folder located under the *Network Tree View* in the main window of PSS/E. Then, under the *Bus* folder it is necessary to locate the number of the bus. Next, right click on the selected bus and then click on *Draw*. The software will locate the bus in the *Single Line Diagram*. When the user draw two buses that are connected between them, the transmission line connecting both buses will appear automatically.

Once the 380kV buses and transmission lines are drawn in the PSS/E *Single Line Diagram*, the data of each transmission line can be read by making double click on the selected line. A window called *Branch Data Record* will appear on the screen. This window looks similar to Figure 2.1. Important data can be obtained from the *Branch Data Record*:

- The values of the resistance R, impedance X and charging B of the line.
- The names and numbers of the buses the transmission line is connected.
- The length of the line.
- The base power of the line.

It is important to point out that the *Charging* of the line is equal to the susceptance, which is the imaginary part of the admittance,

$$Y = G + jB$$

where,

Y is the admittance in Siemens [S].
G is the conductance in Siemens [S].
B is the susceptance in Siemens [S].

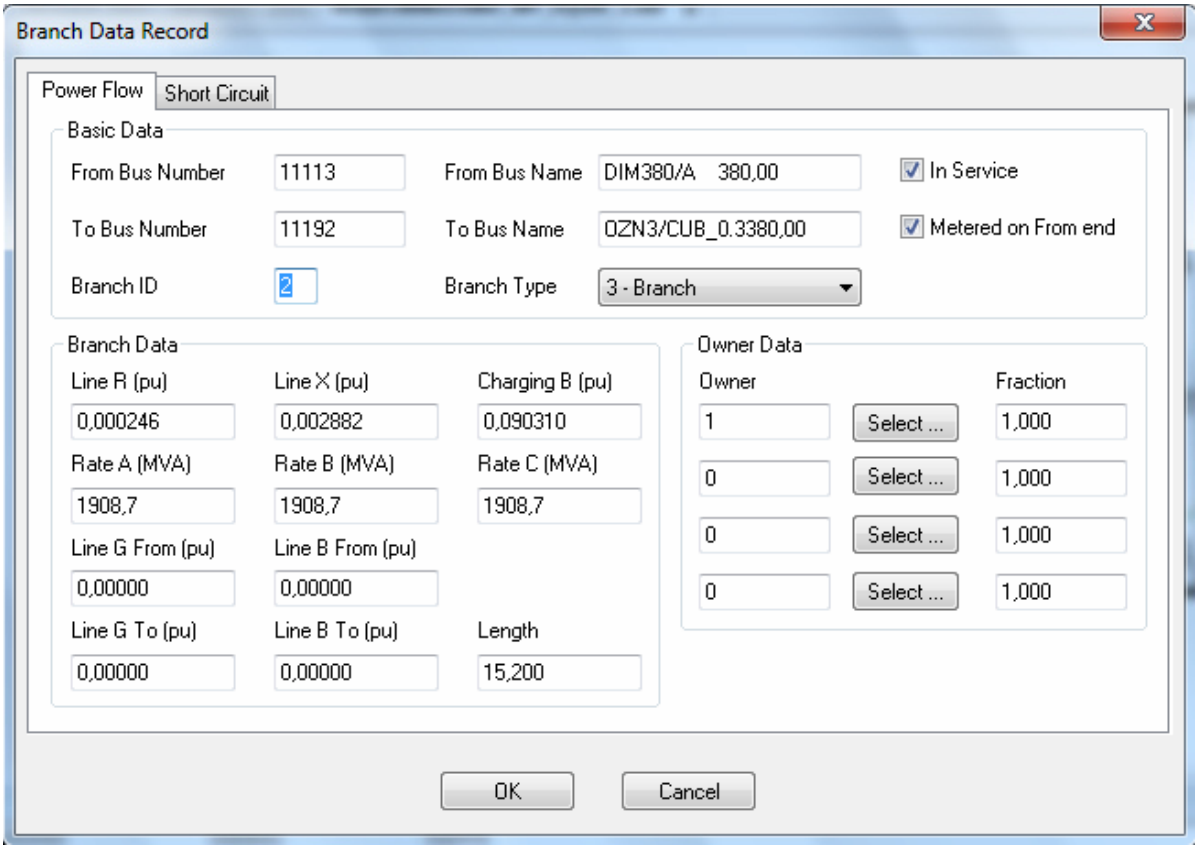

Figure 2.1: *Branch Data Record* in PSS/E

2.2. Transmission line electric values extraction

In order to obtain the values of the resistances, capacitances and inductances of each transmission line of the area of study, it is important to know how PSS/E handles the data for the transmission lines. According to [22, 23] these values can be obtained in agreement with the following equation,

$$Z_{base_i} = \frac{V_{base_i}^2}{S_{base_i}} \tag{2.1}$$

where,

V_{base} is the specified line-to-line voltage in kV.

S_{base} is the rated apparent power of the line in MVA.

For our research the voltage is going to be 380 kV for all transmission lines. The subscript ***i*** indicates one of the transmission lines existing in the area of study.

In order to calculate the impedance of the line it is necessary to extract the values in *p.u.* of the resistance, reactance and susceptance of the line. These values can be found following the steps established in Section 2.1. Then, by using the next equation,

$$Z_i = \frac{(R_i + jX_i)}{l_i} Z_{base_i} \quad \left[\frac{\Omega}{km}\right] \tag{2.2}$$

It can be obtained the resistance of the line, which is going to be the real part of the impedance, and the inductance, which is the imaginary part of the impedance.

$$\begin{aligned} R_i &= Real\{Z_i\} \quad \left[\frac{\Omega}{km}\right] \\ L_i &= Imaginary\{Z_i\} \quad \left[\frac{H}{km}\right] \end{aligned} \tag{2.3}$$

In order to find the capacitance of the line it is necessary to take the *Charge* value,

$$C_{line_i} = \frac{B}{l_i} Z_{base_i} \quad \left[\frac{F}{km}\right] \tag{2.4}$$

Finally, it is important to notice that PSS/E takes the parameter *Charge* as the whole charge of the line. Therefore, it is necessary to divide the capacitance in 2.4 by two to obtain the value of each capacitance.

$$C_i = \frac{C_{line_i}}{2} \quad \left[\frac{F}{km}\right] \tag{2.5}$$

2.3. Transmission line and cable state-space modelling

In PSS/E the modelling approach of the elements that send and receive the power in an electrical power system are represented only by transmission lines. However, as stated earlier in this chapter, the underground cables are also going to be taken into account in the transmission power system. Therefore, in this thesis two different state-space representations are used. One to depict the dynamics of the transmission lines and another to represent the underground cables.

2.3.1. Transmission line modelling

The first model is a typical PI section which is going to be used to represent a transmission line, as can be seen in Figure 2.2.

The first step to express a transmission line in a state-space representation is to obtain the differential equations for the voltage of the capacitors and the current of the inductor.

Using Kirchhoff law, the equation of the first loop of Figure 2.2 can be written as,

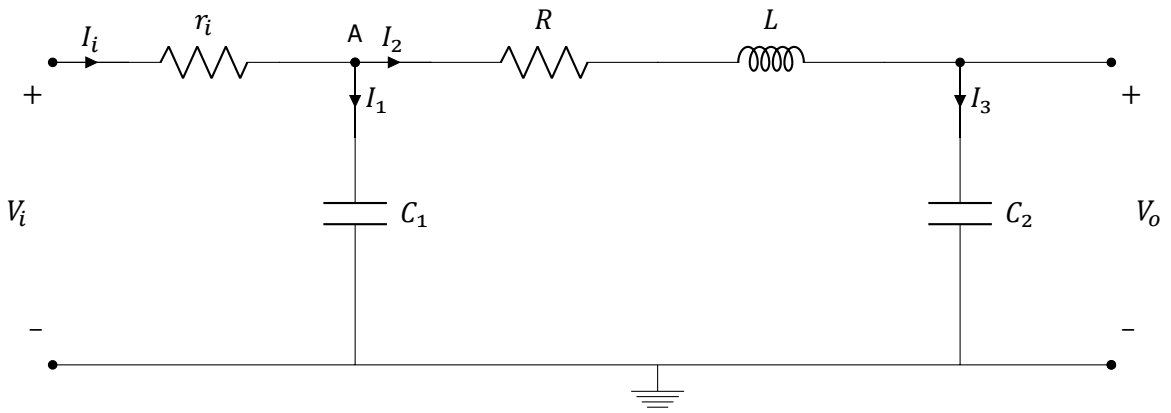

Figure 2.2: PI section

$$V_i = r_i I_i + V_{C_1} \tag{2.6}$$

At node **A** the sum of the currents is,

$$I_i = I_1 + I_2 \tag{2.7}$$

It can be seen in Figure 2.2 that $\boldsymbol{I_1 = i_{C_1}}$ and $\boldsymbol{I_2 = i_L}$. Therefore, 2.7 becomes,

$$I_i = i_{C_1} + i_L \tag{2.8}$$

Substituting 2.8 in 2.6 yields,

$$V_i = r_i i_{C_1} + r_i i_L + V_{C_1} \tag{2.9}$$

From the equation of the current of a capacitor $\boldsymbol{i_C = C\frac{dV}{dt}}$, 2.9 becomes,

$$\frac{dV_{C_1}}{dt} = -\frac{1}{C_1} i_L - \frac{1}{r_i C_1} V_{C_1} + \frac{1}{r_i C_1} V_i \tag{2.10}$$

Using again Kirchhoff law, the equation of the second loop of Figure 2.2 can be written as,

$$V_{C_1} - R i_L - V_L - V_{C_2} = 0 \tag{2.11}$$

From the equation of the voltage of an inductor $\boldsymbol{V_L = L\frac{di}{dt}}$, 2.11 becomes,

$$\frac{di_L}{dt} = -\frac{R}{L} i_L + \frac{1}{L} V_{C_1} - \frac{1}{L} V_{C_2} \tag{2.12}$$

The current that goes through the second capacitor is,

$$i_{C_2} = C_2 \frac{dV_{C_2}}{dt} \tag{2.13}$$

So, from Figure 2.2 it can be observed that $i_L = i_{C_2}$. Therefore, 2.13 becomes,

$$\frac{dV_{C_2}}{dt} = \frac{1}{C_2} i_L \tag{2.14}$$

Finally, it can be observed that,

$$V_{C_2} = V_o \tag{2.15}$$

The second step is to chose the states of the system as the elements that store energy in the system. In this case, the current of the inductor i_L, and the voltages of both capacitors V_{C_1} and V_{C_2} are going to be chosen as the state variables. Thus, the state-space vector becomes,

$$x = \begin{bmatrix} i_L \\ V_{C_1} \\ V_{C_2} \end{bmatrix} \tag{2.16}$$

And the input and the output of the PI section are going to be the voltages,

$$u = V_i \tag{2.17}$$

$$y = V_o \tag{2.18}$$

Hence equations 2.10, 2.12, 2.14 and 2.15 become,

$$\dot{x}_1 = -\frac{R}{L} x_1 + \frac{1}{L} x_2 - \frac{1}{L} x_3 \tag{2.19}$$

$$\dot{x}_2 = -\frac{1}{C_1} x_1 - \frac{1}{r_i C_1} x_2 + \frac{1}{r_i C_1} u \tag{2.20}$$

$$\dot{x}_3 = \frac{1}{C_2} x_1 \tag{2.21}$$

$$y = x_3 \tag{2.22}$$

Finally, the state-space representation for the transmission line is,

$$\dot{x} = \underbrace{\begin{bmatrix} -\frac{R_i}{L_p} & \frac{1}{L_p} & -\frac{1}{L_p} \\ -\frac{1}{C_{1_p}} & -\frac{1}{r_{i_p} C_{1_p}} & 0 \\ \frac{1}{C_{2_p}} & 0 & 0 \end{bmatrix}}_{A_p} x + \underbrace{\begin{bmatrix} 0 \\ \frac{1}{r_{i_p} C_{1_p}} \\ 0 \end{bmatrix}}_{B_p} u \tag{2.23}$$

$$y = \underbrace{\begin{bmatrix} 0 & 0 & 1 \end{bmatrix}}_{C_p} x + \underbrace{\begin{bmatrix} 0 \end{bmatrix}}_{D_p} u$$

Where *p* can be any of the transmission lines in the transmission power system.

It can be seen from 2.23 that each transmission line will have tree states and one input and one output,

$$x \in \mathbb{R}^{3\times1}, \qquad u \in \mathbb{R}^{1\times1}, \qquad y \in \mathbb{R}^{1\times1}$$

Thus, this is a SISO (Single-Input Single-Output) system.

The state-space matrices have the following dimensions:

$$A_p \in \mathbb{R}^{3\times3}, \qquad B_p \in \mathbb{R}^{3\times1}, \qquad C_p \in \mathbb{R}^{1\times3}, \qquad D_p \in \mathbb{R}^{1\times1}$$

2.3.2. Underground cable modelling

The second model is a "fitted PI". This model is basically a PI section with more branches in parallel [24], as it can be seen in Figure 2.3. The elements of the parallel branches have been computed using a fitting algorithm to meet the frequency response of the frequency-dependent elements of a wide-band cable [25].

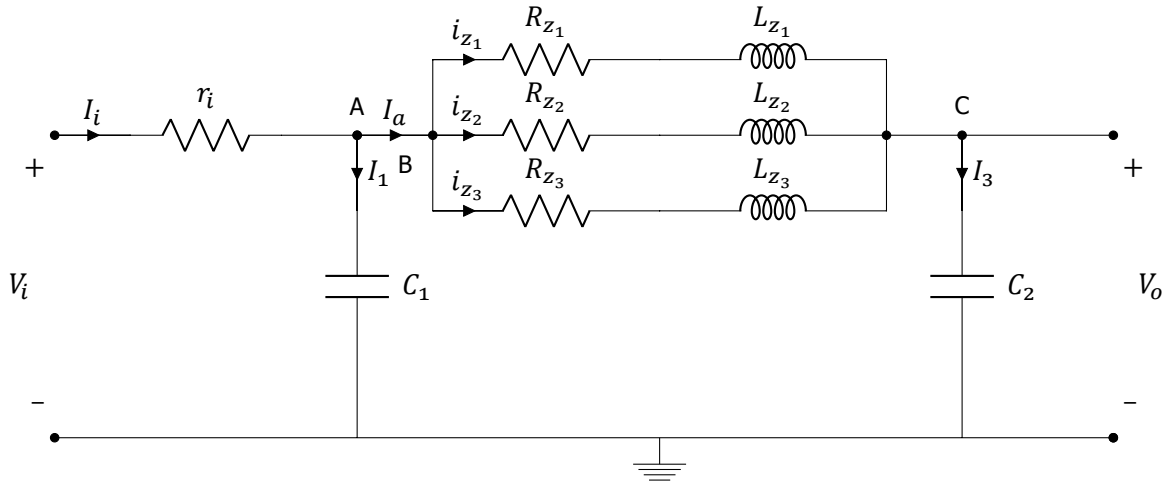

Figure 2.3: Fitted PI

Using Kirchhoff law, the equation of the first loop of Figure 2.3 can be written as,

$$V_i = r_i I_i + V_{C_1} \tag{2.24}$$

At node **A** the sum of the currents is,

$$I_i = I_1 + I_a \tag{2.25}$$

And at node **B** the sum of the currents is,

$$I_a = i_{z_1} + i_{z_2} + i_{z_3} \tag{2.26}$$

Substituting 2.26 in 2.25 yields,

$$I_i = i_{C_1} + i_{z_1} + i_{z_2} + i_{z_3} \tag{2.27}$$

From the equation of the current of a capacitor $i_C = C\frac{dV}{dt}$, 2.27 becomes,

$$I_i = C_1\frac{dV_{C_1}}{dt} + i_{z_1} + i_{z_2} + i_{z_3} \tag{2.28}$$

Substituting 2.28 in 2.24 yields,

$$\frac{dV_{C_1}}{dt} = \frac{1}{r_i C_1}[V_i - r_i i_{z_1} - r_i i_{z_2} - r_i i_{z_3} - V_{C_1}] \tag{2.29}$$

Using again Kirchhoff law, the equation of the second loop of Figure 2.5 can be written as,

$$V_{C_1} - V_{BC} - V_{C_2} = 0 \tag{2.30}$$

Since, the three branches of the ”fitted PI” representation are in parallel it is necessary to study the voltages at each branch separately. Therefore, from top to bottom the first voltage equation can be written as,

$$V_{C_1} - L_{z_1}\frac{di_{z_1}}{dt} - R_{z_1} i_{z_1} - V_{C_2} = 0 \tag{2.31}$$

Solving for $\frac{di_{z_1}}{dt}$, equation 2.31 becomes,

$$\frac{di_{z_1}}{dt} = \frac{1}{L_{z_1}}[V_{C_1} - R_{z_1} i_{z_1} - V_{C_2}] \tag{2.32}$$

Subsequently, for the second and third branch the voltage equations can be written as,

$$\frac{di_{z_2}}{dt} = \frac{1}{L_{z_2}}[V_{C_1} - R_{z_2} i_{z_2} - V_{C_2}] \tag{2.33}$$

$$\frac{di_{z_3}}{dt} = \frac{1}{L_{z_3}}[V_{C_1} - R_{z_3} i_{z_3} - V_{C_2}] \tag{2.34}$$

The current that goes through the second capacitor is,

$$i_{C_2} = C_2\frac{dV_{C_2}}{dt} \tag{2.35}$$

So, from Figure 2.3 it can be observed that $I_a = i_{C_2}$. Therefore, 2.35 becomes,

$$\frac{dV_{C_2}}{dt} = \frac{1}{C_2}[i_{z_1} + i_{z_2} + i_{z_3}] \tag{2.36}$$

Finally, it can be observed that,

$$V_{C_2} = V_o \tag{2.37}$$

Next, by choosing the states of the system as the elements that store energy in the system the state-space vector becomes,

$$x = \begin{bmatrix} i_{z_1} \\ i_{z_2} \\ i_{z_3} \\ V_{C_1} \\ V_{C_2} \end{bmatrix} \tag{2.38}$$

And the input and the output of the PI section are going to be the voltages,

$$u = V_i \tag{2.39}$$

$$y = V_o \tag{2.40}$$

Hence equations 2.29, 2.32, 2.33, 2.34, 2.36 and 2.37 become,

$$\dot{x}_1 = -\frac{R_{z_1}}{L_{z_1}}x_1 + \frac{1}{L_{z_1}}x_4 - \frac{1}{L_{z_1}}x_5 \tag{2.41}$$

$$\dot{x}_2 = -\frac{R_{z_2}}{L_{z_2}}x_2 + \frac{1}{L_{z_2}}x_4 - \frac{1}{L_{z_2}}x_5 \tag{2.42}$$

$$\dot{x}_3 = -\frac{R_{z_3}}{L_{z_3}}x_3 + \frac{1}{L_{z_3}}x_4 - \frac{1}{L_{z_3}}x_5 \tag{2.43}$$

$$\dot{x}_4 = -\frac{1}{C_1}x_1 - \frac{1}{C_1}x_2 - \frac{1}{C_1}x_3 - \frac{1}{r_i C_1}x_4 + \frac{1}{r_i C_1}u \tag{2.44}$$

$$\dot{x}_5 = \frac{1}{C_2}x_1 + \frac{1}{C_2}x_2 + \frac{1}{C_2}x_3 \tag{2.45}$$

$$y = x_5 \tag{2.46}$$

Finally, the state-space representation for the underground cable is,

$$\dot{x} = \underbrace{\begin{bmatrix} -\frac{R_{z_1}}{L_{z_1}} & 0 & 0 & \frac{1}{L_{z_1}} & -\frac{1}{L_{z_1}} \\ 0 & -\frac{R_{z_2}}{L_{z_2}} & 0 & \frac{1}{L_{z_2}} & -\frac{1}{L_{z_2}} \\ 0 & 0 & -\frac{R_{z_3}}{L_{z_3}} & \frac{1}{L_{z_3}} & -\frac{1}{L_{z_3}} \\ -\frac{1}{C_1} & -\frac{1}{C_1} & -\frac{1}{C_1} & -\frac{1}{r_i C_1} & 0 \\ \frac{1}{C_2} & \frac{1}{C_2} & \frac{1}{C_2} & 0 & 0 \end{bmatrix}}_{A_q} x + \underbrace{\begin{bmatrix} 0 \\ 0 \\ 0 \\ \frac{1}{r_i C_1} \\ 0 \end{bmatrix}}_{B_q} u \tag{2.47}$$

$$y = \underbrace{\begin{bmatrix} 0 & 0 & 0 & 0 & 1 \end{bmatrix}}_{C_q} x + \underbrace{\begin{bmatrix} 0 \end{bmatrix}}_{D_q} u$$

Where q can be any of the underground cable in the transmission power system.

It can be seen from 2.47 that each underground cable will have five states and one input and one output,

$$x \in \mathbb{R}^{5\times 1}, \qquad u \in \mathbb{R}^{1\times 1}, \qquad y \in \mathbb{R}^{1\times 1}$$

Thus, this is also a SISO (Single-Input Single-Output) system.

The state-space matrices have the following dimensions:

$$A_q \in \mathbb{R}^{5\times 5}, \qquad B_q \in \mathbb{R}^{5\times 1}, \qquad C_q \in \mathbb{R}^{1\times 5}, \qquad D_q \in \mathbb{R}^{1\times 1}$$

2.4. Introduction to the *small size test system*

As stated earlier in this chapter, a transmission power system is going to be developed with the theory previously derived. For that matter, the system of Figure 2.4 is presented. It can be noticed that there are two wind parks connected to two transmission lines, ***L1*** and ***L2***. Then, both lines are connected to an underground cable ***C1***. Finally, ***C1*** is connected to an external grid. The inputs of the three systems, u_1, u_2 and u_3, are voltage inputs and the outputs, y_1, y_2 and y_3 are voltage outputs.

2.5. SISO state-space representations of the *small size test system*

Following the research methodology of Figure 1.1, first is necessary to obtain the SISO state-space representations of the elements in the system.

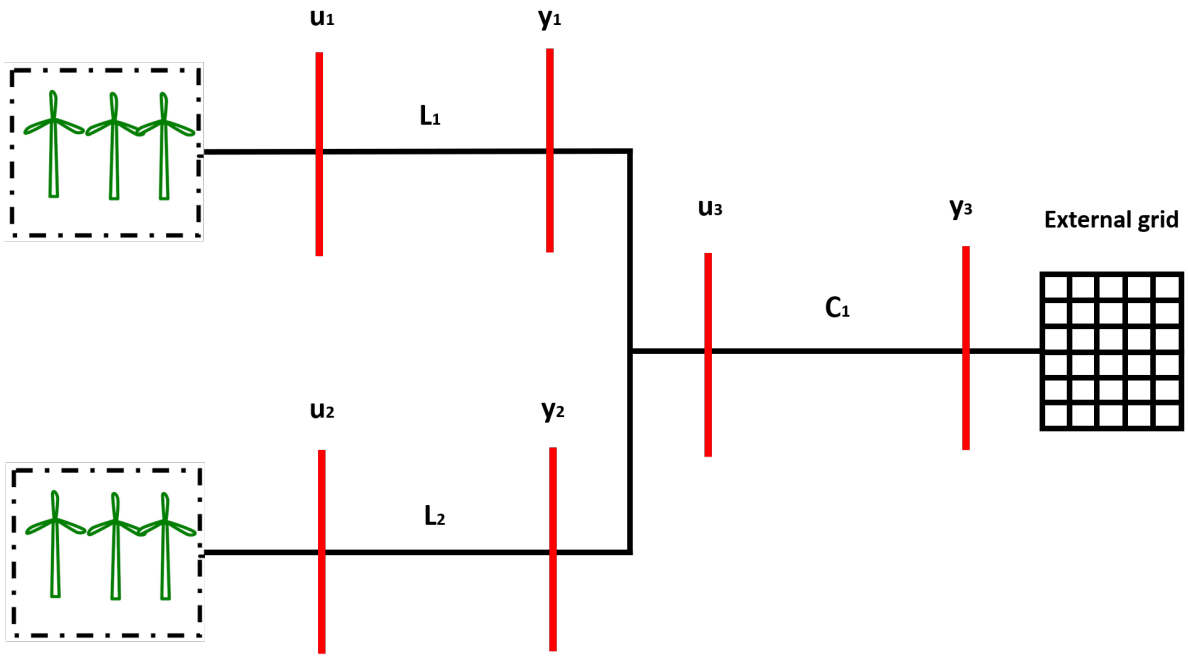

Figure 2.4: *Small size test system*

The electrical parameters for the transmission lines **L1** and **L2** are shown in Table 2.1. These parameters were extracted from the PSS/E software following the steps in Section 2.2, where two 380kV transmission lines existing in the Dutch electrical network were chosen.

Table 2.1: *Small size test system*. Transmission lines parameters

From	To	Length [km]	R [Ω/km]	L [H/km]	$C_1 = C_2$ [μF/km]
u_1	y_1	15.9	0.0012	0.0143	39.26
u_2	y_2	12.1	0.0010	0.0130	135.34

The parameters in Table 2.1 can be used to represent the transmission lines ***L1*** and ***L2*** in a state-space model, as it can be seen in 2.48 and 2.49 respectively.

$$\dot{x}_1 = \begin{bmatrix} -0.08 & 4.38 & -4.38 \\ -1.60 \times 10^3 & -1.60 \times 10^6 & 0 \\ 1.60 \times 10^3 & 0 & 0 \end{bmatrix} x_1 + \begin{bmatrix} 0 \\ 1.60 \times 10^6 \\ 0 \end{bmatrix} u_1 \tag{2.48}$$

$$y_1 = \begin{bmatrix} 0 & 0 & 1 \end{bmatrix} x_1$$

$$\dot{x}_2 = \begin{bmatrix} -0.07 & 6.35 & -6.35 \\ -610.63 & -610.63 \times 10^3 & 0 \\ 610.63 \times 10^3 & 0 & 0 \end{bmatrix} x_2 + \begin{bmatrix} 0 \\ 610.63 \times 10^3 \\ 0 \end{bmatrix} u_2 \tag{2.49}$$

$$y_2 = \begin{bmatrix} 0 & 0 & 1 \end{bmatrix} x_2$$

For the underground cable state-space representation, the parameters were taken from [20] and they can be seen in Tables 2.2 and 2.3.

Table 2.2: *Small size test system*. Underground cable parameters (1)

From	To	Length [km]	R_{z_1} [Ω/km]	R_{z_2} [Ω/km]	R_{z_3} [Ω/km]
u_3	y_3	50	0.11724	0.082072	0.011946

Table 2.3: *Small size test system*. Underground cable parameters (2)

L_{z_1} [mH/km]	L_{z_2} [mH/km]	L_{z_3} [mH/km]	$C_1 = C_2$ [μF/km]
0.22851	1.5522	3.2942	0.19083

With these parameters, the state-space representation for the cable **C1** can be seen in 2.50.

$$\dot{x}_3 = \begin{bmatrix} -513.06 & 0 & 0 & 89.85 & -89.85 \\ 0 & -52.87 & 0 & 13.22 & -13.22 \\ 0 & 0 & 3.62 & 6.23 & -6.23 \\ -107.60 \times 10^3 & -107.60 \times 10^3 & -107.60 \times 10^3 & -107.60 \times 10^6 & 0 \\ 107.60 \times 10^3 & 107.60 \times 10^3 & 107.60 \times 10^3 & 0 & 0 \end{bmatrix} x_3 + \begin{bmatrix} 0 \\ 0 \\ 0 \\ 107.60 \times 10^6 \\ 0 \end{bmatrix} u_3 \tag{2.50}$$

$$y_3 = \begin{bmatrix} 0 & 0 & 0 & 0 & 1 \end{bmatrix} x_3$$

Equations 2.48 to 2.50 represent the SISO state-space representations for the elements in the *small size test system*. However, this power system is a MIMO system. It has two voltage inputs, u_1 and u_2, and three voltage outputs y_1, y_2 and y_3. Therefore, in the next chapter the methodology used to concatenate several linear time invariant systems such as the ones in this example is developed.

3

Multiple-input multiple-output state-space representation

In the present chapter the concatenation of single (SISO) state-space representations is addressed. The objective of this chapter is to develop a MIMO linear time invariant system that depicts the dynamics of an entire transmission power system. At the end of this chapter the theory is applied to the *small size test system* to have a better overview of how this methodology works.

3.1. Concatenation of Linear Time Invariant (LTI) models

For the sake of explaining the theoretical state-space association, two independent (LTI) models are going to be considered [26]. Both of these systems are depicted in the state-space form. As can be seen in 3.1 and 3.2 these systems are linked by an input and an output relationship.

$$\begin{aligned} \dot{x}_1 &= A_1 x_1 + B_1 u_1 \\ y_1 &= C_1 x_1 + D_1 u_1 \end{aligned} \tag{3.1}$$

$$\begin{aligned} \dot{x}_2 &= A_2 x_2 + B_2 u_2 \\ y_2 &= C_2 x_2 + D_2 u_2 \end{aligned} \tag{3.2}$$

The LTI model with subscript **1** has the next characteristics:

- n_1 states that integrate the vector $\boldsymbol{x_1}$.
- m_1 inputs that are part of the vector $\boldsymbol{u_1}$.
- p_1 outputs forming the vector $\boldsymbol{y_1}$.

In the same way, the LTI model with subscript **2**, has:

- n_2 states that integrate the vector $\boldsymbol{x_2}$.
- m_2 inputs that are part of the vector $\boldsymbol{u_2}$.
- p_2 outputs forming the vector $\boldsymbol{y_2}$.

As for their matrices, the LTI model with subscript **1** has:

- A state-space matrix $\boldsymbol{A_1}$ with dimension $n_1 \times n_1$.
- A $n_1 \times m_1$ matrix $\boldsymbol{B_1}$.
- A $p_1 \times n_1$ matrix $\boldsymbol{C_1}$.
- A $p_1 \times m_1$ matrix $\boldsymbol{D_1}$.

In a similar fashion, the matrices in the LTI model with subscript **2** has:

- A state-space matrix $\boldsymbol{A_2}$ with dimension $n_2 \times n_2$.
- A $n_2 \times m_2$ matrix $\boldsymbol{B_2}$
- A $p_2 \times n_2$ matrix $\boldsymbol{C_2}$
- A $p_2 \times m_2$ matrix $\boldsymbol{D_2}$.

Once the components of both systems have been explained, the next steps need to be followed in order to achieve the concatenation of the systems:

Step 1. A sort of ***stack*** is going to be considered for both systems represented by the state-space representation without taking into consideration any feedback between the inputs and the outputs among the systems. This new state-space representation will be called ***open loop***. Therefore, it will have the subscript ***ol***,

$$\begin{aligned} \dot{X}_{ol} &= A_{ol}X_{ol} + B_{ol}U_{ol} \\ Y_{ol} &= C_{ol}X_{ol} + D_{ol}U_{ol} \end{aligned} \tag{3.3}$$

The elements of the state vector, the input vector and the output vector are,

$$X_{ol} = \begin{bmatrix} x_1 \\ x_2 \end{bmatrix} \in \mathbb{R}^{(n_1+n_2)\times 1}, \quad U_{ol} = \begin{bmatrix} u_1 \\ u_2 \end{bmatrix} \in \mathbb{R}^{(m_1+m_2)\times 1}, \quad Y_{ol} = \begin{bmatrix} y_1 \\ y_2 \end{bmatrix} \in \mathbb{R}^{(p_1+p_2)\times 1}$$

The matrices are build as,

$$A_{ol} = \begin{bmatrix} A_1 & 0 \\ 0 & A_2 \end{bmatrix} \in \mathbb{R}^{(n_1+n_2)\times(n_1+n_2)}, \qquad B_{ol} = \begin{bmatrix} B_1 & 0 \\ 0 & B_2 \end{bmatrix} \in \mathbb{R}^{(n_1+n_2)\times(m_1+m_2)},$$
$$C_{ol} = \begin{bmatrix} C_1 & 0 \\ 0 & C_2 \end{bmatrix} \in \mathbb{R}^{(p_1+p_2)\times(n_1+n_2)}, \qquad D_{ol} = \begin{bmatrix} D_1 & 0 \\ 0 & D_2 \end{bmatrix} \in \mathbb{R}^{(p_1+p_2)\times(m_1+m_2)}$$

The graphical representation of this step can be seen in Figure 3.1

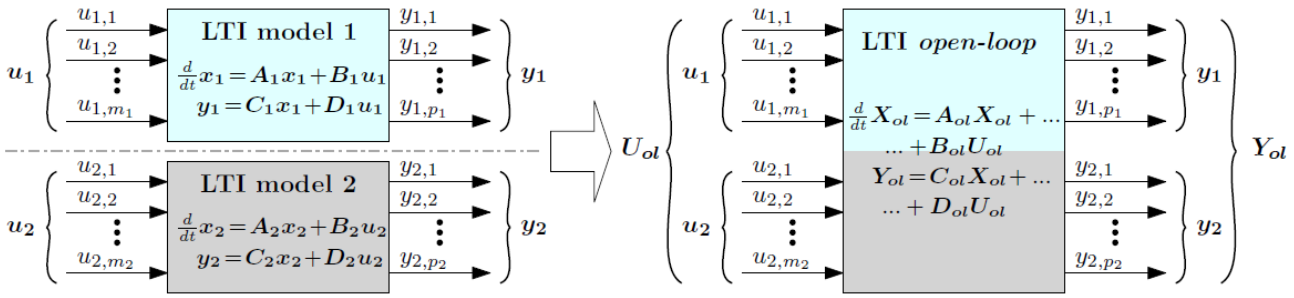

Figure 3.1: Step 1, LTI concatenation [1]

Step 2. In this step is going to be assumed that some of the inputs of the system are connected to some of the outputs. The latter are going to be considered as ***internal inputs*** and will be associated with the matrix U_{int}. The inputs that are not going to be connected to any output are going to be called ***external inputs*** and will be associated with the matrix U_{ext}. The new input vector will be formed as shown in 3.4. This new state-space representation will be called ***closed loop***. Therefore, it will have the subscript ***cl***. The graphical representation of this step can be seen in Figure 3.2.

$$U'_{ol} = U_{int} + U_{ext} \tag{3.4}$$

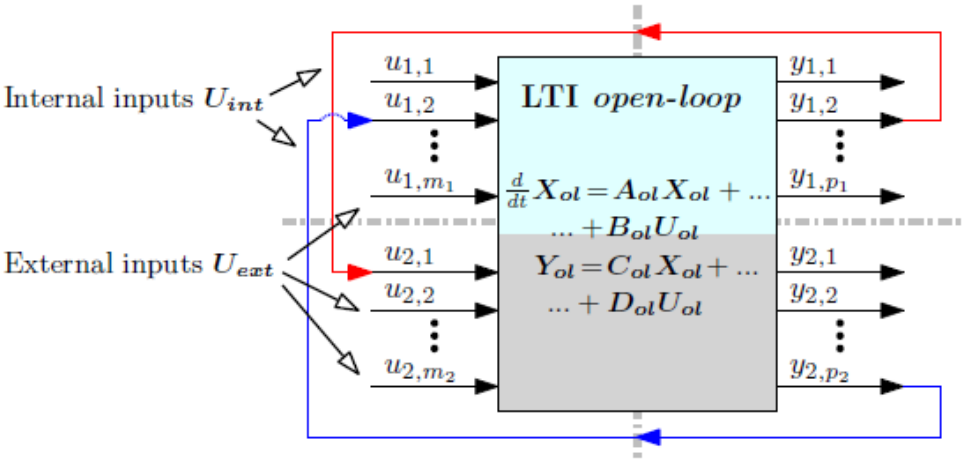

Figure 3.2: Step 2, LTI concatenation [1]

The matrices U_{int} and U_{ext} are given by,

$$U_{int} = M_{int}Y_{ol}, \qquad U_{ext} = M_{ext}U_{ol}$$

On one hand, the matrix M_{int} is known as the ***interconnection matrix*** and relates some outputs of the ***open-loop*** LTI model Y_{ol} which are linked internally to some outputs. On the other hand, the matrix M_{ext} relates the inputs of the ***open-loop*** LTI model U_{ol} which are not being looped back into the ***stacked*** LTI model. Therefore, 3.4 becomes,

$$U'_{ol} = M_{int}Y_{ol} + M_{ext}U_{ol} \tag{3.5}$$

Replacing 3.5 in U_{ol} of 3.4 yields,

$$\begin{aligned} \dot{X}_{ol} &= A_{ol}X_{ol} + B_{ol}(M_{int}Y_{ol} + M_{ext}U_{ol}) \\ Y_{ol} &= C_{ol}X_{ol} + D_{ol}(M_{int}Y_{ol} + M_{ext}U_{ol}) \end{aligned} \tag{3.6}$$

The system in 3.6 can be further developed. In the first line, the term containing the matrix B_{ol} can be expanded. And in the second line the equation can be solved for Y_{ol}, since it appears on both sides of the equation. Therefore, 3.6 can be rewritten as,

$$\begin{aligned} \dot{X}_{ol} &= A_{ol}X_{ol} + B_{ol}M_{int}Y_{ol} + B_{ol}M_{ext}U_{ol} \\ Y_{ol} &= (I - D_{ol}M_{int})^{-1}(C_{ol}X_{ol} + D_{ol}M_{ext}U_{ol}) \end{aligned} \tag{3.7}$$

For the sake of simplicity, the matrix $(I - D_{ol}M_{int})^{-1}$ will be named E_{ol} for the rest of the derivation. Thus, $E_{ol} \triangleq (I - D_{ol}M_{int})^{-1}$ and further introduced in the output equation as $Y_{ol} = E_{ol}C_{ol}X_{ol} + E_{ol}D_{ol}M_{ext}U_{ol}$. Therefore, replacing this last equation of Y_{ol} in 3.7 yields,

$$\begin{aligned} \dot{X}_{ol} &= (A_{ol} + B_{ol}M_{int}E_{ol}C_{ol})X_{ol} + (B_{ol} + B_{ol}M_{int}E_{ol}D_{ol})M_{ext}U_{ol} \\ Y_{ol} &= E_{ol}C_{ol}X_{ol} + E_{ol}D_{ol}M_{ext}U_{ol} \end{aligned} \tag{3.8}$$

Step 3. The last step consists in obtaining the ***closed-loop*** state-space representation of the LTI model from 3.8 as,

$$\begin{aligned} \dot{X}_{cl} &= A_{cl}X_{cl} + B_{cl}U_{cl} \\ Y_{cl} &= C_{cl}X_{cl} + D_{cl}U_{cl} \end{aligned} \tag{3.9}$$

And by comparison, the vectors of the ***closed-loop*** state-space in 3.9 are given by,

$$\begin{aligned} X_{cl} &= X_{ol} \\ U_{cl} &= U_{ext} = M_{ext}U_{ol} \\ Y_{cl} &= Y_{ol} \end{aligned} \tag{3.10}$$

And the matrices as,

$$\begin{aligned} A_{cl} &= A_{ol} + B_{ol}M_{int}E_{ol}C_{ol} \\ B_{cl} &= B_{ol} + B_{ol}M_{int}E_{ol}D_{ol} \\ C_{cl} &= E_{ol}C_{ol} \\ D_{cl} &= E_{ol}D_{ol} \end{aligned} \tag{3.11}$$

The graphical representation of this step can be seen in Figure 3.3. It is important to notice that the vector X_{cl} contains all the states of that integrates the closed-loop system. In the same way, the vector Y_{cl} contains all the outputs of the systems concatenated. Finally, the inputs of the new system are only the external inputs, those who were not fed back internally.

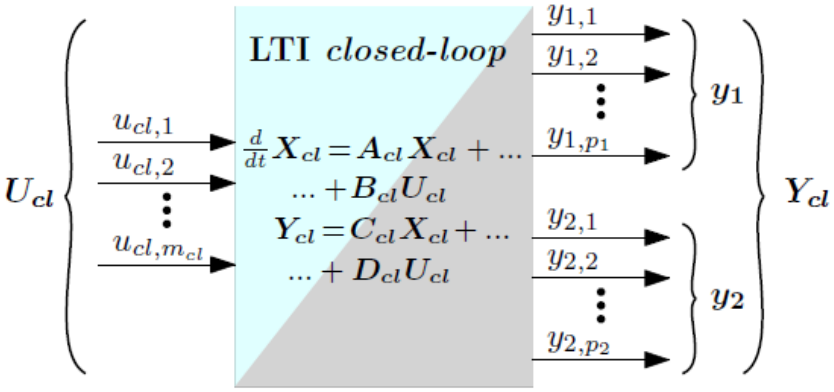

Figure 3.3: Step 3, LTI concatenation [1]

3.2. State-space concatenation of the *small size test system*

In this section the second step of the methodology presented in Figure 1.1 is going to be addressed. In order to explain the steps for the concatenation of LTI systems, the *small size test system* from Section 2.4 is going to be used.

The *small size test system* is going to be represented in a simpler manner to have a better overview of how the concatenation methodology works. In Figure 3.4 can be seen a simplified diagram of the *small size test system*. Some important points need to be discussed in detail:

- The circles represent each transmission line and underground cable state-space representation. In the Figure 3.4, three circles can be found, corresponding to each state-space representation.
- The arrow(s) that point to a certain circle are the inputs that a particular system has.
- The arrow(s) that come out of a certain circle are the outputs that a particular system has.
- The system is considered disconnected form the external grid.

First, in the **Step 1** of the methodology and based on the topology of Figure 3.4 it can be observed that the **open loop** state-space representation will have the following dimensions, where the number of systems to be concatenated is three,

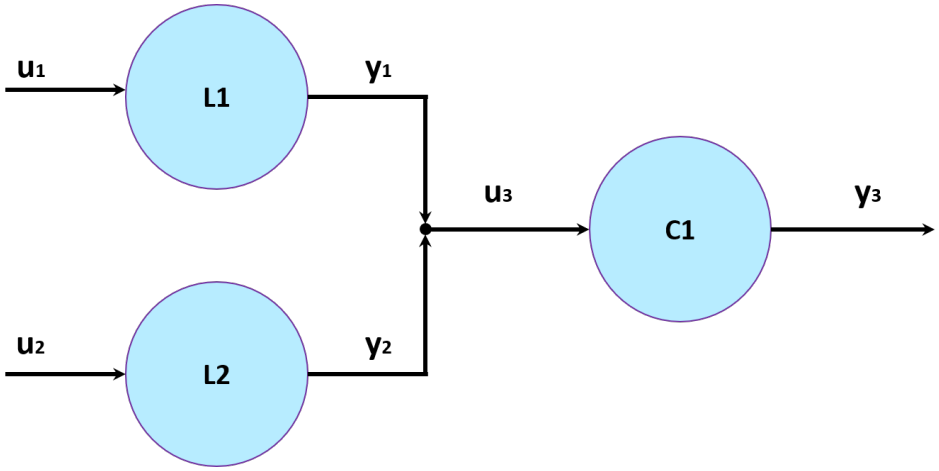

Figure 3.4: Simplified *small size test system*

$$X_{ol} = \begin{bmatrix} x_1 \\ x_2 \\ x_3 \end{bmatrix} \in \mathbb{R}^{11\times 1}, \qquad U_{ol} = \begin{bmatrix} u_1 \\ u_2 \\ u_3 \end{bmatrix} \in \mathbb{R}^{3\times 1}, \qquad Y_{ol} = \begin{bmatrix} y_1 \\ y_2 \\ y_3 \end{bmatrix} \in \mathbb{R}^{3\times 1}$$

Where the elements of the X_{ol} vector are the state-space vectors of each state-space representation. Therefore,

$$x_1 = \begin{bmatrix} i_{L_1} \\ V_{C_{1_1}} \\ V_{C_{2_1}} \end{bmatrix} \in \mathbb{R}^{3\times 1}, \qquad x_2 = \begin{bmatrix} i_{L_2} \\ V_{C_{1_2}} \\ V_{C_{2_2}} \end{bmatrix} \in \mathbb{R}^{3\times 1}, \qquad x_3 = \begin{bmatrix} i_{L_{z_1}} \\ i_{L_{z_2}} \\ i_{L_{z_3}} \\ V_{C_{1_3}} \\ V_{C_{2_3}} \end{bmatrix} \in \mathbb{R}^{5\times 1}$$

From these vectors it can be observed that two correspond to the transmission lines ***L1*** and ***L2***, and one vector corresponds to the underground cable ***C1***. The respective matrices have the next dimensions,

$$A_{ol} = \begin{bmatrix} A_1 & 0_{3\times 3} & 0_{3\times 5} \\ 0_{3\times 3} & A_2 & 0_{3\times 5} \\ 0_{5\times 3} & 0_{5\times 3} & A_3 \end{bmatrix} \in \mathbb{R}^{11\times 11}, \qquad B_{ol} = \begin{bmatrix} B_1 & 0_{3\times 1} & 0_{3\times 1} \\ 0_{3\times 1} & B_2 & 0_{3\times 1} \\ 0_{5\times 1} & 0_{5\times 1} & B_3 \end{bmatrix} \in \mathbb{R}^{11\times 3},$$

$$C_{ol} = \begin{bmatrix} C_1 & 0_{1\times 3} & 0_{1\times 5} \\ 0_{1\times 3} & C_2 & 0_{1\times 5} \\ 0_{1\times 3} & 0_{1\times 3} & C_3 \end{bmatrix} \in \mathbb{R}^{3\times 11}, \qquad D_{ol} = \begin{bmatrix} D_1 & 0_{1\times 1} & 0_{1\times 1} \\ 0_{1\times 1} & D_2 & 0_{1\times 1} \\ 0_{1\times 1} & 0_{1\times 1} & D_3 \end{bmatrix} \in \mathbb{R}^{3\times 3}$$

It is important to note that the dimensions of the matrices A_1, A_2, A_3 in the main diagonal of the matrix A_{ol} are 3×3, 3×3 and 5×5, respectively. The dimensions of the matrices B_1, B_2, B_3 in the main diagonal of the matrix B_{ol} are 3×1, 3×1 and 5×1, respectively. The dimensions of the matrices C_1, C_2, C_3 in the main diagonal of the matrix C_{ol} are 1×3, 1×3

and 1×5, respectively. Finally, the matrices D_1, D_2 and D_3 in the main diagonal of the matrix D_{ol} are zero matrices with dimension 1×1.

In the **Step 2** of the methodology, it is necessary to define the **internal inputs** and the **external inputs** of the system. In the electrical small size test system, there are two external inputs, which are the inputs of the systems *L1* and *L2*, u_1 and u_2; as it can be seen in Figure 3.4. The input u_3 is going to be internal.

In order to build the **interconnection matrix** M_{int}, and the **external matrix** M_{ext} two tables depicting the inputs and outputs of the system were built. In Table 3.1 can be seen the dynamics of the interconnection matrix for the transmission lines *L1* and *L2* and the cable *C1*. It can be observed that when the output of a certain system is the input of a complete different system a number ***1*** appears, depicting the interaction among those systems. Only a few elements in the interconnection matrix will have an internal interaction, these dynamics will depend on how the system is connected.

It can be noticed that the elements of the matrix M_{int} that will be internally connected are:

$$M_{int}(3,1) \qquad\qquad M_{int}(3,2)$$

In Table 3.2 can be seen the external matrix M_{ext} of the electrical small size test system. This matrix M_{ext} shows a ***1*** the intersection of the input and the output of the indicated systems. To summarise, the elements of the M_{ext} which are external inputs are:

$$M_{ext}(1,1) \qquad\qquad M_{ext}(2,2)$$

Table 3.1: Interconnection matrix M_{int}. Electrical small size test system

	y_1	y_2	y_3
u_1	0	0	0
u_2	0	0	0
u_3	1	1	0

Table 3.2: External matrix M_{ext}. Electrical small size test system

	y_1	y_2	y_3
u_1	1	0	0
u_2	0	1	0
u_3	0	0	0

Therefore, the components of the input vector in the open loop $\boldsymbol{U_{ol}^{'} = U_{int} + U_{ext}}$ are,

$$U_{int} = M_{int}Y_{ol} = \begin{bmatrix} 0 \\ 0 \\ y_1 + y_2 \end{bmatrix} \in \mathbb{R}^{3\times 1}, \qquad U_{ext} = M_{ext}U_{ol} = \begin{bmatrix} u_1 \\ u_2 \\ 0 \end{bmatrix} \in \mathbb{R}^{3\times 1}$$

It can be noticed that $\boldsymbol{U_{int}}$ contains only the dynamics of the internal inputs. Thus, from

Figure 3.4, the output of the transmission lines *L1* and *L2* are inputs of the cable *C1*. Hence, in $\boldsymbol{U_{int}}$ can be seen that those outputs are added. Since the inputs of the transmission lines *L1* and *L2* does not receive any output form other system the elements $\boldsymbol{U_{int}(1,1)}$ and $\boldsymbol{U_{int}(2,1)}$ are zero.

For $\boldsymbol{U_{ext}}$, only the inputs that are not fed back to other system are shown. Thus, only the inputs of lines *L1* and *L2* have a value in this vector, while the other elements are zero.

Once defined $\boldsymbol{M_{int}}$ and $\boldsymbol{M_{ext}}$ and the elements of the input vector $\boldsymbol{U_{ol}^{'}}$ the matrix for the open loop in the **Step 2**, $\boldsymbol{E_{ol}}$, can be calculated.

In the **Step 3**, the matrices for the **closed loop** are obtained by identification. Therefore, the state vector as well as the input and output vectors of the global space-state representation are,

$$X_{cl_{pse}} = X_{ol} = \begin{bmatrix} x_1 \\ x_2 \\ x_3 \end{bmatrix} \in \mathbb{R}^{11\times 1}, \quad U_{cl_{pse}} = M_{ext}U_{ol} = \begin{bmatrix} u_1 \\ u_2 \\ 0 \end{bmatrix} \in \mathbb{R}^{3\times 1}, \quad Y_{cl_{pse}} = Y_{ol} = \begin{bmatrix} y_1 \\ y_2 \\ y_3 \end{bmatrix} \in \mathbb{R}^{3\times 1}$$

And the closed-loop matrices dimensions of the global space-state representation are,

$$A_{cl_{pse}} \in \mathbb{R}^{11\times 11}, \qquad B_{cl_{pse}} \in \mathbb{R}^{11\times 3},$$
$$C_{cl_{pse}} \in \mathbb{R}^{3\times 11}, \qquad D_{cl_{pse}} \in \mathbb{R}^{3\times 3}$$

Finally, the state-space representation can be expressed as,

$$\dot{X}_{cl_{pse}} = A_{cl_{pse}}X_{cl_{pse}} + B_{cl_{pse}}U_{cl_{pse}}$$
$$Y_{cl_{pse}} = C_{cl_{pse}}X_{cl_{pse}} + D_{cl_{pse}}U_{cl_{pse}}$$

Where the subscript ***pse*** stands for *small size test system*. The system in this case is a multiple-input multiple-output (MIMO) system. The advantage to follow this methodology is that all of the outputs of the system can be observed.

4

Singular Value Decomposition (SVD) analysis

In this chapter, theory regarding the singular value decomposition is addressed. Then, this mathematical tool is applied to the *small size test system* to discover its harmonic frequencies. Finally, an assessment of the inputs and outputs of the system is performed.

4.1. Singular value decomposition theory

Let a matrix $\Lambda \in \mathbb{C}^{l\times m}$, then Λ can be decomposed into its singular value decomposition [14]. It can be decomposed into three matrices. Thus, it exists a matrix $\Sigma \in \mathbb{R}^{l\times m}$ and two unitary matrices $U \in \mathbb{C}^{l\times l}$ and $V \in \mathbb{C}^{m\times m}$ such that,

$$\Lambda = U\Sigma V^H \tag{4.1}$$

Where Σ is a rectangular diagonal matrix with the singular values $\sigma_1 \dots \sigma_q$ as elements in its main diagonal and in descending order, with $q = \min\{l, m\}$. The columns of the matrix U, $U = [u_1 \dots u_l]$, and the matrix V, $V = [v_1 \dots v_m]$, contain, respectively, the left and right singular vectors. This vectors are orthonormal, hence they are orthogonal and with length equal to the unity. The superscript H denotes the conjugate transpose of the matrix V.

The matrix Λ can be rewritten as,

$$\Lambda = \sum_{k=1}^{r} \sigma_k u_k v_k^H \tag{4.2}$$

Where $r = rank(\Lambda) \leq \min\{l, m\}$, since $\sigma_k = 0 \; k > r$.

In order to explain in a simple and brief manner how the SVD works, in Figure 4.1 an example can be found. It can be noticed in Figure 4.1a two vectors, V_1 and V_2, that exist within a circle of radius equal to one. These vectors have a specific angle with respect to the horizontal axis. When the rotational matrix V^H is applied to this system, the vectors will rotate with a certain angle θ_2. In this new system the vectors are called e_1 and e_2,as it can be seen in Figure 4.1b. The result of the rotation will cause the vectors to have a different orientation than in the beginning. When the diagonal matrix Σ is applied to the system, the

vectors will modify their length σ_1 and σ_2 times, respectively. Thus, the shape of the space in where these two vectors exist is going to be modified. In this specific example the shape of the new space is going to be an ellipse as can be seen in Figure 4.1c. Finally, when the last rotation matrix U is applied to the system, the vectors will change again their orientation. In this case the effect of the rotation is more visible, since the ellipsoid space is going to rotate the same angle θ_1 as the vectors. The effect of this rotational can be seen in Figure 4.1d.

This example can be extrapolated to an $n \times n$ Euclidean system. Thus, by using the SVD it is possible to study how the inputs of a determined MIMO system affect certain outputs of the same system.

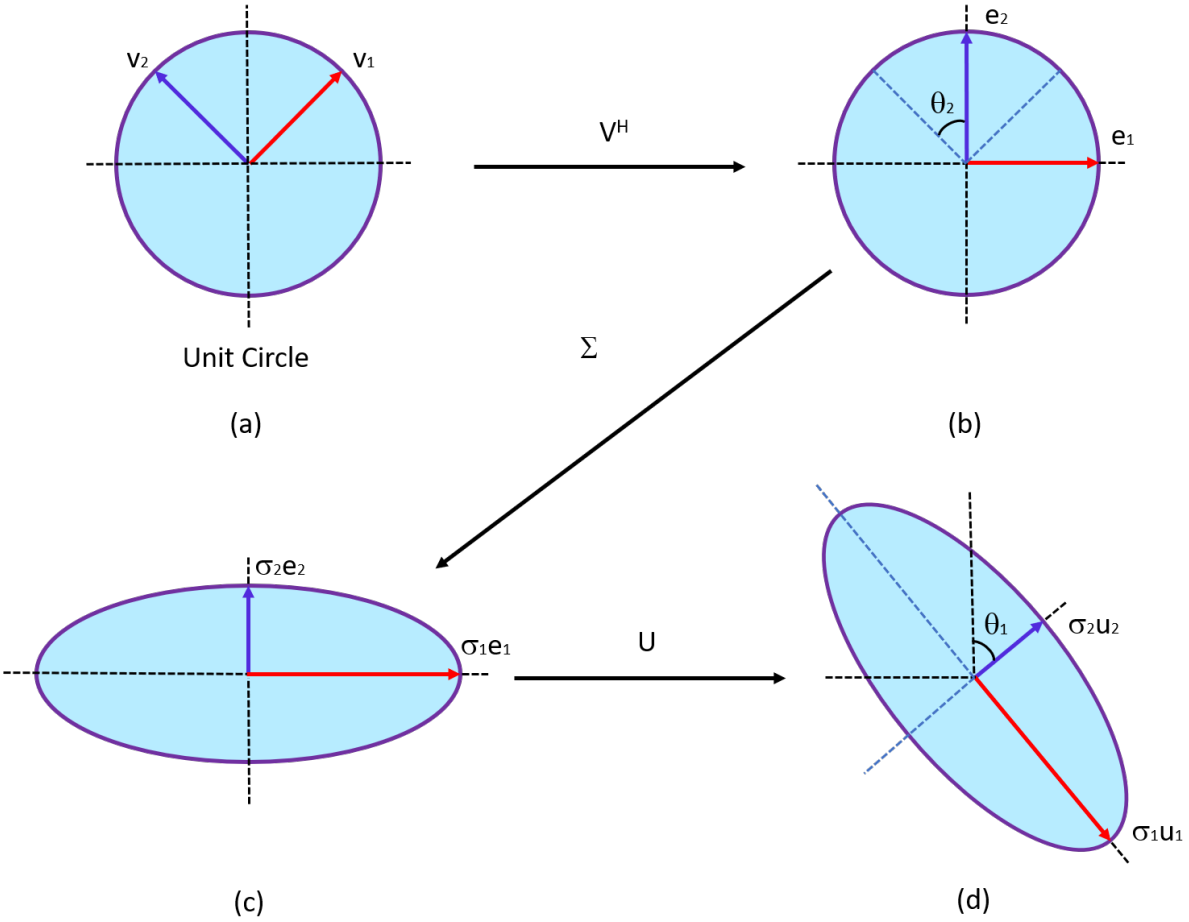

Figure 4.1: SVD representation of 2 vectors

4.2. Obtaining a transfer function from a state-space representation

In Chapter 3, a state-space representation for a MIMO system was obtained. That representation with its respective matrices and vectors can be observed in 4.3 and 4.4.

$$\dot{X}_{cl} = A_{cl}X_{cl} + B_{cl}U_{cl} \tag{4.3}$$

$$Y_{cl} = C_{cl}X_{cl} + D_{cl}U_{cl} \tag{4.4}$$

The objective is to transform 4.3 and 4.4 from a representation in the time domain to the frequency domain. Thus, a transfer function of the system is going to be obtained. Since the state-space representation is a MIMO system the resultant transfer function is going to be a transfer function matrix, whose elements are transfer functions that relates the inputs with the outputs of the system.

Thus, applying the Laplace transform to 4.3,

$$sX_{cl}(s) - x_{cl}(0) = A_{cl}X_{cl}(s) + B_{cl}U_{cl}(s)$$

Where,

$x_{cl}(0)$ is the initial value of the state vector in the time domain.

s is the Laplace transform.

Therefore,

$$\begin{aligned} sX_{cl}(s) - A_{cl}X_{cl}(s) &= x_{cl}(0) + B_{cl}U_{cl}(s) \\ (sI - A_{cl})X_{cl}(s) &= x_{cl}(0) + B_{cl}U_{cl}(s) \\ X_{cl}(s) &= (sI - A_{cl})^{-1}x_{cl}(0) + (sI - A_{cl})^{-1}B_{cl}U_{cl}(s) \end{aligned}$$

Assuming that the initial conditions are equal to zero $x_{cl}(0) = 0$,

$$X_{cl}(s) = (sI - A_{cl})^{-1}B_{cl}U_{cl}(s) \tag{4.5}$$

Following the same approach, the Laplace transform is applied to 4.4. Thus,

$$Y_{cl}(s) = C_{cl}(X_{cl}(s) - x_{cl}(0)) + D_{cl}U_{cl}(s)$$

And assuming initial conditions equal to zero,

$$Y_{cl}(s) = C_{cl}X_{cl}(s) + D_{cl}U_{cl}(s) \tag{4.6}$$

Then, substituting 4.5 in 4.6 yields,

$$\begin{aligned} Y_{cl}(s) &= C_{cl}(sI - A_{cl})^{-1}B_{cl}U_{cl}(s) + D_{cl}U_{cl}(s) \\ Y_{cl}(s) &= [C_{cl}(sI - A_{cl})^{-1}B_{cl} + D_{cl}]U_{cl}(s) \end{aligned}$$

Finally,

$$H_{cl}(s) = \frac{Y_{cl}(s)}{U_{cl}(s)} = C_{cl}(sI - A_{cl})^{-1}B_{cl} + D_{cl} \tag{4.7}$$

Where 4.7 is transfer function matrix whose columns represents the inputs of the system and their rows are the outputs of the system.

4.3. Singular value decomposition of a transfer function

If Λ is substituted by $H_{cl}(s)$ in 4.1. the linearised transfer function is given by,

$$H_{cl}(s) = \sum_{k=1}^{r} \sigma_k(s) u_k(s) v_k^H(s) \tag{4.8}$$

And the frequency response at a selected frequency is given by evaluating H_{cl} at $s = j\omega$.

The maximum $\overline{\sigma}(H_{cl}(j\omega))$ and minimum $\underline{\sigma}(H_{cl}(j\omega))$ system gains (singular values), are given by

$$\underline{\sigma}(H_{cl}(j\omega)) \leqslant \frac{\|H_{cl}(j\omega)d\|_2}{\|d\|_2} \leqslant \overline{\sigma}(H_{cl}(j\omega)) \tag{4.9}$$

With,

$$H_{cl}(j\omega)\overline{v} = \overline{\sigma}\,\overline{u} \tag{4.10}$$

$$H_{cl}(j\omega)\underline{v} = \underline{\sigma}\,\underline{u} \tag{4.11}$$

Where d is any input direction, not in the null space of H_{cl}, and $\|\cdot\|_2$ is the Euclidean norm.

On one hand, the vector $\overline{v}$ corresponds to the input direction with the largest amplification, and $\overline{u}$ is the corresponding output direction in which the inputs are most effective. On the other hand, the least effective input direction which is associated with $\underline{v}$, corresponds to the output $\underline{u}$. With $q = \min\{l, m\}$, the maximum and the minimum system gains, respectively $\overline{\sigma}$ and $\underline{\sigma}$, are given by,

$$\overline{\sigma} = \sigma_1 \tag{4.12}$$

$$\underline{\sigma} = \begin{cases} \sigma_q & l \geqslant m \\ 0 & l < m \end{cases} \tag{4.13}$$

4.4. Obtaining the frequency response from a transfer function

In order to visualise the impact of the first singular value (σ_1) on the response of the transfer function matrix, a sinusoidal signal with a critical harmonic is injected in the inputs of the system in the next manner:

Considering a system $H_{cl}(s)$ with input $d(s)$ and $y(s)$ such that,

$$y(s) = H_{cl}(s)d(s) \tag{4.14}$$

Where d is the input of the system. $h_{cl_{ij}}(j\omega)$ represents the sinusoidal response from input j to output i. Therefore, it is applied to input j a scalar sinusoidal given by,

$$d_j(t) = d_{j0}sin(\omega t + \alpha_j) \tag{4.15}$$

The input signal has been applied since $t = -\infty$. Then the persistent output in i is also a sinusoidal curve with the same frequency,

$$y_i(t) = y_{j0}sin(\omega t + \beta_i) \tag{4.16}$$

Where the gain and phase shift may be obtained from the complex number $h_{cl_{ij}}(j\omega)$ hence,

$$\frac{y_{i0}}{d_{j0}} = |h_{cl_{ij}}(j\omega)|, \qquad \beta_i - \alpha_j = \angle h_{cl_{ij}}(j\omega) \tag{4.17}$$

In phasor notation, the sinusoidal time response described by 4.15, 4.16 and 4.17 can be written as,

$$y_i(\omega) = h_{cl_{ij}}(j\omega)d_j(\omega) \tag{4.18}$$

Where,

$$d_j(\omega) = d_{j0}e^{j\alpha_j}, \qquad y_i(\omega) = y_{i0}e^{j\beta_i} \tag{4.19}$$

The use of ω as the argument in $d_j(\omega)$ and $y_i(\omega)$ implies that they are complex numbers, representing at each frequency the magnitude and the phase of sinusoidal signals in 4.15 and 4.16. The total response to simultaneous input injections of the same frequency in various inputs of the system is, by the superposition principal for linear systems, equal to the sum of the individual responses. Hence, from 4.18,

$$y_i(\omega) = h_{cl_{i1}}(j\omega)d_1(\omega) + h_{cl_{i2}}(j\omega)d_2(\omega) + \ldots = \sum_j h_{cl_{ij}}(j\omega)d_j(\omega) \tag{4.20}$$

Or in matrix form,

$$y_(\omega) = H_{cl}(j\omega)d(\omega) \tag{4.21}$$

Where,

$$d(\omega) = \begin{bmatrix} d_1(\omega) \\ d_2(\omega) \\ \vdots \\ d_m(\omega) \end{bmatrix}, \qquad y(\omega) = \begin{bmatrix} y_1(\omega) \\ y_2(\omega) \\ \vdots \\ y_l(\omega) \end{bmatrix} \tag{4.22}$$

Represent the vectors of sinusoidal input and output signals.

4.5. Singular value decomposition analysis of the *small size test system*

In this section the third and fourth steps of the methodology of Figure 1.1 is addressed. The transfer function matrix of the *small size test system* is obtained following the theory of Section 4.3. Therefore, the resultant transfer function matrix can be expressed as,

$$H_{cl_{pse}}(s) = \frac{Y_{cl_{pse}}(s)}{U_{cl_{pse}}(s)} \tag{4.23}$$

$\boldsymbol{H_{cl_{pse}}}$ is a 3×3 matrix, which links a certain input with a certain output of the system. However, not all the elements of the transfer function matrix are different from zero, some of them are zero due to the topology of the system. In Table 4.1 can be seen which elements of $\boldsymbol{H_{cl_{pse}}}$ have a non-zero value and which ones have a transfer function. The letter ***n*** indicates the degree of the characteristic polynomial of that specific transfer function.

Table 4.1: *Small size test system* transfer function matrix H_{cl}

	u_1	u_2	u_3
y_1	$\frac{y_1(s)}{u_1(s)}$ $n = 3$	0	0
y_2	0	$\frac{y_2(s)}{u_2(s)}$ $n = 3$	0
y_3	$\frac{y_3(s)}{u_1(s)}$ $n = 8$	$\frac{y_3(s)}{u_2(s)}$ $n = 8$	$\frac{y_3(s)}{u_3(s)}$ $n = 5$

The transfer function matrix $H_{cl_{pse}}$ which has all the information of the *small size test system* is going to be studied using the SVD. The next steps were followed,

1. A range of frequencies is previously defined. Within this range it is going to be observed the critical (harmonic) frequencies the system has. Thus, the selected frequency vector was $f = 1\ Hz$ to $f = 1\ kHz$, which is equally spaced.

2. The transfer function matrix $H_{cl_{pse}}$ is going to be evaluated in each of these frequencies. Since $H_{cl_{pse}}(s) = H_{cl_{pse}}(j\omega)$, the elements in this matrix are going to show a complex behaviour. Therefore, it is necessary to obtain the absolute value of each complex component in $H_{cl_{pse}}(j\omega)$.

3. The SVD is performed for every matrix $H_{cl_{pse}}(j\omega)$ evaluated in the frequency vector. Thus, it is obtained a vector of matrices Σ containing the singular values for each frequency ω in the frequency vector.

The resultant singular values can be seen in Figure 4.2. As it was expected there are three singular values curves. The points of these curves corresponds to each singular value matrix Σ evaluated at a certain frequency ω.

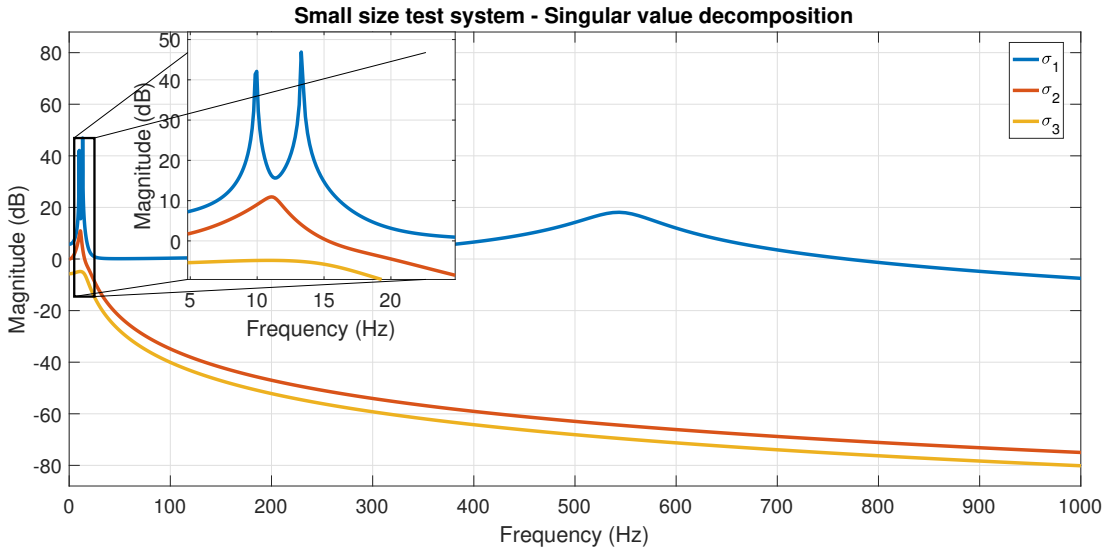

Figure 4.2: *Small size test system* singular value decomposition

As it was seen earlier in this chapter, the first singular value σ_1 has the highest gain and therefore it will have the bigger impact in the inputs and outputs of the system. In Figure 4.3 can be seen the curve of the first singular value (σ_1). It can be noticed that there are three maximum peaks at certain frequencies. The frequencies where these peaks occur are of great interest for this research, since the vectors of the rotational matrices U and V^H associated with the first singular value can be studied and determine which inputs affect more the behaviour of certain outputs. These frequencies can be observed in Table 4.2.

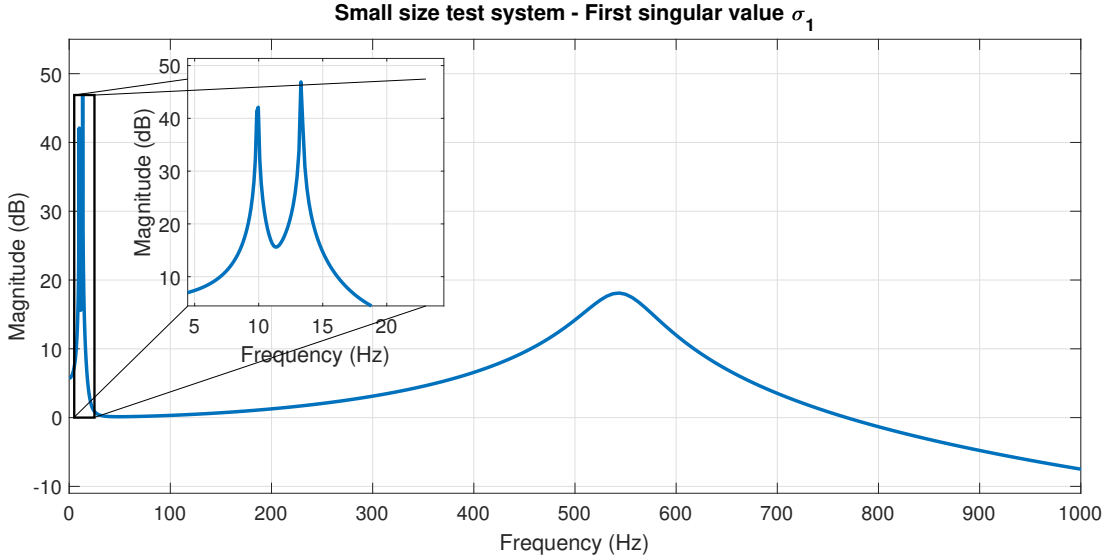

Figure 4.3: *Small size test system* first singular value

Table 4.2: *Small size test system* harmonic frequencies

σ_1 (dB)	Frequency (Hz)
60.33	9.91
57.14	13.34
18.11	550

The frequencies where the peaks of Figure 4.3 occur, belong to the harmonic frequencies of the *small size test system*. These frequencies appear due to the energy exchange between the inductances and capacitances in the PI section and "fitted PI" representations. Using control theory these harmonics can be calculated using the natural frequency of the complex poles of the system [12]. In Table 4.3 can be seen the real and complex poles of the *small size test system*. It can be observed that the harmonic frequencies of the system are calculated from the three complex poles that the system has. They are calculated following the next equation,

$$\omega_{hf} = \omega_n\sqrt{1-\zeta^2}$$

Where the subscript ***hf*** stands for harmonic frequency.

Table 4.3: *Small size test system* damping factors

Pole	Order	Damping ratio	Natural frequency ω_n (rad/s)	Harmonic frequency (rad/s)	Harmonic frequency (Hz)
-9.31	3	1	9.307	-	-
-0.0417$\pm j$62.289	2	6.701$\times 10^{-4}$	62.289	62.289	9.9137
-0.0448$\pm j$83.810	2	5.348$\times 10^{-4}$	83.810	83.810	13.3388
-125.42	3	1	125.423	-	-
-213.84$\pm j$3418.2	3	0.0624	3424.863	3418.18	550
-6.106$\times 10^{5}$	2	1	6.106$\times 10^{5}$	-	-
-1.601$\times 10^{6}$	2	1	1.601$\times 10^{6}$	-	-
-1.076$\times 10^{8}$	3	1	1.076$\times 10^{8}$	-	-

4.6. Input and output assessment of the *small size test system*

In this section the fifth step of the methodology of Figure 1.1 is addressed. In order to assess which input is going to affect the system the most, and which output is going to be the most affected by the latter, in Tables 4.4 and 4.5, the left and right singular vectors associated with the first singular value for the frequencies listed in Table 4.2 are shown. In order to analyse these vectors, the frequency f_1 is going to be taken as an example. The right singular vector or the vector associated with the inputs of the system for the frequency f_1 is V_1^H. It can be noticed that the second element of this vector ($V_1^H(2,1)$) has the highest absolute value among the other components in the vector. This means that the input number 2, u_2 is going to have the biggest direction and will affect the system in a greater manner. On the other hand, when looking at the left singular vector or the vector associated with the outputs of the system U_1, it can be seen that the third element ($U_1(3,1)$) has the highest absolute value among the other components in the vector. Therefore, the output that will be more affected by the input u_2 is going to be the third output y_3, which corresponds to the output of the underground cable, ***C1***.

A similar analysis can be performed with the corresponding singular vectors at frequency f_3. The right singular value vector shows a maximum absolute value in its third component ($V_3^H(3,1)$), followed by the first component ($V_3^H(1,1)$). However, the system only has inputs different from zero in the first (u_1) and second (u_2) components, and since the other directions are zero, the direction that affects more the outputs is the one in the first component ($V_3^H(1,1)$). From the corresponding left singular vector (U_3) it can be clearly seen that the direction that affect the most the input u_1, is the one in the third component ($U_3(3,1)$). Therefore, the most affected output is again, output y_3.

Table 4.4: *Small size test system* left singular vectors associated to the outputs of the system

Frequency (Hz)		
f_1	f_2	f_3
9.91	13.34	550
Left singular vector		
U_1	U_2	U_3
0.000	-0.7065	0.0000
-0.7067	0.0000	0.0000
-0.7075	-0.7077	1.0000

Table 4.5: *Small size test system* right singular vectors associated to the inputs of the system

Frequency (Hz)		
f_1	f_2	f_3
9.91	13.34	550
Right singular vector		
V_1^H	V_2^H	V_3^H
-0.0015	-1.0000	-0.0006
-1.0000	-0.0012	-0.0003
-0.0007	-0.0010	-1.0000

In this part of the In order to visualise the impact of the first singular value (σ_1) on the response of the *small size test system*, a sinusoidal signal with the critical harmonic frequencies are injected at the inputs.

Following the analysis derived in Section 4.4, a sinusoidal input of the form,

$$d = d_0(\cos(\omega t + \alpha) + j\sin(\omega t + \alpha)) \tag{4.24}$$

is applied at the inputs u_1 and u_2 of the *small size test system* transfer function matrix. The magnitude d_0 is chosen as 1, the phase shift is 0 and the frequency ω will take the frequency values of Table 4.2.

When a sinusoidal signal with the first frequency $f_1 = 9.91\ Hz$ is applied to the *small size test system*, the most affected output is the output voltage of the underground cable ***C1***, y_3. As it can be seen in Figure 4.4, the voltage increment is of approximately $7.00\ p.u.$, which is the higher voltage increment the system will have when a sinusoidal with this frequency is injected at the inputs.

A similar behaviour the output y_3 is going to present, when a sinusoidal signal with the second frequency $f_2 = 13.34 Hz$ is injected. In this case the voltage increment is of approximately $5.00\ p.u.$, as it can be seen in Figure 4.5. In both time-domain simulations, the response of the output y_3 has a gradual increment at the beginning of the simulation, and in the end, the oscillations are sustained.

The time-domain response for the highest frequency, $f_3 = 550\,Hz$, is shown in Figure 4.6. In this case the voltage increment at the beginning is higher than in the previous time-domain simulations, but the voltage is lower, approximately $0.80\ p.u.$, when the oscillations are sustained. In Table 4.6 is summarised the injected sinusoidal with the respective critical frequency and the name of the most affected elements of the *small size test system*.

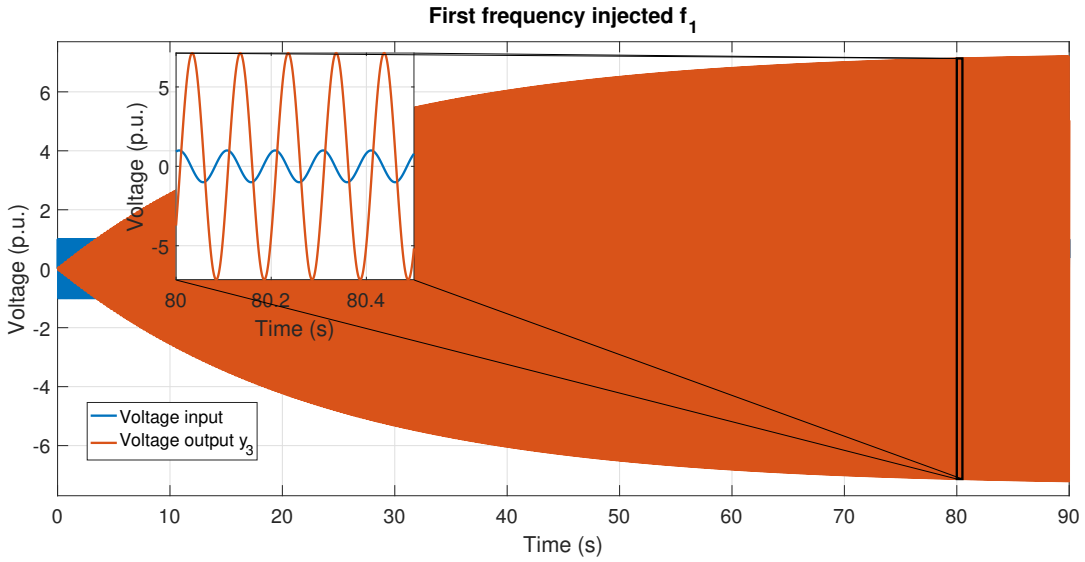

Figure 4.4: *Small size test system* first frequency injected at inputs u_1 and u_2

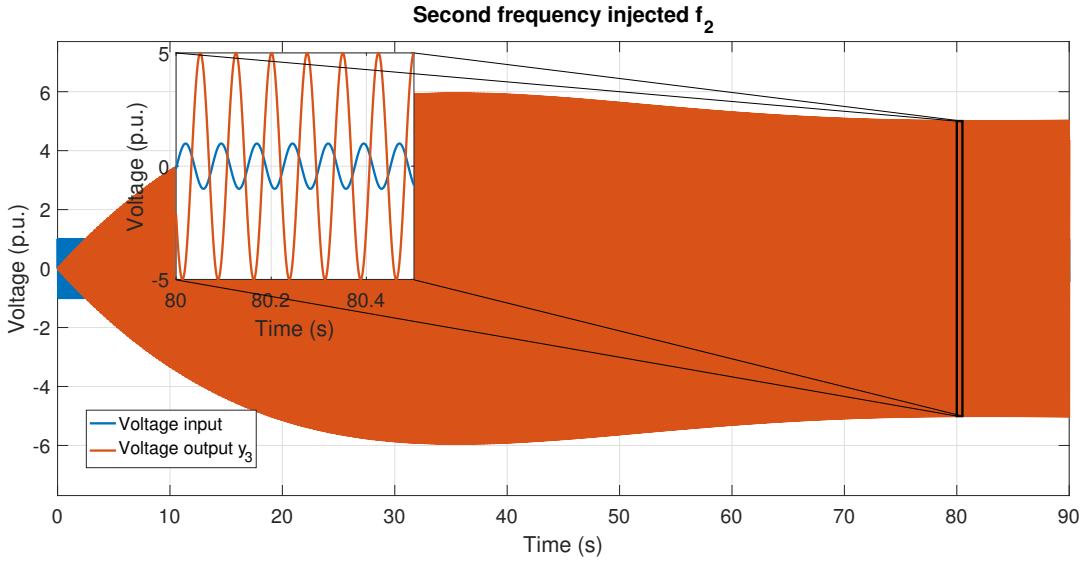

Figure 4.5: *Small size test system* second frequency injected at inputs u_1 and u_2

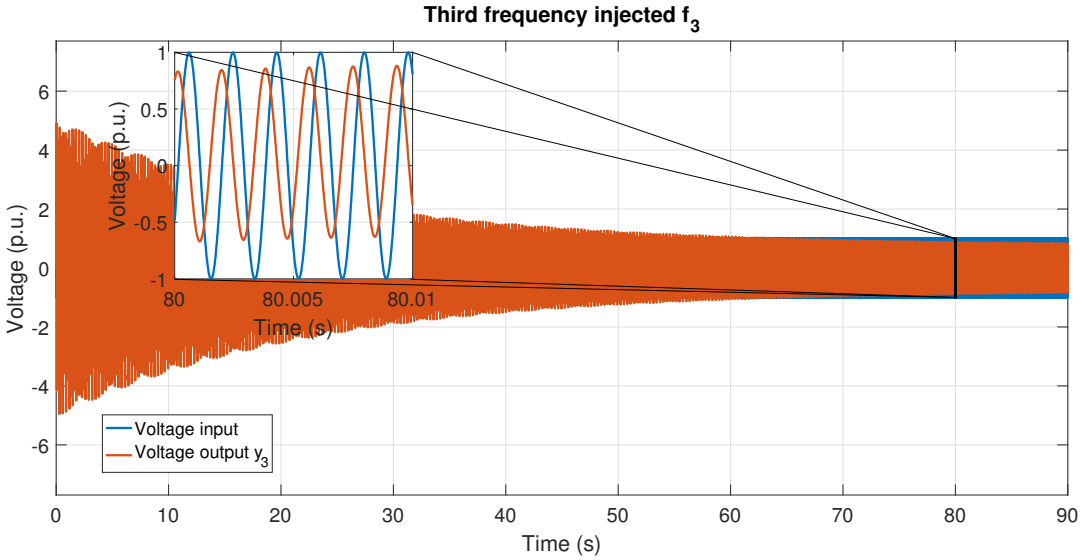

Figure 4.6: *Small size test system* third frequency injected at inputs u_1 and u_2

Table 4.6: *Small size test system* most affected elements

Injected frequency f_i	**Input affecting the system the most** u_i	**Most affected output** y_i	**Transmission line or underground cable**
9.91	u_2	y_3	$C1$
13.34	u_1	y_3	$C1$
550	u_1	y_3	$C1$

For the computation of the SVD and the input and output assessment of the *small size test systemsmall size test system*, a routine in Matlab was created and it can be consulted in Appendix B.1.

4.7. *Small size test system* sensitivity analysis

In the next subsections two sensitivity analysis are performed to observe the system behaviour to the increase or decrease in the length of the *small size test system* elements and the use of lumped PI sections instead of a single PI section.

4.7.1. Length variation

In this subsection an analysis on the variation of the length of the transmission lines and the underground cables is performed.

It can be seen in Figures 4.7 and 4.8 the harmonic response of the *small size test system* when the length of the transmission lines is varied. At first sight, it can be noticed that the frequencies induced by the transmission lines, which are those in the range from $0Hz$ to $50Hz$, shift to higher frequencies when the lines is shorter. Meaning that the shorter the line, the higher the frequencies the system is going to present. Then, when the length is increased the harmonic frequencies shift to lower frequencies. The frequencies related to the under-ground cables, which are those in the range from $200\ Hz$ to $800\ Hz$, does not present any change at all. In both cases the magnitude of the frequencies does not increase nor decrease.

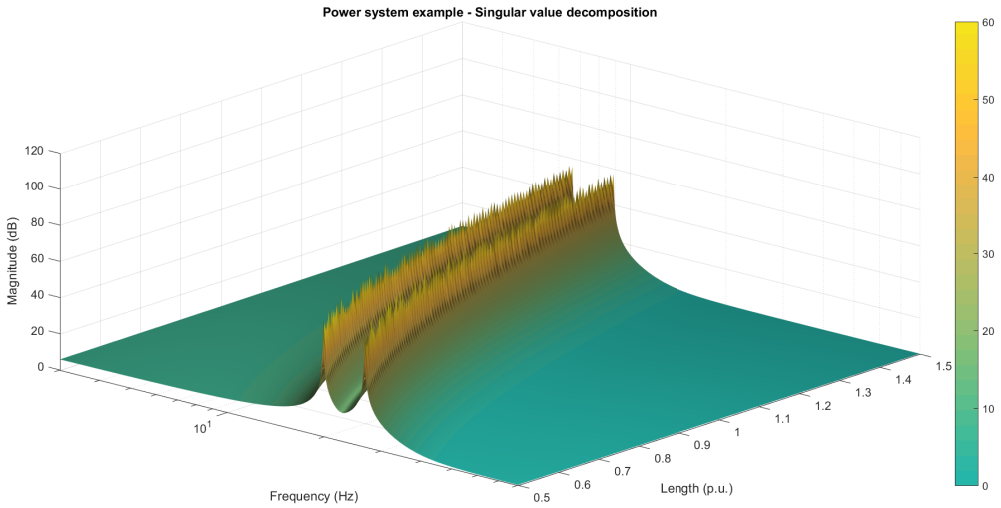

Figure 4.7: Transmission line length variation (1)

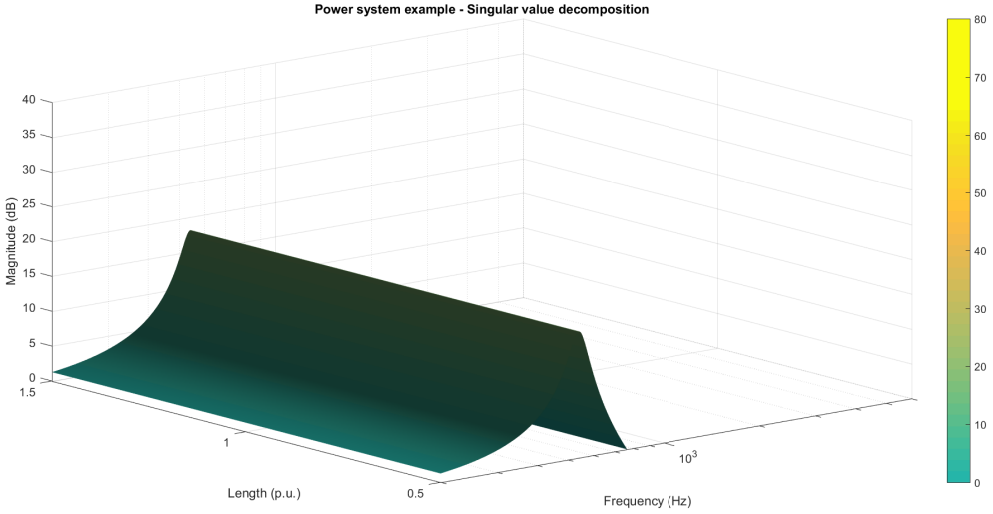

Figure 4.8: Transmission line length variation (2)

In Figures 4.9 and 4.10 can be seen the *small size test system* harmonic response when the length of the underground cables is varied. It can be observed that the frequencies related to the transmission lines do not present any perceptible change. However, the frequencies related to the underground cables does present a change. First, when the length is decreased the frequencies tend to move to lower frequencies. Then, when the length is increased the frequencies tend to move to higher values. Moreover, they increase their magnitude a little, as it can be seen in Figure 4.10, where the magnitude of the frequencies presents a light yellow colour.

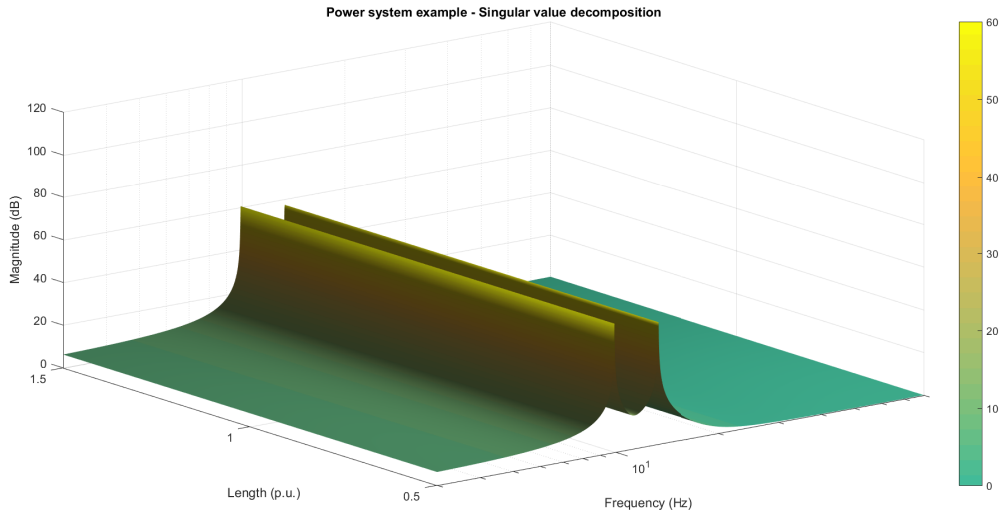

Figure 4.9: Underground cable length variation (1)

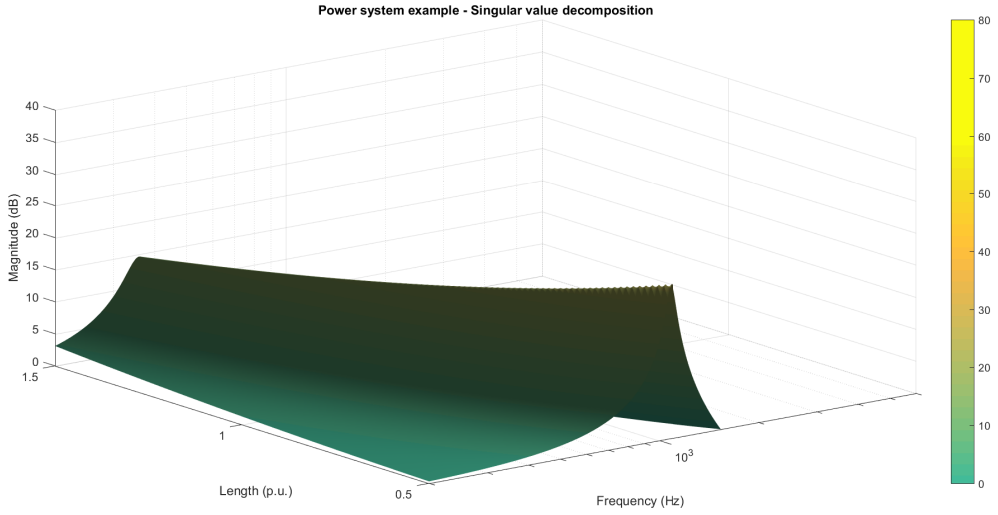

Figure 4.10: Underground cable length variation (2)

4.7.2. Lumped PI sections

In this subsection the use of lumped PI sections to represent a transmission line is addressed. The next steps were performed to observe the harmonic response of the system to this new representation:

1. The transmission line ***L1*** is going to be represented as three PI sections connected in series (lumped PI section). The new *small size test system* can be seen in Figure 4.11.

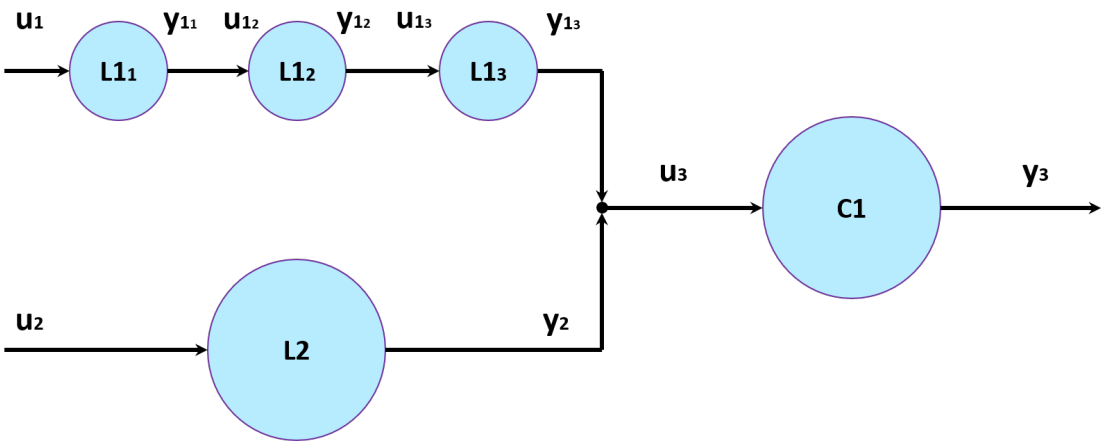

Figure 4.11: New *small size test system*

The values of the inductances and capacitances of $L1_1$, $L1_2$, $L1_3$ PI sections will take the values of ***L1***.

2. The new dimensions of the state-space vector and matrices are,

$$X_{cl_{npse}} = \begin{bmatrix} x_{1_1} \\ x_{1_2} \\ x_{1_3} \\ x_2 \\ x_3 \end{bmatrix} \in \mathbb{R}^{11\times 1}, \qquad U_{cl_{npse}} = \begin{bmatrix} u_1 \\ 0 \\ 0 \\ u_2 \\ 0 \end{bmatrix} \in \mathbb{R}^{3\times 1}, \qquad Y_{cl_{npse}} = \begin{bmatrix} y_{1_1} \\ y_{1_2} \\ y_{1_3} \\ y_2 \\ y_3 \end{bmatrix} \in \mathbb{R}^{3\times 1}$$

And the closed-loop matrices dimensions are,

$$A_{cl_{npse}} \in \mathbb{R}^{17\times 17}, \qquad B_{cl_{npse}} \in \mathbb{R}^{17\times 5},$$
$$C_{cl_{npse}} \in \mathbb{R}^{5\times 17}, \qquad D_{cl_{npse}} \in \mathbb{R}^{5\times 5}$$

3. The elements of the new transfer function H_{ncl} can be seen in Table 4.7

Table 4.7: New *small size test system* transfer function matrix H_{ncl}

	u_1	u_{1_2}	u_{1_3}	u_2	u_3
y_{1_1}	$\frac{y_1(s)}{u_1(s)}$ $n=3$	0	0	0	0
y_{1_2}	0	$\frac{y_2(s)}{u_2(s)}$ $n=3$	0	0	0
y_{1_3}	0	0	$\frac{y_3(s)}{u_3(s)}$ $n=3$	0	0
y_2	0	0	0	$\frac{y_4(s)}{u_4(s)}$ $n=3$	0
y_3	0	0	0	0	$\frac{y_5(s)}{u_5(s)}$ $n=5$

4. When performing the SVD to H_{ncl} the critical frequencies obtained can be seen in Figure 4.12.

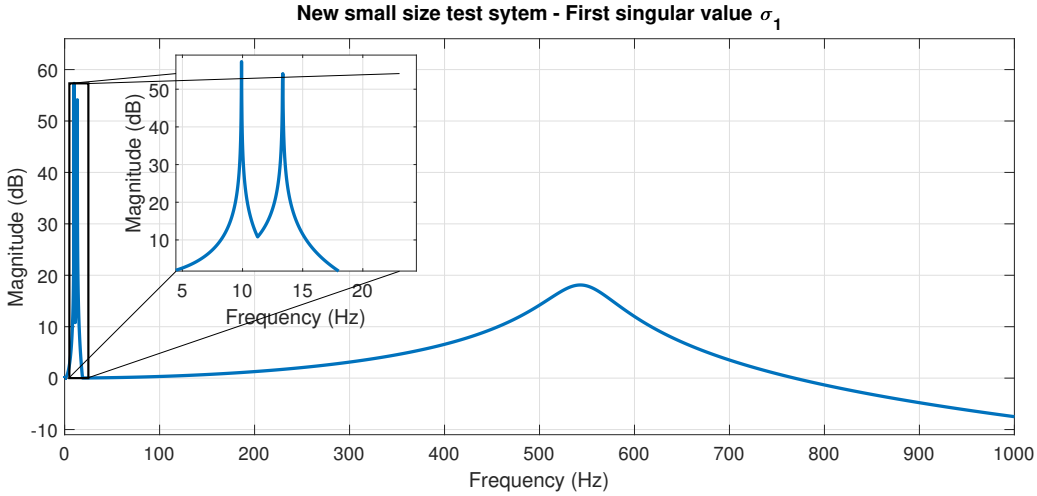

Figure 4.12: New *small size test system* first singular value

It can be observed that the critical frequencies, when representing the transmission line ***L1*** as lumped PI sections, match the critical frequencies of the single PI section used before. Therefore, it can be concluded that this method does not recognise the critical frequencies of several transmission lines when they have the same parameters.

5

Synthetic Randstad transmission system. Harmonic response analysis

In this chapter the Randstad region is discussed in detail. Through the next sections it is depicted where the Randstad region lies geographically and which are the important cities that delimit the region. It is also showed the electric parameters of the transmission lines and underground cables that are going to be used in the present work. Then the research methodology of Chapter 1 is going to be used to find the harmonic frequencies of the region and assess the influence of the inputs in the outputs of the system.

5.1. Geographic location

Within the Randstad region can be found four of the biggest cities in the Netherlands. To have a better overview of where the Randstad lies within the country, in Figure 5.1a this region is delimited by the red contour over the Netherlands territory. It can be observed that it is a vital region in the territory and in the coming years will become even more important due to the new wind power plants that are going to be connected to it. In Figure 5.1b can be observed with more detail the primary cities that represent this region.

5.2. Randstad power transmission system

The Dutch transmission system has four main voltage levels, 110, 150, 220 and 380 kV. The transmission lines, underground cables and buses at 380 kV that integrate the Randstad region can be seen in Figure 5.2 in red. It can be noticed that two rings are formed. The first ring is integrated by the substations located in Beverwijk, Diemen, Bleiswijk and Krimpen aan den IJssel in the north of the region. While in the south, the second ring is integrated by the substations located in Westerlee, Maasvlakte, Bleiswijk and Krimpen aan den IJssel.

These two rings are connected by double-circuit transmission lines as well as XLPE underground cables. The locations of the underground cables are between the substations Wateringen and Bleiswijk and the substations Vijfhuizen and Beverwijk, where underground cables with a length of 10.8 km and 9.3 km respectively, are implemented.

The substations mentioned before as well as those in between are the matter of study of the present work.

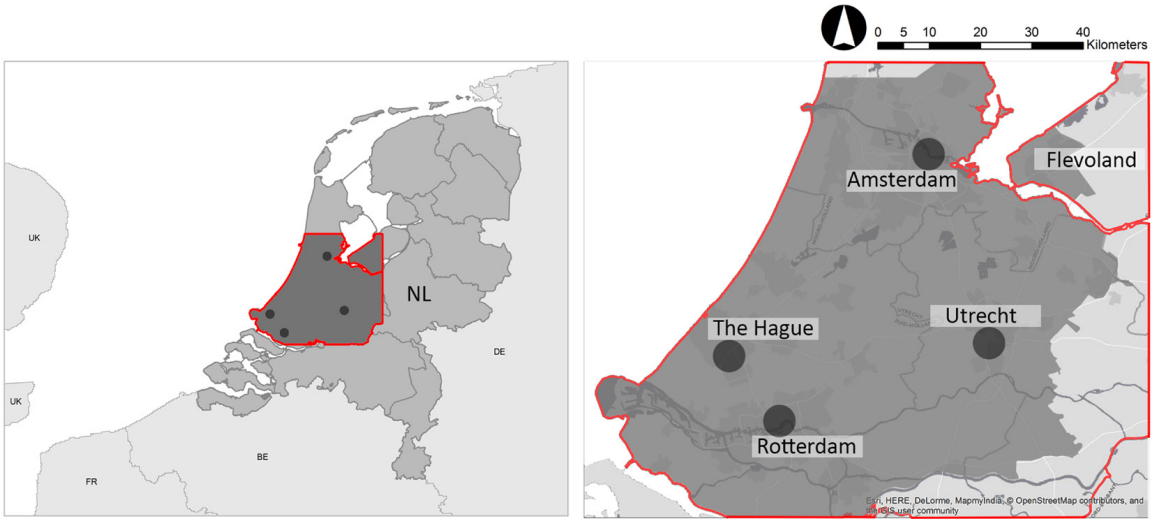

Figure 5.1: Randstad region [2]

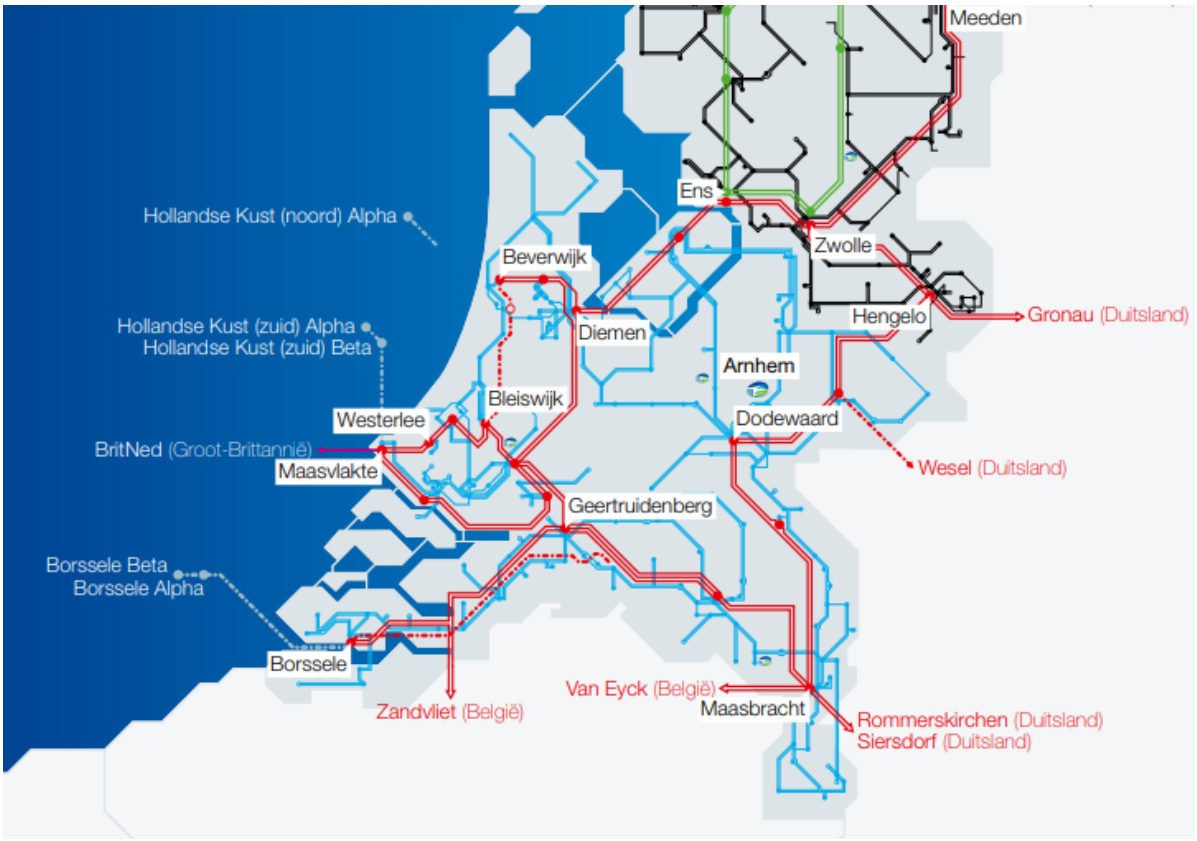

Figure 5.2: 380 kV buses in the Randstad [3]

5.3. Randstad SISO state-space representations

In order to model the SISO state-space representations of the elements within the Randstad region, first of all, it is necessary to delimit the area of study.

Table 5.1: Buses tags in PSS/E

City	Voltage [kV]	Name in PPS/E	Bus number in PPS/E
Diemen	380	DIM	11113
Oostzaan	380	OZN	11192
Beverwijk	380	BVW	11105
Vijfhuizen	380	VHZ	11213
Bleiswijk	380	BWK	11107
Wateringen	380	WTR	11221
Westerlee	380	WL	11217
Terminal SP	380	TERMINAL SP	11208
Maasvlakte	380	MVL	11177
Simonshaven	380	TERMINAL SMH	11201
Crayestein	380	CST	11110
Krimpen aan den Ijssel	380	KIJ	11161
Breukelen Kortrijk	380	BKK	11100

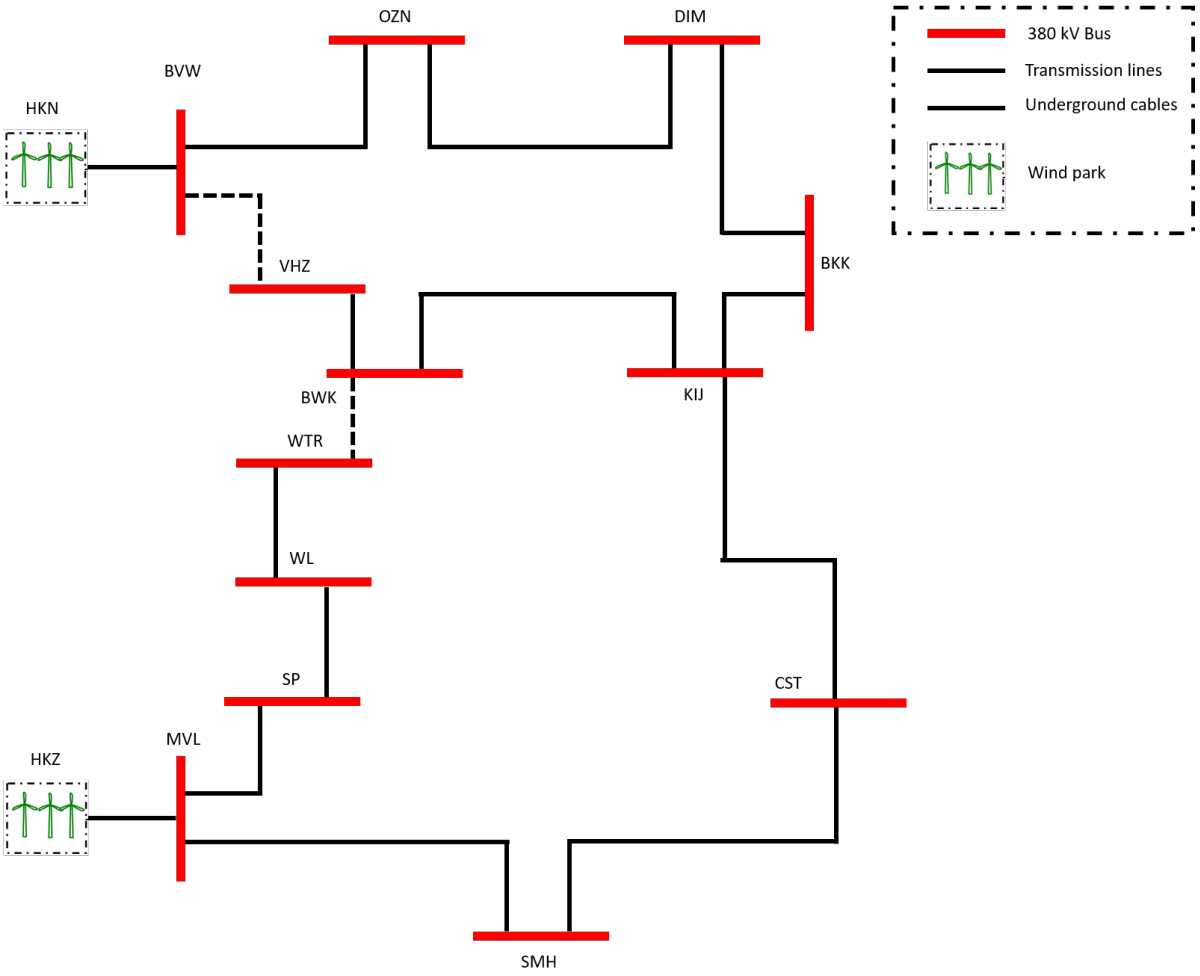

Figure 5.3: Randstad region single line diagram

Therefore, it is necessary to choose the buses that are going to be part of the Randstad area in order to extract their electrical parameters from the PSS/E software. In Table 5.1 can be seen the names and the numbers that the buses have in the PSS/E software.

The area delimited by these buses can be seen in Figure 5.3. Within this area lie twelve transmission lines and two underground cables, and the values of their respective electrical components are enlisted in Appendix A in Table A.1. With this information it is possible to build the fourteen SISO state-space representations that lie in the Randstad region. For that matter, a routine in Matlab was created and it can be consulted in Appendix B.2.

5.4. Randstad state-space concatenation

The steps explained in Section 3.1 are going to be followed to concatenate the twelve state-space representations for the transmission lines and the two state-space representations for the underground cables.

A simpler representation of the Randstad region can be seen in Figure 5.4. A few important points need to be pointed out:

- The circles represent the state-space representations of each element in the Randstad region. It can be seen that there are fourteen of them.
- The arrow(s) that point to a certain circle are the inputs that a particular system has.
- The arrow(s) that come out of a certain circle are the outputs that a particular system has.

For **Step 1** of the methodology presented in Section 3.1 and based on the topology of Figure 5.4 it can be observed that the **open loop** state-space representation will have the following dimensions, where the number of systems to be concatenated is fourteen,

$$X_{ol} = \begin{bmatrix} x_1 \\ x_2 \\ \vdots \\ x_{13} \\ x_{14} \end{bmatrix} \in \mathbb{R}^{46\times 1}, \qquad U_{ol} = \begin{bmatrix} u_1 \\ u_2 \\ \vdots \\ u_{13} \\ u_{14} \end{bmatrix} \in \mathbb{R}^{14\times 1}, \qquad Y_{ol} = \begin{bmatrix} y_1 \\ y_2 \\ \vdots \\ y_{13} \\ y_{14} \end{bmatrix} \in \mathbb{R}^{14\times 1}$$

Where the elements of the state-space vectors for the transmission lines are of the form,

$$x_i = \begin{bmatrix} i_{L_i} \\ V_{C_{1_i}} \\ V_{C_{2_i}} \end{bmatrix} \in \mathbb{R}^{3\times 1}$$

It is important to point out that the transmission lines have the subscripts 1, 2, 3, 4, 5, 7, 8, 9, 10, 12, 13, 14. The elements of the state-space vectors for the underground cables are of the form,

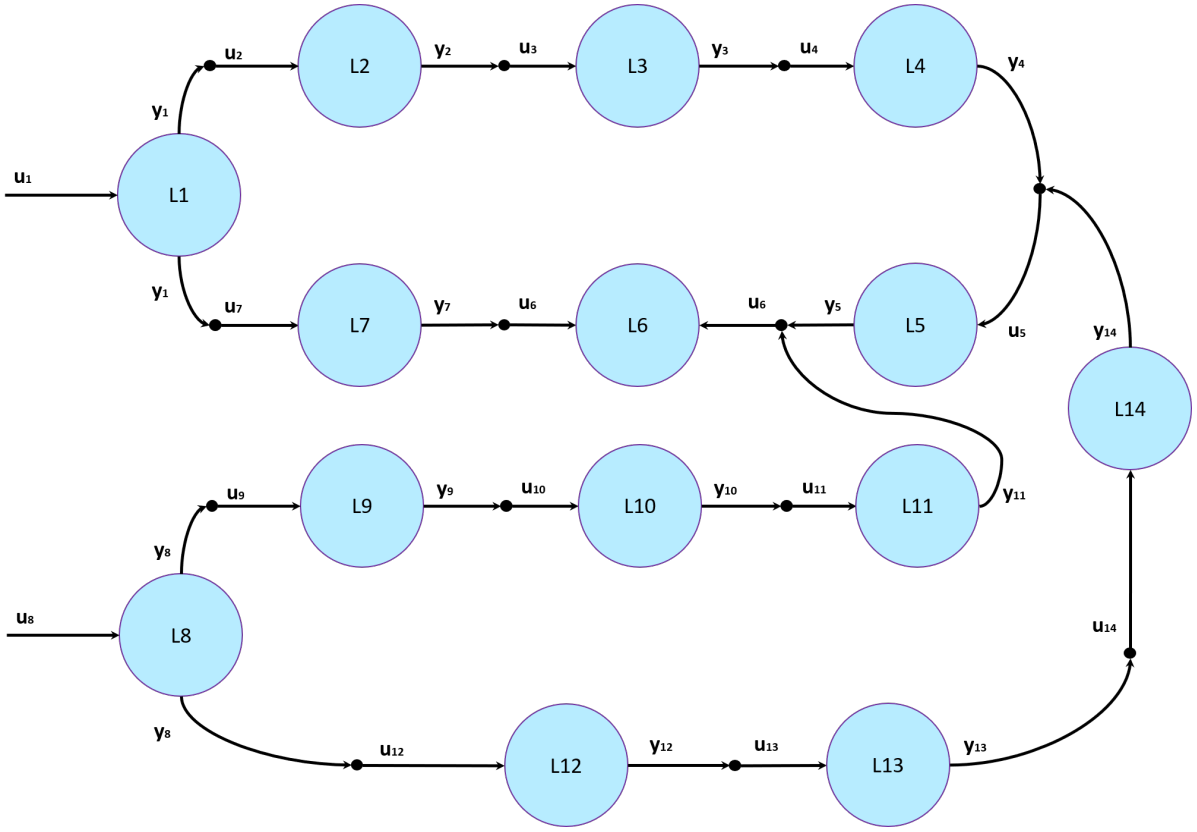

Figure 5.4: Randstad simplified electrical system

$$x_i = \begin{bmatrix} i_{L_{z_{1,i}}} \\ i_{L_{z_{2,i}}} \\ i_{L_{z_{3,i}}} \\ V_{C_{1_i}} \\ V_{C_{2_i}} \end{bmatrix} \in \mathbb{R}^{5\times 1}$$

The underground cables have the subscripts 6 and 11. The respective matrices have the next dimensions,

$$A_{ol} = \begin{bmatrix} A_1 & 0_{3\times3} & \cdots & 0_{3\times3} & 0_{3\times3} \\ 0_{3\times3} & A_2 & \cdots & 0_{3\times3} & 0_{3\times3} \\ \vdots & \vdots & \ddots & \vdots & \vdots \\ 0_{3\times3} & 0_{3\times3} & \cdots & A_{13} & 0_{3\times3} \\ 0_{3\times3} & 0_{3\times3} & \cdots & 0_{3\times3} & A_{14} \end{bmatrix} \in \mathbb{R}^{46\times46}, \quad B_{ol} = \begin{bmatrix} B_1 & 0_{3\times1} & \cdots & 0_{3\times1} & 0_{3\times1} \\ 0_{3\times1} & B_2 & \cdots & 0_{3\times1} & 0_{3\times1} \\ \vdots & \vdots & \ddots & \vdots & \vdots \\ 0_{3\times1} & 0_{3\times1} & \cdots & B_{13} & 0_{3\times1} \\ 0_{3\times1} & 0_{3\times1} & \cdots & 0_{3\times1} & B_{14} \end{bmatrix} \in \mathbb{R}^{46\times14},$$

$$C_{ol} = \begin{bmatrix} C_1 & 0_{1\times3} & \cdots & 0_{1\times3} & 0_{1\times3} \\ 0_{1\times3} & C_2 & \cdots & 0_{1\times3} & 0_{1\times3} \\ \vdots & \vdots & \ddots & \vdots & \vdots \\ 0_{1\times3} & 0_{1\times3} & \cdots & C_{13} & 0_{1\times3} \\ 0_{1\times3} & 0_{1\times3} & \cdots & 0_{1\times3} & C_{14} \end{bmatrix} \in \mathbb{R}^{14\times46}, \quad D_{ol} = \begin{bmatrix} D_1 & 0_{1\times1} & \cdots & 0_{1\times1} & 0_{1\times1} \\ 0_{1\times1} & D_2 & \cdots & 0_{1\times1} & 0_{1\times1} \\ \vdots & \vdots & \ddots & \vdots & \vdots \\ 0_{1\times1} & 0_{1\times1} & \cdots & D_{13} & 0_{1\times1} \\ 0_{1\times1} & 0_{1\times1} & \cdots & 0_{1\times1} & D_{14} \end{bmatrix} \in \mathbb{R}^{14\times14}$$

It is important to note that the size of the matrices A_6 and A_{11} in the main diagonal of A_{ol}

is 5×5. The size of the rest of the matrices is 3×3. The size of the matrices B_6 and B_{11} in the main diagonal of B_{ol} is 5×1. The rest has a size of 3×1. The size of the matrices C_6 and C_{11} in the main diagonal of C_{ol} is 1×5. The rest has a size of 1×3. Finally, the size of the matrices in the main diagonal of D_{ol} is 1×1 and they are zero matrices.

In **Step 2** of the methodology, it is necessary to define the **internal inputs** and the **external inputs**. In our system there are only two external inputs, which are the inputs of the systems *L1* and *L8* as can be seen in Figure 5.4. The rest of the inputs are going to be internal.

In order to build the **interconnection matrix** M_{int}, and the **external matrix** M_{ext} two tables depicting the inputs and outputs of the system were built. In Appendix A in Tables A.2 and A.3 can be seen the dynamics of the interconnection matrix for systems 1 to 7 and 8 to 14, respectively. It can be observed that when the output of a certain system is the input of a complete different system a number ***1*** appears, depicting the interaction among those systems. Only a few elements in the interconnection matrix will have an internal interaction, these dynamics will depend on the topology of the power system.

To summarise, the elements of M_{int} that will be internally connected are:

$M_{int}(2,1)$	$M_{int}(7,1)$	$M_{int}(3,2)$
$M_{int}(4,3)$	$M_{int}(5,4)$	$M_{int}(6,5)$
$M_{int}(6,7)$	$M_{int}(9,8)$	$M_{int}(12,8)$
$M_{int}(10,9)$	$M_{int}(11,10)$	$M_{int}(6,11)$
$M_{int}(13,12)$	$M_{int}(14,13)$	$M_{int}(5,14)$

The external matrix has a simpler construction due to the nature of the system depicted in Figure 5.4. As it can be seen in Tables A.4 and A.5, only the inputs u_1 and u_8 are external inputs, meaning that they do not receive any output from other system. The matrix M_{ext} shows a ***1*** in the intersection of the input and the output of the indicated systems. To summarise, the elements of M_{ext} which are external inputs are:

$$M_{ext}(1,1) \qquad M_{ext}(8,8)$$

It is important to notice that both matrices have the following dimensions,

$$M_{int} \in \mathbb{R}^{14\times14}, \qquad M_{ext} \in \mathbb{R}^{14\times14},$$

Then, the components of the input vector in the open loop $\boldsymbol{U_{ol}^{'} = U_{int} + U_{ext}}$ are,

$$U_{int} = M_{int}Y_{ol} = \begin{bmatrix} 0 \\ y_1 \\ y_2 \\ y_3 \\ y_4 + y_{14} \\ y_5 + y_7 + y_{11} \\ y_1 \\ 0 \\ y_8 \\ y_9 \\ y_{10} \\ y_8 \\ y_{12} \\ y_{13} \end{bmatrix} \in \mathbb{R}^{14\times1}, \qquad U_{ext} = M_{ext}U_{ol} = \begin{bmatrix} u_1 \\ 0 \\ 0 \\ 0 \\ 0 \\ 0 \\ 0 \\ u_8 \\ 0 \\ 0 \\ 0 \\ 0 \\ 0 \\ 0 \end{bmatrix} \in \mathbb{R}^{14\times1}$$

It can be noticed that $\boldsymbol{U_{int}}$ contains only the dynamics of the internal inputs. As an example, from Figure 5.4, the output of the lines *L4* and *L14* are inputs of the line *L5*. Therefore, in the element $(5, 1)$ of $\boldsymbol{U_{int}}$, it can be seen that those outputs are added. In the same manner, the output of lines *L5*, *L7*, *L11* are the inputs to the line *L6* and this dynamics can be observed in the element $(6, 1)$. Since the inputs of the lines *L1* and *L8* does not receive any output form other system the elements $\boldsymbol{U_{int}(1, 1)}$ and $\boldsymbol{U_{int}(8, 1)}$ are zero.

For $\boldsymbol{U_{ext}}$, only the inputs that are not fed back to other system are shown. Thus only the inputs of lines *L1* and *L8* have a value in this vector, while the other elements are zero.

Once defined $\boldsymbol{M_{int}}$ and $\boldsymbol{M_{ext}}$ and the elements of the input vector $\boldsymbol{U_{ol}^{'}}$ the matrix for the open loop in the **Step 2**, $\boldsymbol{E_{ol}}$, can be calculated.

In the **Step 3**, the last step of the methodology, the matrices for the **closed loop** are obtained by identification. Therefore, the state, input and output vectors of the global space-state representation are,

$$X_{cl_{Rs}} = X_{ol} = \begin{bmatrix} x_1 \\ x_2 \\ x_3 \\ x_4 \\ x_5 \\ x_6 \\ x_7 \\ x_8 \\ x_9 \\ x_{10} \\ x_{11} \\ x_{12} \\ x_{13} \\ x_{14} \end{bmatrix} \in \mathbb{R}^{46\times1}, \quad U_{cl_{Rs}} = M_{ext}U_{ol} = \begin{bmatrix} u_1 \\ 0 \\ 0 \\ 0 \\ 0 \\ 0 \\ 0 \\ u_8 \\ 0 \\ 0 \\ 0 \\ 0 \\ 0 \\ 0 \end{bmatrix} \in \mathbb{R}^{14\times1}, \quad Y_{cl_{Rs}} = Y_{ol} \begin{bmatrix} y_1 \\ y_2 \\ y_3 \\ y_4 \\ y_4 \\ y_6 \\ y_7 \\ y_8 \\ y_9 \\ y_{10} \\ y_{11} \\ y_{12} \\ y_{13} \\ y_{14} \end{bmatrix} \in \mathbb{R}^{14\times1}$$

And the closed-loop matrices dimensions of the global space-state representation are,

$$A_{cl_{Rs}} \in \mathbb{R}^{46\times46}, \qquad B_{cl_{Rs}} \in \mathbb{R}^{46\times14},$$
$$C_{cl_{Rs}} \in \mathbb{R}^{14\times46}, \qquad D_{cl_{Rs}} \in \mathbb{R}^{14\times14}$$

Finally, the MIMO system of the Ranstad region can be expressed in a state-space representation point of view as,

$$\begin{aligned} \dot{X}_{cl_{Rs}} &= A_{cl_{Rs}} X_{cl_{Rs}} + B_{cl_{Rs}} U_{cl_{Rs}} \\ Y_{cl_{Rs}} &= C_{cl_{Rs}} X_{cl_{Rs}} + D_{cl_{Rs}} U_{cl_{Rs}} \end{aligned} \tag{5.1}$$

Where the subscript ***Rs*** stands for *Randstad*.

5.5. Randstad singular value decomposition

In the previous section, a state-space representation for the Randstad region was obtained an can be seen in 5.1. In order to obtain the transfer function matrix of the system, the theory of Section 4.3 is used. Therefore, the resultant transfer function matrix can be expressed as,

$$H_{cl_{Rs}}(s) = \frac{Y_{cl_{Rs}}(s)}{U_{cl_{Rs}}(s)} \tag{5.2}$$

$\boldsymbol{H_{cl_{Rs}}}$ is a 14×14 matrix, which links a certain input with a certain output of the system. However, not all the elements of the transfer function matrix are different from zero, some of them are zero due to the topology of the system. In Table A.6 can be seen which elements of $\boldsymbol{H_{cl_{Rs}}}$ have a non-zero value and which ones have a transfer function. The letter ***n*** indicates the degree of the characteristic polynomial of that specific transfer function.

The transfer function matrix $H_{cl_{Rs}}$ which has all the information of the Randstad region is going to be studied using the SVD. The next steps were followed,

1. A range of frequencies is previously defined. Within this range it is going to be observed the critical (harmonic) frequencies the system has. Thus, the selected frequency vector was $f = 1\ Hz$ to $f = 10\ kHz$, which is equally spaced.

2. The transfer function matrix $H_{cl_{Rs}}$ is going to be evaluated in each of these frequencies. Since $H_{cl_{Rs}}(s) = H_{cl_{Rs}}(j\omega)$, the elements in this matrix are going to show a complex behaviour. Therefore, it is necessary to obtain the absolute value of each complex component in $H_{cl_{Rs}}(j\omega)$.

3. The SVD is performed for every matrix $H_{cl_{Rs}}(j\omega)$ evaluated in the frequency vector. Thus, it is obtained a vector of matrices Σ containing the singular values for each frequency ω in the frequency vector.

The resultant singular values can be seen in Figure 5.5. As it was expected there are fourteen singular values curves that corresponds to each singular value matrix Σ.

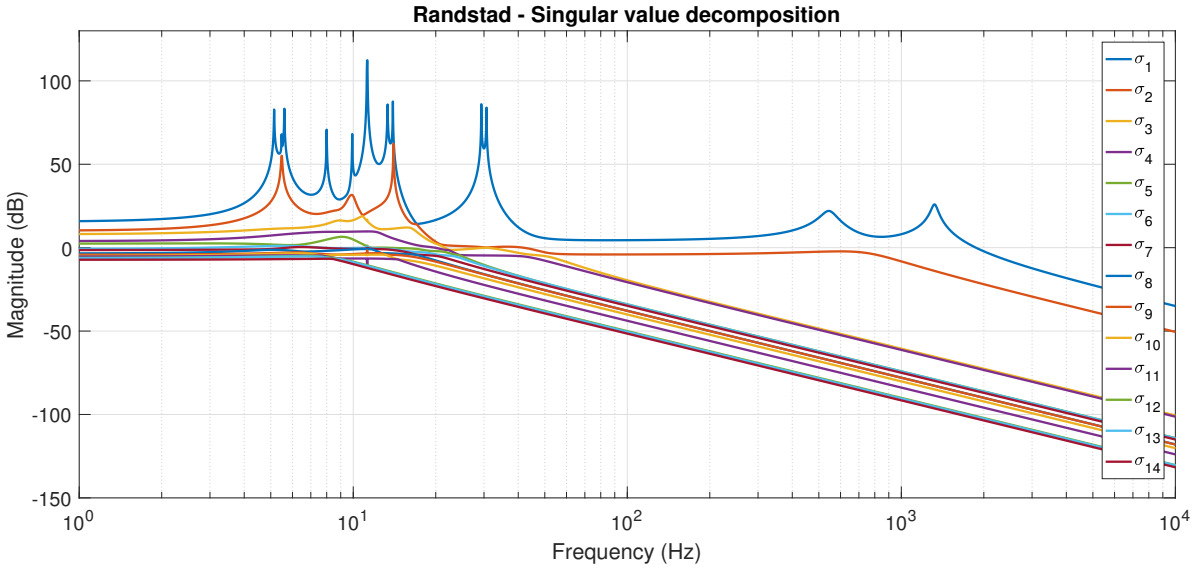

Figure 5.5: Randstad region singular value decomposition

As stated earlier in this chapter, the first singular value σ_1 has the highest gain and therefore it will have the bigger impact in the inputs and outputs of the system. In Figure 5.6 can be seen the curve of the first singular value. It can be noticed that there are twelve maximum peaks at certain frequencies. The frequencies where these peaks occur are of great interest for this research, since the vectors of the rotational matrices U and V^H associated with the first singular value can be studied and determine which inputs affect more the behaviour of certain outputs. These frequencies can be observed in Table 5.2.

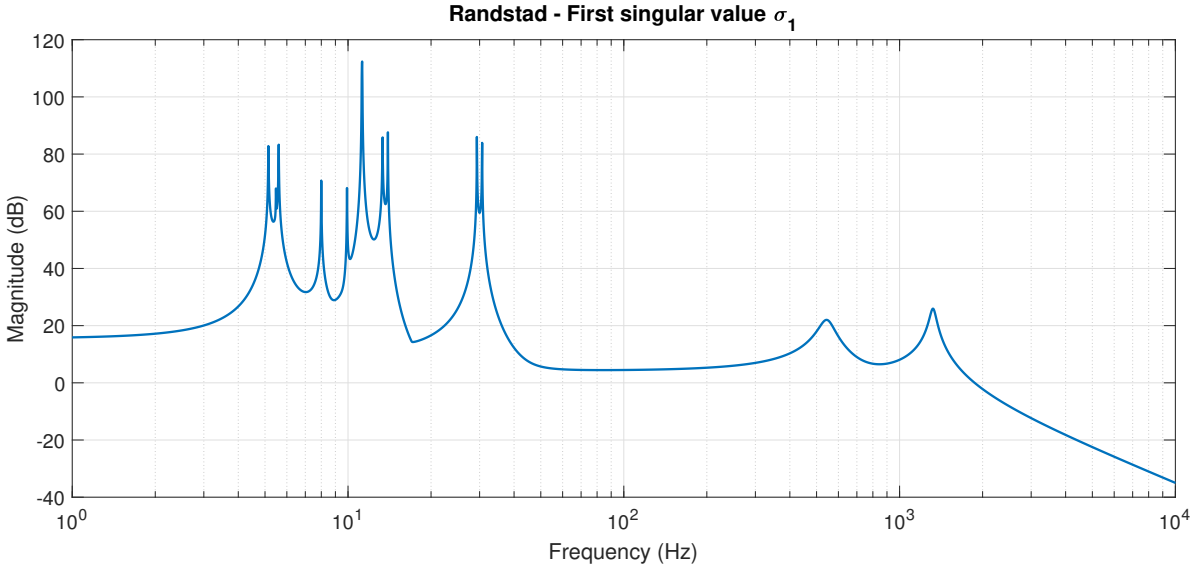

Figure 5.6: Randstad region first singular value

5.6. Randstad input and output assessment

In this section, an analysis of which input is going to have more influence in the system and which output is going to be the most affected is addressed. For that matter in Tables A.7 and A.8, the left and right singular vectors associated with the first singular value for the

frequencies listed in Table 5.2 are shown. In order to analyse these vectors, the frequency f_1 is going to be taken as an example. The right singular vector or the vector associated with the inputs of the system for the frequency f_1 is V_1^H. It can be noticed that the eighth element of this vector ($V_1^H(8,1)$) has the highest absolute value among the other components in this vector. This means that the input number 1, u_8 is going to have the biggest direction and will affect the system in a greater manner. On the other hand, when looking at the left singular vector or the vector associated with the outputs of the system, U_1, it can be seen that the fifth element ($U_1(5,1)$) has the highest absolute value among the other components in the vector. Therefore, the output that will be more affected by the this input is going to be the fifth output, y_5.

Table 5.2: Randstad region harmonic frequencies

σ_1 (dB)	Frequency (Hz)
82.8058	5.1432
67.9747	5.4795
83.2872	5.6071
70.6988	7.9971
68.1276	9.9148
112.3707	11.2536
85.8286	13.3497
87.6124	13.9522
85.9835	29.3222
83.9243	30.6455
22.0145	550
25.9352	1300

A similar analysis can be done with the corresponding singular vectors at frequency f_{12}. The right singular value vector shows a maximum absolute value in its eleventh component ($V_{12}^H(11,1)$), followed by the sixth component ($V_{12}^H(6,1)$). However, the system only has inputs different from zero in the first (u_1) and eighth (u_8) components, and since the other directions are zero the direction that affects more the outputs is the one in the first component ($V_{12}^H(1,1)$). From the corresponding left singular vector (U_{12}), it can be clearly seen that the direction that affect the most the input is the one in the eleventh component ($U_{12}(11,1)$). Therefore, output y_{11} is the most affected.

In order to visualise the impact of the first singular value (σ_1) on the response of the Randstad region, a sinusoidal signal with the critical harmonic frequencies are injected at the inputs.

Following the analysis derived in Section 4.4, a sinusoidal input of the form,

$$d_{Rd} = d_0(\cos(\omega t + \alpha) + j\sin(\omega t + \alpha)) \tag{5.3}$$

is applied as input in u_1 and u_8 of the Randstad region transfer function matrix. The magnitude d_0 is chosen as 1, the phase shift is 0 and the frequency ω will take the frequency values of Table 5.2.

When a sinusoidal signal with the first frequency $f_1 = 5.14\,Hz$ is injected to the system at the first and eighth inputs corresponding to the Hollandse Kust Nord and South wind parks,

the output that will be the most affected in terms of voltage increment is the output y_5, that corresponds to the voltage at the Krimpen aan den IJssel (KIJ) substation. In Figure 5.7 can be seen that when injecting a voltage with a magnitude of $1\ p.u.$, the voltage at output y_5 increases to approximately $7.6\ p.u.$ and the oscillation behaviour that presents is persistent. The same behaviour will present the outputs y_5, y_3 and y_6 when injecting a sinusoidal with a frequency of $f_3 = 5.60\ Hz$, $f_7 = 13.34\ Hz$, $f_{10} = 30.64\ Hz$, respectively.

Another frequency of interest is $f_4 = 7.99\ Hz$, if a sinusoidal with this frequency is injected to the Randstad system, the output voltage that presents the higher increment is $y = 6$, that corresponds to the voltage at the Beverwijk substation. In Figure 5.8 can be seen that the increment has a maximum of $1.4\ p.u.$, and the oscillation behaviour is sustained. A similar behaviour present the output voltages y_5, y_6 when is injected a sinusoidal with the frequencies $f_2 = 5.4\ Hz$, $f_5 = 9.91\ Hz$, respectively.

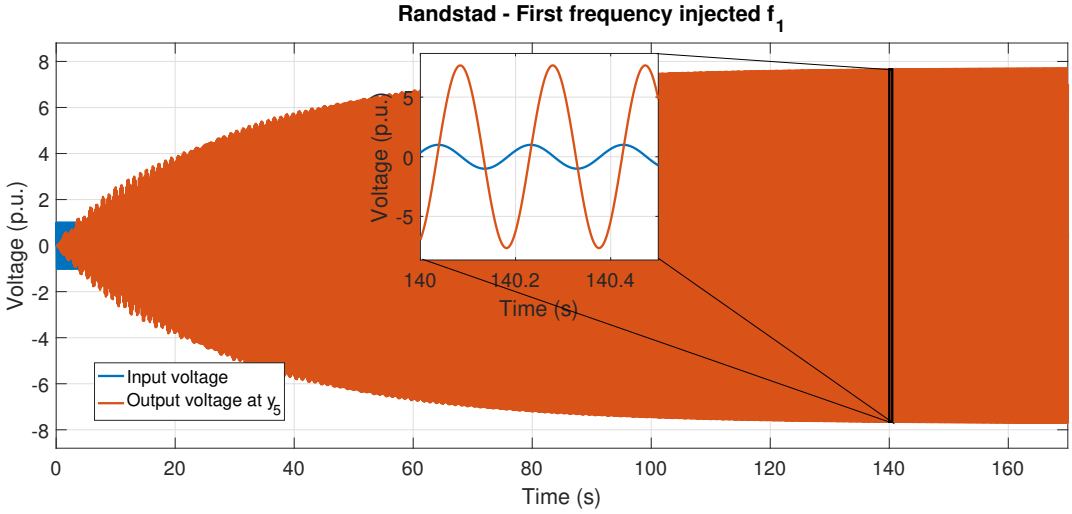

Figure 5.7: Randstad first frequency injected in inputs u_1 and u_8

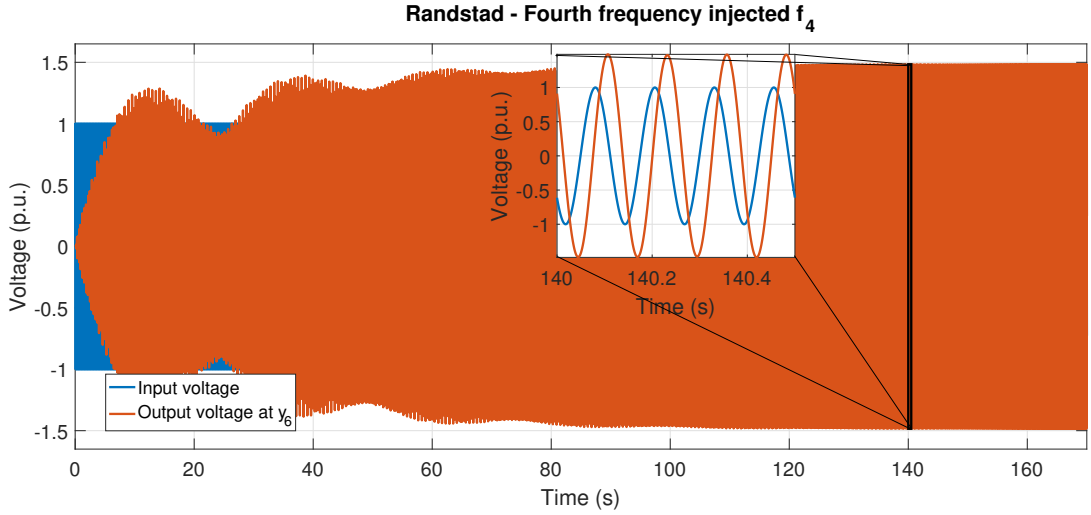

Figure 5.8: Randstad fourth frequency injected in inputs u_1 and u_8

The most critical frequency is $f_6 = 11.25\ Hz$. At this frequency the singular value decomposition presents the higher magnitude, as it can be seen in Figure 5.6. When injecting a sinusoidal with this frequency at the inputs of the system, the most affected output is y_6,

which is the voltage at the Krimpen aan den IJssel (KIJ) substation. The increment of the voltage is $27.8\ p.u.$.

In Figure 5.6 can be seen two frequencies beyond $50\,Hz$, this two frequencies corresponds to the two underground cables that exists in the Randstad region. The time-domain simulation for these frequencies have a different behaviour than those below $50\ Hz$. In Figure 5.10 can be seen the time-domain simulation when a sinusoidal with a frequency of $f_{11} = 550\ Hz$ is injected to the system. In this case, the most affected output is y_6, that corresponds to the voltage at the Beverwijk substation. It can be noticed that the voltage amplification increases really fast in the first seconds of the simulations, in contrast to the previous time-domain simulations where the voltage increases gradually with time. Then, the voltage starts to decrease and after a while it settles to $0.71\ p.u.$ and maintains this value through the rest of the simulation.

In Table 5.3 are summarised the injected sinusoidal signals with the respective harmonic frequency and the substation of the most affected transmission line or underground cable.

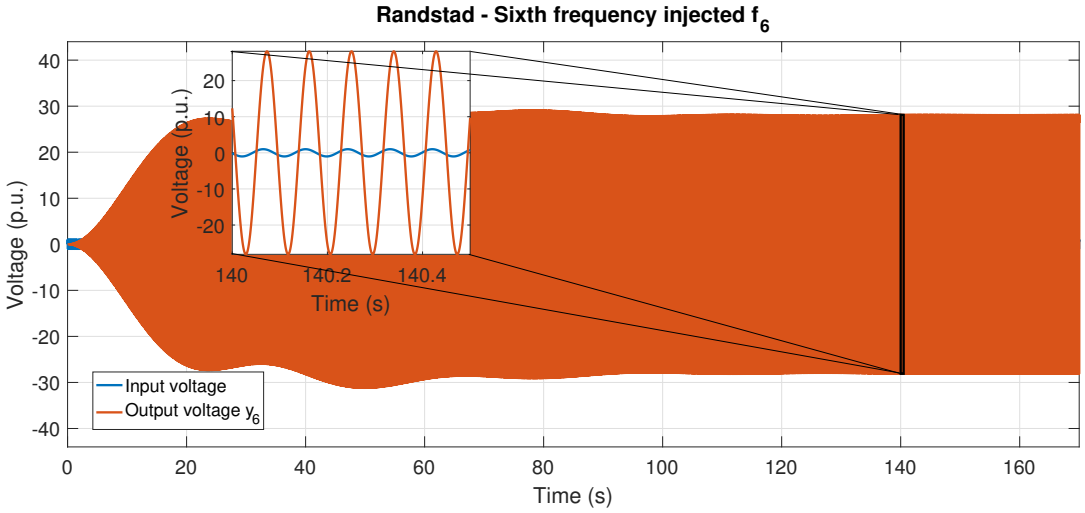

Figure 5.9: Randstad sixth frequency injected in inputs u_1 and u_8

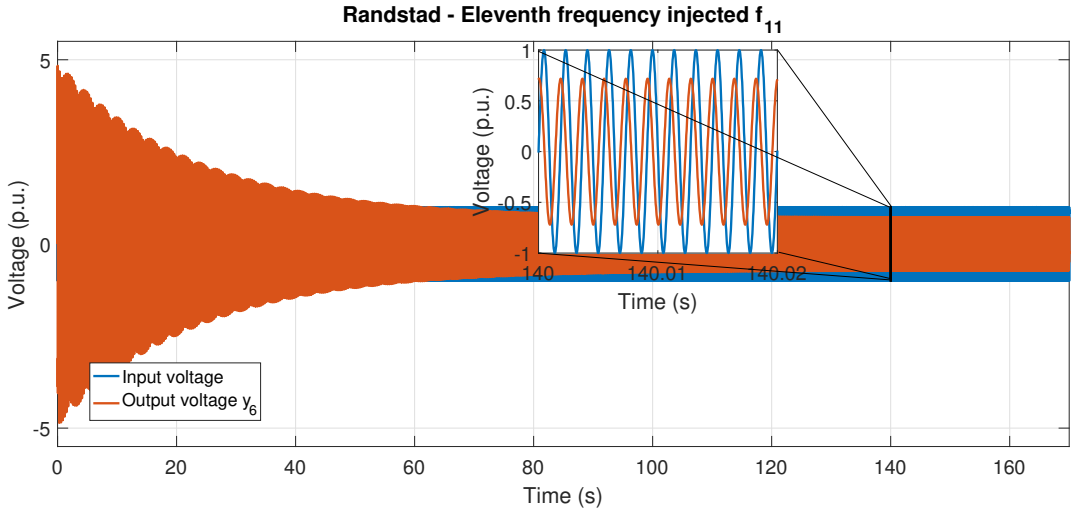

Figure 5.10: Randstad eleventh frequency injected in inputs u_1 and u_8

Table 5.3: Randstad region most affected elements

Injected frequency f_i	Input affecting the system the most u_i	Most affected output y_i	Transmission line or underground cable
5.1432	u_8 - HKZ	y_5	BWK to KIJ - Voltage at KIJ
5.4795	u_1 - HKN	y_5	BWK to KIJ - Voltage at KIJ
5.6071	u_8 - HKZ	y_5	BWK to KIJ - Voltage at KIJ
7.9971	u_8 - HKZ	y_6	VHZ to BWK - Voltage at BWK
9.9148	u_1 - HKN	y_6	VHZ to BWK - Voltage at BWK
11.2536	u_1 - HKN	y_6	VHZ to BWK - Voltage at BWK
13.3497	u_1 - HKN	y_3	DIM to BKK - Voltage at BKK
13.9522	u_1 - HKN	y_3	DIM to BKK - Voltage at BKK
29.3222	u_8 - HKZ	y_6	VHZ to BWK - Voltage at BWK
30.6455	u_8 - HKZ	y_6	VHZ to BWK - Voltage at BWK
550	u_1 - HKN	y_6	VHZ to BWK - Voltage at BWK
1300	u_1 - HKN	y_{11}	WTR to BWK - Voltage at BWK

5.7. Randstad sensitivity analysis

In this section, an analysis on the variation of the length of the transmission lines and the underground cables is performed. The first task to achieve is to variate only the length of the transmission lines in order to observe if the frequencies induced by the underground cables are influenced by this variation. The second task is to do the opposite, the length of the underground cables are going to be varied, in order to observe if the frequencies induced by the transmission lines are affected.

On one hand, in Figure 5.11 and 5.12 can be seen the harmonic response of the Randstad region when the length of the transmission lines is varied. At first sight, it can be noticed that the frequencies induced by the transmission lines, which are those in the range from $0\,Hz$ to $50\,Hz$, shift to higher frequencies when the lines is shorter. Meaning that the shorter the line, the higher the frequencies the system is going to present. Then, when the length is increased the harmonic frequencies shift to lower frequencies. The frequencies related to the underground cables, which are those in the range from $100\,Hz$ to $1500\,Hz$, does not present any change at all. In both cases the magnitude of the frequencies does not increase nor decrease.

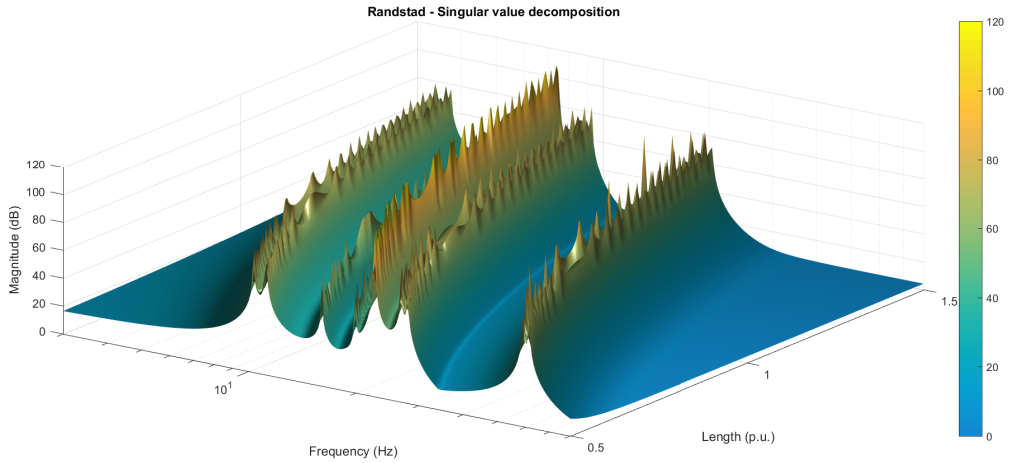

Figure 5.11: Transmission line length variation (1)

On the other hand, in Figure 5.13 and 5.14 can be seen the Randstad harmonic response when the length of the underground cables is varied. It can be observed that the frequen-

cies related to the transmission lines do not present any perceptible change. However, the frequencies related to the underground cables does present a change. First, when the length is decreased the frequencies tend to move to lower frequencies. Then, when the length is increased the frequencies tend to move to higher values. Moreover, they increase their magnitude a little, as it can be seen in Figure 5.14, where the magnitude of the frequencies present a light green colour.

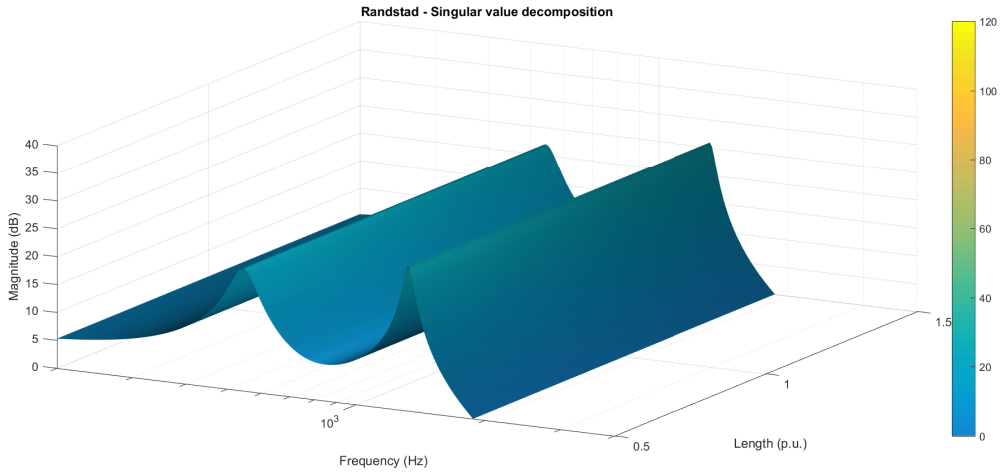

Figure 5.12: Transmission line length variation (2)

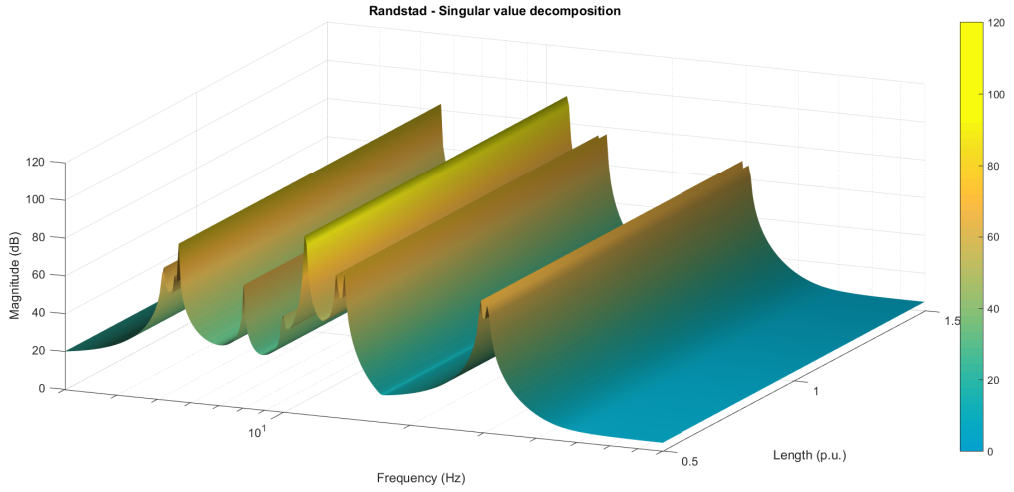

Figure 5.13: Underground cable length variation (1)

Performing this analysis can be observed that the transmission line that shows the highest impact in the observed harmonics, in terms of magnitude, is the transmission line that lies between the *Diemen* and the *Breukelen Kortrijk* substations. This transmission line has the input u_3 and the output y_3. To this transmission line is associated the frequency number eleven f_{11}, which in Table 5.2 depicts the highest magnitude in the system. It was seen in this sensitivity analysis that the frequencies associated to this transmission line always depicts the highest amplitude. Therefore, this is the most critical frequency in the Randstad region because it will present the highest voltage increment when injected to the system.

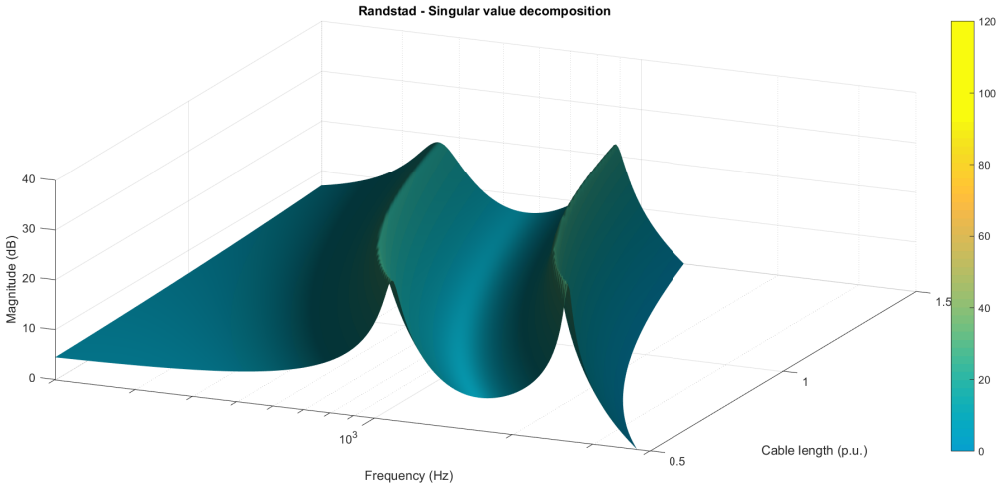

Figure 5.14: Underground cable length variation (2)

6

Conclusions and recommendations

This chapter contains the main conclusions that can be drawn from the research developed in the previous chapters. It also contains the answers to the research questions presented in Chapter 1. Finally, recommendations and future work are also discussed.

6.1. Conclusions

In the present work the harmonic frequencies of an electrical power system were obtained when the system is modelled in a MIMO point of view. A representation of the system in this way is necessary because a power system has many voltage injections and injects many voltage signals. The classical methods are not suitable for the study of a MIMO system since they only take into account SISO representations of a power system.

It was seen that the singular value decomposition is useful to find the harmonic frequencies of the system. Moreover, this tool is helpful to asses the voltage input that affect the system the most and the voltage output that is the most affected by that input. This can be seen in the time-domain simulations when a certain harmonic frequency is injected to the system. The most affected output will present an increment in terms of voltage magnitude and will show sustained oscillations.

The main conclusions derived from the present work are:

1. It is possible to represent the elements of a transmission power system as linear-time-invariant systems and represent them in a state-space representation.
2. A methodology can be developed to concatenate the state-space representation of each element in the transmission power system, and represent it as a multiple-input multiple-output system.
3. The dynamics of the multiple-input multiple-output system can be expressed in time domain via the state-space representation and in frequency domain via the transfer function matrix of the system.
4. It is possible to obtain the harmonic frequencies of the transmission power system represented as a MIMO system, using the singular value decomposition.
5. Using this mathematical tool, an input-output analysis can be performed to assess which element of the MIMO system is the most affected by a certain harmonic frequency.

6.2. Answers to research questions

The answers to the research questions of Chapter 1 are summarised as follows:

1. **How to derive a model of a transmission electrical power system to asses the harmonic response by considering a multiple-input multiple-output point of view?**

   There are two ways of building a MIMO system. The first one, is to obtain each differential equation describing the dynamics of the system under study. Then, choose the relevant states of the system and build the state-space matrices. It is important to point out that the more inputs and outputs the system has, the more difficult is to obtain the differential equations. The second way is to obtain the single-input single-output (SISO) representation of each element in the transmission power system and then, concatenate each representation to obtain a MIMO system. In order to perform the latter a methodology to connect each SISO state-space representation is needed. The last approach was used in this research, not only to concatenate the SISO representations, but to depict the system in time domain and frequency domain. The latter is necessary to answer the next research question.

2. **How to analytically determine the influence of harmonic voltage injections on the harmonic performance observed in different buses of a transmission electrical power system?**

   In order to obtain the harmonic performance of a transmission power system which is modelled as a MIMO system, a mathematical tool called singular value decomposition can be used. As stated earlier in this chapter, this tool has been used in many transmission power related studies, and in the present work is discussed whether it can be useful to show the harmonic response of a determined transmission system or not. The analysis developed in the chapters of the present work has shown that not only the harmonic response of a transmission power system can be easily extracted, this tool is also useful to determine which output of the system is being affected the most, and which input has more influence in the dynamics of the system.

6.3. Future work recommendations

Although a lot of researchers have used the singular value decomposition for the study of transmission power systems, the use of this tool to analyse their harmonic response is still under study. Therefore, some suggestions that can be followed to improve the study of this topic can be pointed out:

1. Include a state-space representation of the harmonic elements of a certain wind turbine. This can be achieved by performing a Fourier analysis of the voltage signal extracted from the turbine and find a linear-time-invariant representation of the harmonic content found by the Fourier analysis.

2. A more detailed state-space representation of the elements of the transmission power system can be used. In the present work, PI sections and fitted PI sections were used to describe the transmission lines and underground cables, respectively. However, transient and frequency-dependent models can also be studied and used [27].

3. Consider more elements of the transmission power system to concatenate, such as, three phase transformers, generators, stabilisers, governors. However, it is important to point out that the higher the elements to be concatenated, the bigger the computational effort is.

4. An unbalanced transmission line or underground cable representation can be used to study the harmonic response of the system.

A

Relevant information tables

In this appendix the tables that contain an enormous amount of relevant information from the chapters included in this thesis are presented.

Table A.1: Transmission lines electric parameters

Number	Transmission Line	V_{base} $[kV]$	S_{base} $[MVA]$	Length $[km]$	R $[\Omega]$	L $[H]$	C $[\mu F]$
1	Beverwijk to Oostzaan	380	1908.7	15.9	0.0194	0.2280	624.36
2	Oostzaan to Diemen	380	1908.7	15.2	0.0186	0.2180	596.87
3	Diemen to Breukelen Kortrijk	380	1645.4	18.83	0.0268	0.3133	637.48
4	Breukelen Kortrijk to Krimpen aan den IJssel	380	1645.4	1	0.0549	0.6438	1309.93
5	Krimpen aan den IJssel to Bleiswijk	380	2632.7	18.560	0.0108	0.1717	1171.31
6	Bleiswijk to Vijfhuizen	380	1974.5	47.3	0.0473	0.6151	6401.605
7	Vijfhuizen to Beverwijk	380	1974.5	12.1	0.0121	0.1574	1637.64
8	Maasvlakte to Terminal SP	380	2632.7	1	0.0101	0.1815	4442.68
9	Terminal SP to Westerlee	380	2650.0	1	0.000381	0.3207	91.759
10	Westerlee to Wateringen	380	2632.7	6.8	0.0039	0.0631	427.72
11	Wateringen to Bleiswijk	380	2632.7	1	0.0181	0.1387	21363.33
12	Maasvlakte to Simonshaven	380	2632.7	26	0.0151	0.2394	1654.09
13	Simonshaven to Crayestein	380	2632.7	40.43	0.0235	0.3722	2572.16
14	Crayestein to Krimpen aan den Ijssel	380	2632.7	14.84	0.0086	0.1366	943.78

Table A.2: Interconnection Matrix M_{int}. Systems 1 to 7

		BVW to OZN L1	**OZN to DIM L2**	**DIM to BKK L3**	**BKK to KIJ L4**	**KIJ to BWK L5**	**BWK to VHZ L6**	**VHZ to BVW L7**
		y_1	y_2	y_3	y_4	y_5	y_6	y_7
BVW to OZN L1	u_1	0	0	0	0	0	0	0
OZN to DIM L2	u_2	**1**	0	0	0	0	0	0
DIM to BKK L3	u_3	0	**1**	0	0	0	0	0
BKK to KIJ L4	u_4	0	0	**1**	0	0	0	0
KIJ to BWK L5	u_5	0	0	0	**1**	0	0	0
BWK to VHZ L6	u_6	0	0	0	0	**1**	0	**1**
VHZ to BVW L7	u_7	**1**	0	0	0	0	0	0
MVL to SP L8	u_8	0	0	0	0	0	0	0
SP to WL L9	u_9	0	0	0	0	0	0	0
WL to WTR L10	u_{10}	0	0	0	0	0	0	0
WTR to BWK L11	u_{11}	0	0	0	0	0	0	0
MVL to SMH L12	u_{12}	0	0	0	0	0	0	0
SMH to CST L13	u_{13}	0	0	0	0	0	0	0
CST to KIJ L14	u_{14}	0	0	0	0	0	0	0

Table A.3: Interconnection Matrix M_{int}. Systems 8 to 14

		MVL to SP L8	**SP to WL L9**	**WL to WTR L10**	**WTR to BWK L11**	**MVL to SMH L12**	**SMH to CST L13**	**CST to KIJ L14**
		y_8	y_9	y_{10}	y_{11}	y_{12}	y_{13}	y_{14}
BVW to OZN L1	u_1	0	0	0	0	0	0	0
OZN to DIM L2	u_2	0	0	0	0	0	0	0
DIM to BKK L3	u_3	0	0	0	0	0	0	0
BKK to KIJ L4	u_4	0	0	0	0	0	0	0
KIJ to BWK L5	u_5	0	0	0	0	0	0	**1**
BWK to VHZ L6	u_6	0	0	0	**1**	0	0	0
VHZ to BVW L7	u_7	0	0	0	0	0	0	0
MVL to SP L8	u_8	0	0	0	0	0	0	0
SP to WL L9	u_9	**1**	0	0	0	0	0	0
WL to WTR L10	u_{10}	0	**1**	0	0	0	0	0
WTR to BWK L11	u_{11}	0	0	**1**	0	0	0	0
MVL to SMH L12	u_{12}	**1**	0	0	0	0	0	0
SMH to CST L13	u_{13}	0	0	0	0	**1**	0	0
CST to KIJ L14	u_{14}	0	0	0	0	0	**1**	0

Table A.4: External Matrix M_{ext}. Systems 1 to 7

		BVW to OZN L1	**OZN to DIM L2**	**DIM to BKK L3**	**BKK to KIJ L4**	**KIJ to BWK L5**	**BWK to VHZ L6**	**VHZ to BVW L7**
		y_1	y_2	y_3	y_4	y_5	y_6	y_7
BVW to OZN L1	u_1	**1**	0	0	0	0	0	0
OZN to DIM L2	u_2	0	0	0	0	0	0	0
DIM to BKK L3	u_3	0	0	0	0	0	0	0
BKK to KIJ L4	u_4	0	0	0	0	0	0	0
KIJ to BWK L5	u_5	0	0	0	0	0	0	0
BWK to VHZ L6	u_6	0	0	0	0	0	0	0
VHZ to BVW L7	u_7	0	0	0	0	0	0	0
MVL to SP L8	u_8	0	0	0	0	0	0	0
SP to WL L9	u_9	0	0	0	0	0	0	0
WL to WTR L10	u_{10}	0	0	0	0	0	0	0
WTR to BWK L11	u_{11}	0	0	0	0	0	0	0
MVL to SMH L12	u_{12}	0	0	0	0	0	0	0
SMH to CST L13	u_{13}	0	0	0	0	0	0	0
CST to KIJ L14	u_{14}	0	0	0	0	0	0	0

Table A.5: External Matrix M_{ext}. Systems 8 to 14

		MVL to SP L8	**SP to WL L9**	**WL to WTR L10**	**WTR to BWK L11**	**MVL to SMH L12**	**SMH to CST L13**	**CST to KIJ L14**
		y_8	y_9	y_{10}	y_{11}	y_{12}	y_{13}	y_{14}
BVW to OZN L1	u_1	0	0	0	0	0	0	0
OZN to DIM L2	u_2	0	0	0	0	0	0	0
DIM to BKK L3	u_3	0	0	0	0	0	0	0
BKK to KIJ L4	u_4	0	0	0	0	0	0	0
KIJ to BWK L5	u_5	0	0	0	0	0	0	0
BWK to VHZ L6	u_6	0	0	0	0	0	0	0
VHZ to BVW L7	u_7	0	0	0	0	0	0	0
MVL to SP L8	u_8	**1**	0	0	0	0	0	0
SP to WL L9	u_9	0	0	0	0	0	0	0
WL to WTR L10	u_{10}	0	0	0	0	0	0	0
WTR to BWK L11	u_{11}	0	0	0	0	0	0	0
MVL to SMH L12	u_{12}	0	0	0	0	0	0	0
SMH to CST L13	u_{13}	0	0	0	0	0	0	0
CST to KIJ L14	u_{14}	0	0	0	0	0	0	0

Table A.6: Transfer function matrix $H_{cl_{Rs}}$

	u_1	u_2	u_3	u_4	u_5	u_6	u_7	u_8	u_9	u_{10}	u_{11}	u_{12}	u_{13}	u_{14}
y_1	$\frac{y_1(s)}{u_1(s)}$ $n=3$	0	0	0	0	0	0	0	0	0	0	0	0	0
y_2	$\frac{y_2(s)}{u_1(s)}$ $n=6$	$\frac{y_2(s)}{u_2(s)}$ $n=3$	0	0	0	0	0	0	0	0	0	0	0	0
y_3	$\frac{y_3(s)}{u_1(s)}$ $n=9$	$\frac{y_3(s)}{u_2(s)}$ $n=6$	$\frac{y_3(s)}{u_3(s)}$ $n=3$	0	0	0	0	0	0	0	0	0	0	0
y_4	$\frac{y_4(s)}{u_1(s)}$ $n=12$	$\frac{y_4(s)}{u_2(s)}$ $n=9$	$\frac{y_4(s)}{u_3(s)}$ $n=6$	$\frac{y_4(s)}{u_4(s)}$ $n=3$	0	0	0	0	0	0	0	0	0	0
y_5	$\frac{y_5(s)}{u_1(s)}$ $n=15$	$\frac{y_5(s)}{u_2(s)}$ $n=12$	$\frac{y_5(s)}{u_3(s)}$ $n=9$	$\frac{y_5(s)}{u_4(s)}$ $n=6$	$\frac{y_5(s)}{u_5(s)}$ $n=3$	0	0	$\frac{y_5(s)}{u_8(s)}$ $n=15$	0	0	0	$\frac{y_5(s)}{u_{12}(s)}$ $n=12$	$\frac{y_5(s)}{u_{13}(s)}$ $n=9$	$\frac{y_5(s)}{u_{14}(s)}$ $n=6$
y_6	$\frac{y_6(s)}{u_1(s)}$ $n=23$	$\frac{y_6(s)}{u_2(s)}$ $n=17$	$\frac{y_6(s)}{u_3(s)}$ $n=14$	$\frac{y_6(s)}{u_4(s)}$ $n=11$	$\frac{y_6(s)}{u_5(s)}$ $n=8$	$\frac{y_6(s)}{u_6(s)}$ $n=5$	$\frac{y_6(s)}{u_7(s)}$ $n=8$	$\frac{y_6(s)}{u_8(s)}$ $n=31$	$\frac{y_6(s)}{u_9(s)}$ $n=16$	$\frac{y_6(s)}{u_{10}(s)}$ $n=13$	$\frac{y_6(s)}{u_{11}(s)}$ $n=10$	$\frac{y_6(s)}{u_{12}(s)}$ $n=17$	$\frac{y_6(s)}{u_{13}(s)}$ $n=14$	$\frac{y_6(s)}{u_{14}(s)}$ $n=11$
y_7	$\frac{y_7(s)}{u_1(s)}$ $n=6$	0	0	0	0	0	$\frac{y_7(s)}{u_7(s)}$ $n=3$	0	0	0	0	0	0	0
y_8	0	0	0	0	0	0	0	$\frac{y_8(s)}{u_8(s)}$ $n=3$	0	0	0	0	0	0
y_9	0	0	0	0	0	0	0	$\frac{y_9(s)}{u_8(s)}$ $n=6$	$\frac{y_9(s)}{u_9(s)}$ $n=3$	0	0	0	0	0
y_{10}	0	0	0	0	0	0	0	$\frac{y_{10}(s)}{u_8 s)}$ $n=9$	$\frac{y_{10}(s)}{u_9(s)}$ $n=6$	$\frac{y_{10}(s)}{u_{10}(s)}$ $n=3$	0	0	0	0
y_{11}	0	0	0	0	0	0	0	$\frac{y_{11}(s)}{u_8(s)}$ $n=14$	$\frac{y_{11}(s)}{u_9(s)}$ $n=11$	$\frac{y_{11}(s)}{u_{10}(s)}$ $n=8$	$\frac{y_{11}(s)}{u_{11}(s)}$ $n=5$	0	0	0
y_{12}	0	0	0	0	0	0	0	$\frac{y_{12}(s)}{u_8(s)}$ $n=6$	0	0	0	$\frac{y_{12}(s)}{u_{12}(s)}$ $n=3$	0	0
y_{13}	0	0	0	0	0	0	0	$\frac{y_{13}(s)}{u_8(s)}$ $n=9$	0	0	0	$\frac{y_{13}(s)}{u_{12}(s)}$ $n=6$	$\frac{y_{13}(s)}{u_{13}(s)}$ $n=3$	0
y_{14}	0	0	0	0	0	0	0	$\frac{y_{14}(s)}{u_8(s)}$ $n=12$	0	0	0	$\frac{y_{14}(s)}{u_{12}(s)}$ $n=9$	$\frac{y_{14}(s)}{u_{13}(s)}$ $n=6$	$\frac{y_{14}(s)}{u_{14}(s)}$ $n=3$

Table A.7: Randstad left singular vectors associated to the outputs of the system

Frequency (Hz)											
f_1	f_2	f_3	f_4	f_5	f_6	f_7	f_8	f_9	f_{10}	f_{11}	f_{12}
5.1432	5.4795	5.6071	7.9971	9.9148	11.2536	13.3497	13.9522	29.3222	30.6455	550	1300
Left singular vectors											
U_1	U_2	U_3	U_4	U_5	U_6	U_7	U_8	U_9	U_{10}	U_{11}	U_{12}
0.0000	-0.0003	0.0000	0.0000	-0.0008	0.0000	-0.0260	-0.0004	0.0000	0.0000	0.0000	0.0000
0.0000	-0.0006	0.0000	0.0000	-0.0016	0.0000	-0.3082	-0.4306	0.0000	0.0000	0.0000	0.0000
0.0000	-0.0010	0.0000	0.0000	-0.0072	-0.0132	-0.7606	-0.8050	0.0000	0.0000	0.0000	0.0000
-0.0001	-0.4449	0.0000	0.0000	-0.0032	-0.0041	-0.1542	-0.1469	0.0000	0.0000	0.0000	0.0000
-0.5701	-0.6333	-0.5907	-0.6232	-0.0145	-0.7066	-0.3713	-0.2691	0.0000	0.0000	0.0000	0.0000
-0.5681	-0.6312	-0.5527	-0.6236	-0.7087	-0.7075	-0.4039	-0.2695	-0.5787	-0.5795	-0.9973	0.2013
0.0000	-0.0004	0.0000	0.0000	-0.7053	0.0000	-0.0320	-0.0004	0.0000	0.0000	0.0000	0.0000
-0.0021	-0.0023	-0.0357	-0.0002	0.0000	0.0000	0.0000	0.0000	0.0000	0.0000	0.0000	0.0000
-0.0022	-0.0023	-0.0370	-0.0002	0.0000	0.0000	0.0000	0.0000	-0.0480	-0.0007	0.0000	0.0000
-0.0023	-0.0024	-0.0383	-0.0002	0.0000	0.0000	0.0000	0.0000	-0.5754	-0.5760	0.0000	0.0000
-0.0023	-0.0024	-0.0383	-0.0002	0.0000	0.0000	0.0000	0.0000	-0.5759	-0.5765	-0.0736	0.9795
-0.0037	-0.0043	-0.0701	-0.2932	0.0000	0.0000	0.0000	0.0000	0.0000	0.0000	0.0000	0.0000
-0.3880	-0.0317	-0.3723	-0.2069	0.0000	0.0000	0.0000	0.0000	0.0000	0.0000	0.0000	0.0000
-0.4491	-0.0374	-0.4432	-0.3067	0.0000	0.0000	0.0000	0.0000	0.0000	0.0000	0.0000	0.0000

Table A.8: Randstad right singular vectors associated to the inputs of the system

Frequency (Hz)											
f_1	f_2	f_3	f_4	f_5	f_6	f_7	f_8	f_9	f_{10}	f_{11}	f_{12}
5.1432	5.4795	5.6071	7.9971	9.9148	11.2536	13.3497	13.9522	29.3222	30.6455	550	1300
Right singular vectors											
V_1^H	V_2^H	V_3^H	V_4^H	V_5^H	V_6^H	V_7^H	V_8^H	V_9^H	V_{10}^H	V_{11}^H	V_{12}^H
-0.001568	-0.615546	-0.004225	-0.002257	-0.913139	-0.956420	-0.999998	-0.995592	-0.000001	-0.000001	0.000000	0.001200
-0.001278	-0.511621	-0.003534	-0.001967	-0.005148	-0.275652	-0.001936	-0.093687	0.000000	0.000000	0.000000	0.000000
-0.001105	-0.432700	-0.002963	-0.001321	-0.002548	-0.096298	-0.000148	-0.000079	0.000000	0.000000	0.000000	0.000000
-0.000874	-0.330261	-0.002228	-0.000655	-0.000570	-0.000183	-0.000021	-0.000009	0.000000	0.000000	0.000000	0.000000
-0.000104	-0.000663	-0.000104	-0.000739	-0.001295	-0.000588	-0.000096	-0.000041	-0.000005	-0.000006	-0.000271	0.000000
-0.000041	-0.000252	-0.000038	-0.000182	-0.000278	-0.000002	-0.000021	-0.000011	-0.000029	-0.000037	-0.635726	0.002089
-0.000056	-0.000363	-0.000056	-0.000521	-0.407591	-0.000006	-0.000027	-0.000011	-0.000004	-0.000004	-0.000212	0.000000
-0.983644	-0.250757	-0.999976	-0.694521	-0.001000	-0.000146	-0.000015	-0.000061	-0.037896	-0.034445	0.000000	0.000000
-0.000044	-0.000273	-0.000049	-0.000211	-0.000351	-0.000002	-0.000032	-0.000018	-0.999281	-0.995280	-0.000007	0.000000
-0.000042	-0.000262	-0.000045	-0.000196	-0.000311	-0.000002	-0.000026	-0.000014	-0.001043	-0.090721	-0.002462	0.000538
-0.000041	-0.000253	-0.000040	-0.000182	-0.000278	-0.000002	-0.000021	-0.000011	-0.000058	-0.000074	-0.771910	0.999998
-0.155358	-0.011365	-0.001951	-0.719462	-0.001778	-0.000446	-0.000100	-0.000334	0.000000	0.000000	0.000000	0.000000
-0.091122	-0.006030	-0.000987	-0.000910	-0.000954	-0.000437	-0.000179	-0.000683	0.000000	0.000000	0.000000	0.000000
-0.000158	-0.000800	-0.000160	-0.001229	-0.002590	-0.001654	-0.001025	-0.004342	-0.000001	-0.000002	0.000000	0.000000

B

Matlab routines

In the next lines, the routines for the *small size test system* and the synthetic Randstad region system is presented.

B.1. *Small size test system* routine

```
clc;clear variables;
%% Common values
sizesys = 3;
Vbase = 380e3;
ri = 1e-3;

%% Transmission lines - TL1
Sbase1 = 1908.7e6;
Zbase1 = (Vbase^2)/Sbase1;

l_1 = 15.9;

Z1 = ((0.000257+0.003014*i)*Zbase1)/15.9;
B1 = (0.094470/Zbase1)/15.9;

R1 = real(Z1)*l_1;
L1 = imag(Z1)*l_1;
C1_1 = (B1/2)*l_1;
C2_1 = (B1/2)*l_1;

A1 = [-R1/L1 1/L1 -1/L1; -1/C1_1 -1/(ri*C1_1) 0; 1/C2_1 0 0];
B1 = [0; 1/(ri*C1_1); 0];
C1 = [0 0 1];
D1 = 0;

syms u1 y1 i_L_1 V_C1_1 V_C2_1

x1 = [i_L_1; V_C1_1; V_C2_1];

%% TL2
```

```
Sbase2 = 1974.5e6;
Zbase2 = (Vbase^2)/Sbase2;

l_2 = 12.1;

Z2 = ((0.000166+0.002152*i)*Zbase2)/12.1;
B2 = (0.239530/Zbase2)/12.1;

R2 = real(Z2)*l_2;
L2 = imag(Z2)*l_2;
C1_2 = (B2/2)*l_2;
C2_2 = (B2/2)*l_2;

A2 = [-R2/L2 1/L2 -1/L2; -1/C1_2 -1/(ri*C1_2) 0; 1/C2_2 0 0];
B2 = [0; 1/(ri*C1_2); 0];
C2 = [0 0 1];
D2 = 0;

syms u2 y2 i_L_2 V_C1_2 V_C2_2

x2 = [i_L_2; V_C1_2; V_C2_2];

%% Underground cable - C1
l_3 = 48.7;
rz1_3 = (1.1724e-1)*l_3; rz2_3 = (8.2072e-2)*l_3; rz3_3 = (1.1946e
    -2)*l_3;
Lz1_3 = (2.2851e-4)*l_3; Lz2_3 = (1.5522e-3)*l_3; Lz3_3 = (3.2942e
    -3)*l_3;
Cc_3 = (1.9083e-7)*l_3;

A3 = [-rz1_3/Lz1_3 0 0 1/Lz1_3 -1/Lz1_3;...
     0 -rz2_3/Lz2_3 0 1/Lz2_3 -1/Lz2_3;...
     0 0 rz3_3/Lz3_3 1/Lz3_3 -1/Lz3_3;...
     -1/Cc_3 -1/Cc_3 -1/Cc_3 -1/(ri*Cc_3) 0;...
     1/Cc_3 1/Cc_3 1/Cc_3 0 0];
B3 = [0; 0; 0; 1/(ri*Cc_3); 0];
C3 = [0 0 0 0 1];
D3 = 0;

syms u3 y3 i_L1_3 i_L2_3 i_L3_3 V_C1_3 V_C2_3

x3 = [i_L1_3; i_L2_3; i_L3_3; V_C1_3; V_C2_3];

%% Concatenation - Open  loop
Adiag = {A1,A2,A3};
Bdiag = {B1,B2,B3};
Cdiag = {C1,C2,C3};
Ddiag = {D1,D2,D3};

```

```
78 Xol = [x1; x2; x3];
79 Uol = [u1; u2; u3];
80 Yol = [y1; y2; y3];
81
82 Mint = zeros(sizesys);
83 Mint(3,1) = 1; Mint(3,2) = 1;
84
85 Mext = zeros(sizesys);
86 Mext(1,1) = 1; Mext(2,2) = 1;
87
88 Aol = blkdiag(Adiag{:});
89 Bol = blkdiag(Bdiag{:});
90 Col = blkdiag(Cdiag{:});
91 Dol = blkdiag(Ddiag{:});
92
93 Uolp = (Mint*Yol)+(Mext*Uol);
94 Eol = inv(eye(sizesys)-Dol*Mint);
95
96 %% Closed Loop
97 Acl = Aol+(Bol*Mint*Eol*Col);
98 Bcl = Bol+(Bol*Mint*Eol*Dol);
99 Ccl = Eol*Col;
100 Dcl = Eol*Dol;
101
102 Xcl = Xol;
103
104 Ucl = Mext*Uol;
105
106 Ycl = Yol;
107
108 %% State space & transfer function
109 ssT = ss(Acl,Bcl,Ccl,Dcl);
110 H = tf(ssT);
111
112 %% Singular value decomposition
113 W = logspace(0,5,6000);
114 [SV] = sigma(H,W);
115 [pk, pkindx] = findpeaks(SV(1,:));
116 pkdb = 20*log10(pk);
117 freqrad = W(pkindx);
118 freqdeg = freqrad/(2*pi);
119 %% Evaluation in time domain
120 f1 = 1300;
121 w1 = f1*2*pi;
122 T = 1/f1; period = 100000; ns = 1e-2;
123 t = 0:T*ns:T*period;
124 u = sin(w1*t);
125 zer = zeros(size(u));
126
```

```
U = [u; u; zer];
y = lsim(H,U,t);
```

B.2. Synthetic Randstad region system routine

```
function [SV,W] = tlinesycables(distline,discabl)
%% Common values
sizesys = 14;
Vbase = 380e3;
ri = 1e-3;

%% BVW380/A to OZN3/CUB_0.3
Sbase1 = 1908.7e6;
Zbase1 = (Vbase^2)/Sbase1;

l_1 = 15.9*distline;

Z1 = ((0.000257+0.003014*i)*Zbase1)/15.9;
B1 = (0.094470/Zbase1)/15.9;

R1 = real(Z1)*l_1;
L1 = imag(Z1)*l_1;
C1_1 = (B1/2)*l_1;
C2_1 = (B1/2)*l_1;

A1 = [-R1/L1 1/L1 -1/L1; -1/C1_1 -1/(ri*C1_1) 0; 1/C2_1 0 0];
B1 = [0; 1/(ri*C1_1); 0];
C1 = [0 0 1];
D1 = 0;

syms u1 y1 i_L_1 V_C1_1 V_C2_1

x1 = [i_L_1; V_C1_1; V_C2_1];

%% OZN3/CUB_0.3 to DIM380/A
Sbase2 = 1908.7e6;
Zbase2 = (Vbase^2)/Sbase2;

l_2 = 15.2*distline;

Z2 = ((0.000246+0.002882*i)*Zbase2)/15.2;
B2 = (0.090310/Zbase2)/15.2;

R2 = real(Z2)*l_2;
L2 = imag(Z2)*l_2;
C1_2 = (B2/2)*l_2;
C2_2 = (B2/2)*l_2;

A2 = [-R2/L2 1/L2 -1/L2; -1/C1_2 -1/(ri*C1_2) 0; 1/C2_2 0 0];
```

```
45 B2 = [0; 1/(ri*C1_2); 0];
46 C2 = [0 0 1];
47 D2 = 0;
48
49 syms u2 y2 i_L_2 V_C1_2 V_C2_2
50
51 x2 = [i_L_2; V_C1_2; V_C2_2];
52
53 %% DIM380/A to BKK380/A
54 Sbase3 = 1645.4e6;
55 Zbase3 = (Vbase^2)/Sbase3;
56
57 l_3 = 18.830*distline;
58
59 Z3 = ((0.000305+0.003570*i)*Zbase3)/18.830;
60 B3 = (0.111890/Zbase3)/18.830;
61
62 R3 = real(Z3)*l_3;
63 L3 = imag(Z3)*l_3;
64 C1_3 = (B3/2)*l_3;
65 C2_3 = (B3/2)*l_3;
66
67 A3 = [-R3/L3 1/L3 -1/L3; -1/C1_3 -1/(ri*C1_3) 0; 1/C2_3 0 0];
68 B3 = [0; 1/(ri*C1_3); 0];
69 C3 = [0 0 1];
70 D3 = 0;
71
72 syms u3 y3 i_L_3 V_C1_3 V_C2_3
73
74 x3 = [i_L_3; V_C1_3; V_C2_3];
75
76 %% BKK380/A to KIJ380/A
77 Sbase4 = 1645.4e6;
78 Zbase4 = (Vbase^2)/Sbase4;
79
80 l_4 = 1*distline;
81
82 Z4 = ((0.000626+0.007336*i)*Zbase4)/1;
83 B4 = (0.229920/Zbase4)/1;
84
85 R4 = real(Z4)*l_4;
86 L4 = imag(Z4)*l_4;
87 C1_4 = (B4/2)*l_4;
88 C2_4 = (B4/2)*l_4;
89
90 A4 = [-R4/L4 1/L4 -1/L4; -1/C1_4 -1/(ri*C1_4) 0; 1/C2_4 0 0];
91 B4 = [0; 1/(ri*C1_4); 0];
92 C4 = [0 0 1];
93 D4 = 0;
```

```
94
95 syms u4 y4 i_L_4 V_C1_4 V_C2_4
96
97 x4 = [i_L_4; V_C1_4; V_C2_4];
98
99 %% KIJ380/A to BWK380/A
100 Sbase5 = 2632.7e6;
101 Zbase5 = (Vbase^2)/Sbase5;
102
103 l_5 = 18.560*distline;
104
105 Z5 = ((0.000196+0.003131*i)*Zbase5)/18.560;
106 B5 = (0.128490/Zbase5)/18.560;
107
108 R5 = real(Z5)*l_5;
109 L5 = imag(Z5)*l_5;
110 C1_5 = (B5/2)*l_5;
111 C2_5 = (B5/2)*l_5;
112
113 A5 = [-R5/L5 1/L5 -1/L5; -1/C1_5 -1/(ri*C1_5) 0; 1/C2_5 0 0];
114 B5 = [0; 1/(ri*C1_5); 0];
115 C5 = [0 0 1];
116 D5 = 0;
117
118 syms u5 y5 i_L_5 V_C1_5 V_C2_5
119
120 x5 = [i_L_5; V_C1_5; V_C2_5];
121
122 %% BWK380/A to VHZ380/B
123 l_6 = 48.7*discabl;
124 rz1_6 = (1.1724e-1)*l_6; rz2_6 = (8.2072e-2)*l_6; rz3_6 = (1.1946e
    -2)*l_6;
125 Lz1_6 = (2.2851e-4)*l_6; Lz2_6 = (1.5522e-3)*l_6; Lz3_6 = (3.2942e
    -3)*l_6;
126 Cc_6 = (1.9083e-7)*l_6;
127
128 A6 = [-rz1_6/Lz1_6 0 0 1/Lz1_6 -1/Lz1_6;...
129     0 -rz2_6/Lz2_6 0 1/Lz2_6 -1/Lz2_6;...
130     0 0 -rz3_6/Lz3_6 1/Lz3_6 -1/Lz3_6;...
131     -1/Cc_6 -1/Cc_6 -1/Cc_6 -1/(ri*Cc_6) 0;...
132     1/Cc_6 1/Cc_6 1/Cc_6 0 0];
133 B6 = [0; 0; 0; 1/(ri*Cc_6); 0];
134 C6 = [0 0 0 0 1];
135 D6 = 0;
136
137 syms u6 y6 i_L1_6 i_L2_6 i_L3_6 V_C1_6 V_C2_6
138
139 x6 = [i_L1_6; i_L2_6; i_L3_6; V_C1_6; V_C2_6];
140
```

```
%% VHZ380/B to BVW380/A
Sbase7 = 1974.5e6;
Zbase7 = (Vbase^2)/Sbase7;

l_7 = 12.1*distline;

Z7 = ((0.000166+0.002152*i)*Zbase7)/12.1;
B7 = (0.239530/Zbase7)/12.1;

R7 = real(Z7)*l_7;
L7 = imag(Z7)*l_7;
C1_7 = (B7/2)*l_7;
C2_7 = (B7/2)*l_7;

A7 = [-R7/L7 1/L7 -1/L7; -1/C1_7 -1/(ri*C1_7) 0; 1/C2_7 0 0];
B7 = [0; 1/(ri*C1_7); 0];
C7 = [0 0 1];
D7 = 0;

syms u7 y7 i_L_7 V_C1_7 V_C2_7

x7 = [i_L_7; V_C1_7; V_C2_7];

%% MVL3/CUB_0.4 to Terminal SP
Sbase8 = 2632.7e6;
Zbase8 = (Vbase^2)/Sbase8;

l_8 = 1*distline;

Z8 = ((0.000184+0.003309*i)*Zbase8)/1;
B8 = (0.487350/Zbase8)/1;

R8 = real(Z8)*l_8;
L8 = imag(Z8)*l_8;
C1_8 = (B8/2)*l_8;
C2_8 = (B8/2)*l_8;

A8 = [-R8/L8 1/L8 -1/L8; -1/C1_8 -1/(ri*C1_8) 0; 1/C2_8 0 0];
B8 = [0; 1/(ri*C1_8); 0];
C8 = [0 0 1];
D8 = 0;

syms u8 y8 i_L_8 V_C1_8 V_C2_8

x8 = [i_L_8; V_C1_8; V_C2_8];

%% Terminal SP to WL380/W
Sbase9 = 2650.0e6;
Zbase9 = (Vbase^2)/Sbase9;
```

```
190
191 l_9 = 1*distline;
192
193 Z9 = ((0.000007+0.005886*i)*Zbase9)/1;
194 B9 = (0.01/Zbase9)/1;
195
196 R9 = real(Z9)*l_9;
197 L9 = imag(Z9)*l_9;
198 C1_9 = (B9/2)*l_9;
199 C2_9 = (B9/2)*l_9;
200
201 A9 = [-R9/L9 1/L9 -1/L9; -1/C1_9 -1/(ri*C1_9) 0; 1/C2_9 0 0];
202 B9 = [0; 1/(ri*C1_9); 0];
203 C9 = [0 0 1];
204 D9 = 0;
205
206 syms u9 y9 i_L_9 V_C1_9 V_C2_9
207
208 x9 = [i_L_9; V_C1_9; V_C2_9];
209
210 %% WL380/W to WTR380/A
211 Sbase10 = 2632.7e6;
212 Zbase10 = (Vbase^2)/Sbase10;
213
214 l_10 = 6.8*distline;
215
216 Z10 = ((0.000072+0.001151*i)*Zbase10)/6.8;
217 B10 = (0.046920/Zbase10)/6.8;
218
219 R10 = real(Z10)*l_10;
220 L10 = imag(Z10)*l_10;
221 C1_10 = (B10/2)*l_10;
222 C2_10 = (B10/2)*l_10;
223
224 A10 = [-R10/L10 1/L10 -1/L10; -1/C1_10 -1/(ri*C1_10) 0; 1/C2_10 0
      0];
225 B10 = [0; 1/(ri*C1_10); 0];
226 C10 = [0 0 1];
227 D10 = 0;
228
229 syms u10 y10 i_L_10 V_C1_10 V_C2_10
230
231 x10 = [i_L_10; V_C1_10; V_C2_10];
232
233 %% WTR380/A to BWK380/A
234 l_11 = 20.1*discabl;
235 rz1_11 = (1.1724e-1)*l_11; rz2_11 = (8.2072e-2)*l_11; rz3_11 =
      (1.1946e-2)*l_11;
```

```
236 Lz1_11 = (2.2851e-4)*l_11; Lz2_11 = (1.5522e-3)*l_11; Lz3_11 =
       (3.2942e-3)*l_11;
237 Cc_11 = (1.9083e-7)*l_11;
238
239 A11 = [-rz1_11/Lz1_11 0 0 1/Lz1_11 -1/Lz1_11;...
240     0 -rz2_11/Lz2_11 0 1/Lz2_11 -1/Lz2_11;...
241     0 0 -rz3_11/Lz3_11 1/Lz3_11 -1/Lz3_11;...
242     -1/Cc_11 -1/Cc_11 -1/Cc_11 -1/(ri*Cc_11) 0;...
243     1/Cc_11 1/Cc_11 1/Cc_11 0 0];
244 B11 = [0; 0; 0; 1/(ri*Cc_11); 0];
245 C11 = [0 0 0 0 1];
246 D11 = 0;
247
248 syms u11 y11 i_L1_11 i_L2_11 i_L3_11 V_C1_11 V_C2_11
249
250 x11 = [i_L1_11; i_L2_11; i_L3_11; V_C1_11; V_C2_11];
251
252 %% MVL3/CUB_0.4 to TERMINAL SMH
253 Sbase12 = 2632.7e6;
254 Zbase12 = (Vbase^2)/Sbase12;
255
256 l_12 = 26*distline;
257
258 Z12 = ((0.000275+0.004364*i)*Zbase12)/26;
259 B12 = (0.181450/Zbase12)/26;
260
261 R12 = real(Z12)*l_12;
262 L12 = imag(Z12)*l_12;
263 C1_12 = (B12/2)*l_12;
264 C2_12 = (B12/2)*l_12;
265
266 A12 = [-R12/L12 1/L12 -1/L12; -1/C1_12 -1/(ri*C1_12) 0; 1/C2_12 0
       0];
267 B12 = [0; 1/(ri*C1_12); 0];
268 C12 = [0 0 1];
269 D12 = 0;
270
271 syms u12 y12 i_L_12 V_C1_12 V_C2_12
272
273 x12 = [i_L_12; V_C1_12; V_C2_12];
274
275 %% TERMINAL SMH to CST380/A
276 Sbase13 = 2632.7e6;
277 Zbase13 = (Vbase^2)/Sbase13;
278
279 l_13 = 40.430*distline;
280
281 Z13 = ((0.000428+0.006786*i)*Zbase13)/40.430;
282 B13 = (0.282160/Zbase13)/40.430;
```

```
283
284 R13 = real(Z13)*l_13;
285 L13 = imag(Z13)*l_13;
286 C1_13 = (B13/2)*l_13;
287 C2_13 = (B13/2)*l_13;
288
289 A13 = [-R13/L13 1/L13 -1/L13; -1/C1_13 -1/(ri*C1_13) 0; 1/C2_13 0
       0];
290 B13 = [0; 1/(ri*C1_13); 0];
291 C13 = [0 0 1];
292 D13 = 0;
293
294 syms u13 y13 i_L_13 V_C1_13 V_C2_13
295
296 x13 = [i_L_13; V_C1_13; V_C2_13];
297
298 %% CST380/A to KIJ380/A
299 Sbase14 = 2632.7e6;
300 Zbase14 = (Vbase^2)/Sbase14;
301
302 l_14 = 14.840*distline;
303
304 Z14 = ((0.000157+0.002490*i)*Zbase14)/14.840;
305 B14 = (0.103530/Zbase14)/14.840;
306
307 R14 = real(Z14)*l_14;
308 L14 = imag(Z14)*l_14;
309 C1_14 = (B14/2)*l_14;
310 C2_14 = (B14/2)*l_14;
311
312 A14 = [-R14/L14 1/L14 -1/L14; -1/C1_14 -1/(ri*C1_14) 0; 1/C2_14 0
       0];
313 B14 = [0; 1/(ri*C1_14); 0];
314 C14 = [0 0 1];
315 D14 = 0;
316
317 syms u14 y14 i_L_14 V_C1_14 V_C2_14
318
319 x14 = [i_L_14; V_C1_14; V_C2_14];
320
321 %% Open  loop
322 Adiag = {A1,A2,A3,A4,A5,A6,A7,A8,A9,A10,A11,A12,A13,A14};
323 Bdiag = {B1,B2,B3,B4,B5,B6,B7,B8,B9,B10,B11,B12,B13,B14};
324 Cdiag = {C1,C2,C3,C4,C5,C6,C7,C8,C9,C10,C11,C12,C13,C14};
325 Ddiag = {D1,D2,D3,D4,D5,D6,D7,D8,D9,D10,D11,D12,D13,D14};
326
327 Xol = [x1; x2; x3; x4; x5; x6; x7; x8; x9; x10; x11; ...
328        x12; x13; x14];
329 Uol = [u1; u2; u3; u4; u5; u6; u7; u8; u9; u10; u11; ...
```

```
330         u12; u13; u14];
331 Yol = [y1; y2; y3; y4; y5; y6; y7; y8; y9; y10; y11; ...
332         y12; y13; y14];
333
334 Mint = zeros(sizesys);
335 Mint(2,1) = 1;
336 Mint(7,1) = 1;
337 Mint(3,2) = 1;
338 Mint(4,3) = 1;
339 Mint(5,4) = 1;
340 Mint(6,5) = 1;
341 Mint(6,7) = 1;
342 Mint(9,8) = 1;
343 Mint(12,8) = 1;
344 Mint(10,9) = 1;
345 Mint(11,10) = 1;
346 Mint(6,11) = 1;
347 Mint(13,12) = 1;
348 Mint(14,13) = 1;
349 Mint(5,14) = 1;
350
351 Mext = zeros(sizesys);
352 Mext(1,1) = 1;
353 Mext(8,8) = 1;
354
355 Aol = blkdiag(Adiag{:});
356 Bol = blkdiag(Bdiag{:});
357 Col = blkdiag(Cdiag{:});
358 Dol = blkdiag(Ddiag{:});
359
360 Uolp = (Mint*Yol)+(Mext*Uol);
361 Eol = inv(eye(sizesys)-Dol*Mint);
362
363 %% Closed Loop
364 Acl = Aol+(Bol*Mint*Eol*Col);
365 Bcl = Bol+(Bol*Mint*Eol*Dol);
366 Ccl = Eol*Col;
367 Dcl = Eol*Dol;
368
369 Xcl = Xol;
370 Ucl = Mext*Uol;
371 Ycl = Yol;
372
373 %% State space & Transfer function
374 ssT = ss(Acl,Bcl,Ccl,Dcl);
375 H = tf(ssT);
376
377 %% Singular value decomposition
378 W = logspace(0,5,1000);
```

```
[SV] = sigma(H,W);
[pk, pkindx] = findpeaks(SV(1,:));
pkdb = 20*log10(pk);
freqrad = W(pkindx);
freqdeg = freqrad/(2*pi);
```

```
clc;clear variables;
% distline = 1; discabl = 1;
% distline = 0.5:0.01:1.5; discabl = ones(size(distline));
discabl = 0.5:0.01:1.5; distline = ones(size(discabl));

for n = 1:length(distline)
    [SV(:,:,n),W(:,:,n)] = tlinesycables(distline(n),discabl(n));
end

for n = 1:length(distline)
    sv(n,:) = SV(1,:,n);
    omeg(n,:) = W(:,:,n);
    dis(n,:) = ones(1,length(W))*discabl(n);
end

figure(1);clf
surf(omeg/(2*pi),dis,20*log10(sv),'FaceColor','interp',...
   'EdgeColor','none',...
   'FaceLighting','gouraud');
camlight left
h = colorbar;
set(h, 'ylim', [0 120])
zlim([0 120])
set(gca,'XScale','log');
xlim([3 80])
title('Transmission Line Length Variation')
xlabel('Frequency (Hz)')
ylabel('Line length (p.u.)')
zlabel('First Singular Value')

figure(2);clf
surf(omeg/(2*pi),dis,20*log10(sv),'FaceColor','interp',...
   'EdgeColor','none',...
   'FaceLighting','gouraud');
camlight left
h = colorbar;
set(h, 'ylim', [0 120])
zlim([0 40])
set(gca,'XScale','log');
xlim([200 4000])
title('Cable Line Length Variation')
xlabel('Frequency (Hz)')
ylabel('Cable length (p.u.)')
zlabel('First Singular Value')
```

Bibliography

[1] J. Freytes, *Small-signal stability analysis of Modular Multilevel Converters and application to MMC–based Multi-Terminal DC grids*, Ph.D. thesis, Ecole Centrale de Lille (2017).

[2] D. Kasraian, K. Maat, and B. van Wee, *Development of rail infrastructure and its impact on urbanization in the Randstad, the Netherlands,* Journal of Transport and Land Use **9** (2015).

[3] *Kwaliteits- en Capaciteitsdocument 2017. Deel II: Investeringen Net op Land 2018-2027,* (2017), TenneT TSO B.V., Available at https://www.tennet.eu/.

[4] *Offshore Wind in Europe. Key trends and statistics 2018,* (2018), Wind Europe, Available at https://windeurope.org/.

[5] *Kwaliteits- en Capaciteitsdocument 2017. Deel III: Investeringen Net op Zee 2018-2027,* (2017), TenneT TSO B.V., Available at https://www.tennet.eu/.

[6] S. Cole, D. Van Hertem, I. Pardon, and R. Belmans, *Randstad hvdc,* Research group Electa, Dept. of Electrical Engineering, KULeuven, Belgium (2006).

[7] Y. Qiu, C. Dai, and R. Jin, *Impact of power electronic device development on power grids,* in *2016 28th International Symposium on Power Semiconductor Devices and ICs (ISPSD)* (IEEE, 2016) pp. 9–14.

[8] V. Klema and A. Laub, *The singular value decomposition: Its computation and some applications,* IEEE Transactions on automatic control **25**, 164 (1980).

[9] A. D. Torres Acosta, *EMT model of Randstad electrical regional network and near shore wind power plants for real-time digital simulation,* (2019), Delft University of Technology.

[10] M. Amin and M. Molinas, *Small-signal stability assessment of power electronics based power systems: A discussion of impedance-and eigenvalue-based methods,* IEEE Transactions on Industry Applications **53**, 5014 (2017).

[11] J. Sun, *Impedance-based stability criterion for grid-connected inverters,* IEEE Transactions on Power Electronics **26**, 3075 (2011).

[12] G. F. Franklin, J. D. Powell, A. Emami-Naeini, and J. D. Powell, *Feedback control of dynamic systems*, Vol. 3 (Addison-Wesley Reading, MA, 1994).

[13] Y. Wang, X. Wang, F. Blaabjerg, and Z. Chen, *Harmonic instability assessment using state-space modeling and participation analysis in inverter-fed power systems,* IEEE Transactions on Industrial Electronics **64**, 806 (2016).

[14] S. Skogestad and I. Postlethwaite, *Multivariable feedback control: analysis and design*, Vol. 2 (Wiley New York, 2007).

[15] A. Bonner, T. Grebe, E. Gunther, L. Hopkins, M. Marz, J. Mahseredjian, N. Miller, T. Ortmeyer, V. Rajagopalan, S. Ranade, *et al.*, *Modeling and simulation of the propagation of harmonics in electric power networks. 1. Concepts, models, and simulation techniques,* IEEE Transactions on Power Delivery **11**, 452 (1996).

[16] Z. Huang, Y. Cui, and W. Xu, *Application of modal sensitivity for power system harmonic resonance analysis,* IEEE Transactions on Power Systems **22**, 222 (2007).

[17] E. Prieto-Araujo, F. D. Bianchi, A. Junyent-Ferre, and O. Gomis-Bellmunt, *Methodology for droop control dynamic analysis of multiterminal VSC-HVDC grids for offshore wind farms,* IEEE Transactions on power delivery **26**, 2476 (2011).

[18] E. Prieto-Araujo, A. Egea-Alvarez, S. Fekriasl, and O. Gomis-Bellmunt, *DC voltage droop control design for multiterminal HVDC systems considering AC and DC grid dynamics,* IEEE Transactions on Power Delivery **31**, 575 (2016).

[19] R. Eriksson, J. Beerten, M. Ghandhari, and R. Belmans, *Optimizing DC voltage droop settings for AC/DC system interactions,* IEEE Transactions on Power Delivery **29**, 362 (2014).

[20] S. Akkari, E. Prieto-Araujo, J. Dai, O. Gomis-Bellmunt, and X. Guillaud, *Impact of the DC cable models on the SVD analysis of a multi-terminal HVDC system,* in *2016 Power Systems Computation Conference (PSCC)* (IEEE, 2016) pp. 1–6.

[21] *Nederlands Transpornet,* (2017), TenneT TSO B.V., Available at https://www.tennet.eu/.

[22] *PSS®E 33.5 Program Application Guide Volume 1,* (2013), Siemens Industry Inc., Siemens Power Technologies International.

[23] *PSS®E 33.5 Program Application Guide Volume 2,* (2013), Siemens Industry Inc., Siemens Power Technologies International.

[24] J. Beerten, S. D'Arco, and J. A. Suul, *Cable model order reduction for HVDC systems interoperability analysis,* (2015).

[25] O. Ramos-Leaños, J. L. Naredo, J. Mahseredjian, C. Dufour, J. A. Gutiérrez-Robles, and I. Kocar, *A wideband line/cable model for real-time simulations of power system transients,* IEEE Transactions on Power Delivery **27**, 2211 (2012).

[26] S. Akkari, *Control of a multi-terminal HVDC (MTDC) system and study of the interactions between the MTDC and the AC grids.*, Ph.D. thesis, Université Paris-Saclay (2016).

[27] J. Marti, L. Marti, and H. Dommel, *Transmission line models for steady-state and transients analysis,* in *Proceedings. Joint International Power Conference Athens Power Tech,*, Vol. 2 (IEEE, 1993) pp. 744–750.